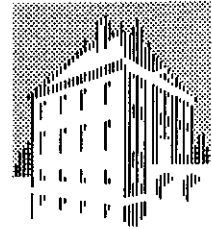


APRIL 1990

---

FOM-INSTITUUT  
VOOR  
PLASMAFYSICA  
RIJNHUIZEN



ASSOCIATIE  
EURATOM-FOM

---

# MICROWAVE INTERFEROMETER AND REFLECTOMETER TECHNIQUES FOR THERMONUCLEAR PLASMAS

C.A.J. HUGENHOLTZ

RIJNHUIZEN REPORT 90-192

This work was performed as part of the research programme of the association agreement of Euratom and the 'Stichting voor Fundamenteel Onderzoek der Materie' (FOM) with financial support from the 'Nederlandse Organisatie voor Wetenschappelijk Onderzoek' (NWO) and Euratom.

POSTBUS 1207  
3430 BE NIEUWEGEIN  
NEDERLAND  
EDISONBAAN 14  
3439 MN NIEUWEGEIN  
TEL. 03402 - 31224  
TELEFAX 03402 - 31204  
TELEX 47380 RIJNHZ NL

---

# **MICROWAVE INTERFEROMETER AND REFLECTOMETER TECHNIQUES FOR THERMONUCLEAR PLASMAS**

## **PROEFSCHRIFT**

ter verkrijging van de graad van doctor aan de  
Technische Universiteit Eindhoven, op gezag van  
de Rector Magnificus, prof. ir. M. Tels, voor  
een commissie aangewezen door het College van  
Dekanen in het openbaar te verdedigen op  
dinsdag 10 april 1990 te 14.00 uur

door

**COENRAAD ALBERTUS JACOBUS HUGENHOLTZ**  
geboren te Klaaswaal

Dit proefschrift is goedgekeurd door  
de promotoren  
prof. dr. L.Th.M. Ornstein  
en  
prof. dr. F.W. Sluijter

*The work described in this thesis was performed as part of the research programme of the 'Stichting voor Fundamenteel Onderzoek der Materie' (FOM) and the Association EURATOM-FOM, with financial support from the 'Nederlandse Organisatie voor Wetenschappelijk Onderzoek' (NWO) and EURATOM. The work was carried out at the FOM-Instituut voor Plasmafysica Rijnhuizen, Nieuwegein, the Netherlands, and at the JET Joint Undertaking at Culham, UK.*

*Aan Eefje*

## CONTENTS

<b>General introduction</b>	9
<b>Summary</b>	12

### PART 1

## INTERFEROMETRY

<b>Chapter 1</b>	<b>Introduction to interferometry</b>	15
1.1	Principle of plasma density measurements	15
1.2	Refraction of electromagnetic waves	18
1.3	Microwave components	19
1.4	Phase modulation techniques	22
1.5	Phase detectors	26
<b>Chapter 2</b>	<b>Multi-radian 2-mm interferometer for JET</b>	35
2.1	Introduction	35
2.2	Proposal for the 2-mm interferometer	36
2.3	Horn antenna matched to oversized waveguide and vacuum window	42
2.4	Plasma electron density measurements in JET with the 2-mm microwave interferometer	47
<b>Chapter 3</b>	<b>Heterodyne CO<sub>2</sub>-laser interferometry</b>	59
3.1	Introduction	59
3.2	CO <sub>2</sub> -laser interferometer with a Doppler-wheel	61
3.3	CO <sub>2</sub> -laser interferometer with acousto-optic modulators	67
3.4	Multi-channel CO <sub>2</sub> -laser interferometer using a PbSnTe detector array	69
<b>Appendix A</b>	<b>A simple method to obtain polar information with a normal microwave interferometer</b>	75
<b>Appendix B</b>	<b>A rigid microwave access lens into copper-shielded plasma physics experiments</b>	78

**PART 2**  
**REFLECTOMETRY**

<b>Chapter 4</b>	<b>Introduction to reflectometry</b>	83
4.1	Principle of reflectometry	83
4.2	Profile measurements from phase information with swept frequency	86
4.3	Complications due to external magnetic fields	88
<b>Chapter 5</b>	<b>The multi-channel reflectometer for JET</b>	91
5.1	Introduction	91
5.2	Construction of the multi-channel reflectometer	93
5.3	Technical description of the sources, detection systems, and data acquisition systems of the multi-channel reflectometer	97
5.4	Performance tests in a mock-up of the JET reflectometer	113
5.5	First results of the multi-channel reflectometer	118
<b>Appendix C</b>	<b>Proposal for a multi-channel reflectometer for RTP</b>	123
<b>Epilogue</b>	<b>Measurements at 33 GHz of Doppler frequency shift</b>	127
	<b>References</b>	135
	<b>Inhoud</b>	139
	<b>Samenvatting</b>	142
	<b>Dankwoord</b>	143
	<b>Curriculum vitae</b>	144

## GENERAL INTRODUCTION

The tokamak has become the predominant research tool in the world-wide endeavour to develop useful electrical power based on controlled thermonuclear fusion. To achieve thermonuclear conditions in a tokamak it is necessary to confine the plasma and, in particular, its energy for a sufficiently long time. The confinement is limited by thermal conduction, convection processes, and by radiation. Detailed analysis of experiments indicates that thermal losses through electrons exceed the classical predictions by up to two orders of magnitude, whereas ion thermal losses are closer to theoretical predictions.

In order to assess the viability of a tokamak reactor it is necessary to diagnose the plasma. A large group of diagnostics is based on the analysis of radiation emerging from the plasma [Luhm-84, Orli-88]. This may concern either radiation emitted by the plasma itself or it may be radiation originating from an external source, transmitted through the plasma and affected by it. Microwave diagnostics play an important role in this respect.

Measuring techniques based on microwaves have been playing an important role in thermonuclear plasma experiments for many years. The most useful microwave diagnostic techniques can be divided into a number of categories:

- detection of electron cyclotron emission or synchrotron radiation, to obtain information on the temperature of the electrons in the plasma,
- study of collective scattering of incident waves to follow density fluctuations in plasmas,
- interferometry to measure plasma densities,
- reflectometry to determine the location of plasmas with specific densities, often combined with the measurement of fluctuations thereof,
- polarimetry to measure the distribution of the magnetic field in the plasma.

This is an appreciable number of different methods, each of them based on interaction of electromagnetic waves with plasmas. The propagation of electromagnetic waves in plasmas is treated in detail by several authors [Chen-77, Ginz-61, Heal-65, Stix-62]. Though the complete picture of the interaction of electromagnetic waves with plasmas is quite complicated, the description can be simplified considerably for tokamak plasmas: in the frequency range used here the ion may be considered to be infinitely heavy. In tokamak plasmas, the electron temperature is usually  $\leq 10$  keV. So the average thermal velocity of the electrons is much less than the velocity of the waves which is close to the velocity of light; consequently, relativistic effects are in general negligible. The electron-ion collision frequency is much less than the frequency of the wave and, therefore, collisional damping effects can also be neglected.

## 10 General introduction

In this thesis two types of microwave diagnostics are treated: Interferometry and Reflectometry. Most emphasis will be placed on technical aspects. In addition, an exposé of the underlying theories will be given in chapters 1 and 4. At this point the basic principles underlying these techniques may be illustrated by the following. The phase velocity of an electromagnetic wave travelling through plasma depends of the density: the index of refraction is  $\mu(n_e) = c/v$ , where  $c$  is the velocity of light and  $v$  the phase velocity of the electromagnetic wave in a plasma with an electron density  $n_e$ . At a certain –critical– density,  $n_c$ , the phase velocity becomes infinite, so electromagnetic waves of a chosen frequency cannot propagate any more through the plasma (cut-off) but are reflected \*).

Waves, when transmitted through a plasma, can be used to measure the electron density with interferometers, provided that a proper choice of the applied frequency is made as long as  $n_e$  remains smaller than  $n_c$ . Interferometry is basically the measurement of the phase change due to the presence of the plasma. If the plasma density is non-homogeneous and has a certain spatial distribution (e.g. parabolic) a wave passing through the plasma undergoes varying refractive effects all along its path and may therefore not travel along a straight line. The resulting angle of refraction depends on the chosen frequency, on the values of  $n_e/n_c$ , and on the spatial gradient of  $n_e$  [Shmo-61]. For this reason the wavelength of the probing beam should be chosen far away from cut-off, i.e. as short as possible, but still within the range where the phase changes, due to the presence of the plasma, are still detectable. However, smaller wavelengths require a higher mechanical stability of the instrument to avoid spurious phase-effects due to vibrations. Thus, the choice of the operating frequency always implies a compromise and it also depends on the availability of microwave oscillators. Single-beam interferometers are generally used. In most cases the microwave beam, with a limited angular spread, is directed parallel to the density gradient through the centre of the plasma, thus the influence of refractive effects is relatively small. Interferometry may yield density profiles when applied along a number of (parallel) chords. Since line-integrated densities are measured, one must unfold the interferometric information, e.g. by Abel inversion [Gott-77], to find the density profile. Multi-channel interferometers for large thermonuclear plasma experiments actually become physically dominating obstacles in the crowded space around such experiments and may also occupy many observational ports. It is hard to believe that next step thermonuclear experiments will apply this kind of set up.

---

\*) This is, of course, approximately true. In fact, reflection is a continuous effect in an inhomogeneous medium [Slui-70]. However, within the limits of applicability of the so-called WKB (Wenzel Kramers Brillouin) approximation, i.e. in essence as long as the wavelengths concerned are very small with respect to the scale length of the inhomogeneity, the effect of the inhomogeneity is almost exclusively felt in the phase of the wave and reflection is either non-present or total.

In reflectometry a wave of a specific frequency is launched towards the plasma to be (almost exclusively) reflected from the layer in the immediate vicinity of the critical density. The phase difference of the launched wave and the reflected wave contains information on the position of the reflecting layer. Reflectometers can be operated in two different modes: with a fixed frequency to follow movements of a reflecting layer or with swept frequency to find the absolute position of the reflecting layer. As the wave travels through plasma before it reflects at the cut-off layer, the phase change in this transparent layer must be taken into account. Since the critical density is dependent on the frequency of the waves a number of different frequencies must be used to determine the density profile on the side where the reflectometer is located. Reflectometer measurements from two sides are needed to find a complete single-humped plasma profile. Since the reflectometer cannot look over the rim of a hollow profile, extra information to determine details of the profile beyond the rim must be obtained from other diagnostics. One of the attractive aspects of reflectometry, compared with multi-channel interferometry, is the small interference with the experimental installations, since this technique occupies little space. Another advantage of reflectometry is the lower frequency that can be used, for which various oscillators are more readily available. Reflectometry is under development in different laboratories.

## SUMMARY

### Part 1. Interferometry

Chapter 1 is an introduction to interferometry in which also the theoretical background is given. Some microwave components are discussed briefly. Phase-modulation techniques, to ensure unambiguous phase measurements, are discussed in detail. A number of digital phase detectors, which can yield a high resolution, are described.

Chapter 2 gives a description of the 2-mm microwave interferometer, designed and built for the JET-tokamak, the joint European experiment in Culham, England. Calculations are given of the waveguide losses, losses of the microwave beam through the plasma, and the expected signal-to-noise ratio. Results of measurements of the plasma density show a high phase-resolution (1 in 5000).

Chapter 3 describes CO<sub>2</sub>-laser interferometers, built for the RINGBOOG-experiment, a gas blanket tokamak in the FOM-Instituut voor Plasmafysica Rijnhuizen, Nieuwegein, the Netherlands. The first instrument is a single-channel interferometer giving unambiguous phase information through the application of a moving mirror. In the second instrument two Bragg-cell modulators are used. The third instrument is a 15-channel interferometer using a sheet-like beam which gives a 'phase image' of the plasma on a detector array.

### Part 2. Reflectometry

Chapter 4 is an introduction to reflectometry in which different possibilities and limitations of the method are discussed. The relation between the phase measurement and the density profile is given.

Chapter 5 gives a detailed description of the 12-channel heterodyne reflectometer designed and built for JET. The reflectometer can be operated in two modes as mentioned in the general introduction. Measurements in a mock-up, using a plane mirror, show that it is possible to obtain the required accuracy. First results of measurements with this reflectometer of the JET-plasma are shown.

An appendix gives a proposal of a 24-channel reflectometer for the RTP-tokamak experiment at the FOM-Instituut voor Plasmafysica Rijnhuizen.

In the epilogue, looking back as far as 1963, a description is given of a heterodyne reflectometer to measure high velocities of plasmoids.

**PART 1**

**INTERFEROMETRY**



## Chapter 1

### INTRODUCTION TO INTERFEROMETRY

#### 1.1 Principle of plasma density measurements

An interferometer is in fact used to measure the difference in path length between a reference beam, which is kept constant in optical length, and a beam transmitted through the plasma. The optical length through the plasma varies because of the change in refractive index, connected with the increase and the decrease of the electron density, during the experimental sequence (Fig. 1.1).

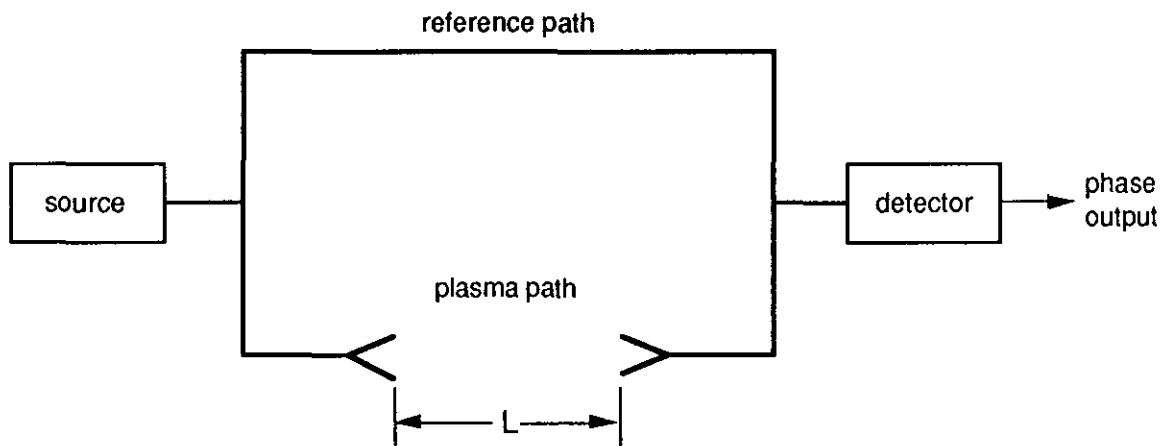


Fig. 1.1. Mach-Zehnder interferometer.

The path length  $L$  contains a number of vacuum wavelengths  $\lambda_0$ ,  $a$ :

$$L = a \lambda_0, \text{ where } a = \frac{\varphi_0}{2\pi}, \quad (1.1)$$

and in the presence of plasma a number plasma wavelengths  $\lambda_p$ ,  $b$ :

$$L = b \lambda_p, \text{ where } b = \frac{\varphi_p}{2\pi}, \quad (1.2)$$

where  $\varphi_0$  and  $\varphi_p$  are the phases of the waves after travelling through vacuum or through plasma, respectively. From the Eqs (1.1 and 1.2) one can see

$$\varphi_0 = \frac{L}{\lambda_0} 2\pi \text{ and } \varphi_p = \frac{L}{\lambda_p} 2\pi. \quad (1.3)$$

The refractive index  $\mu$  is given by

$$\mu = \frac{c}{v} = \frac{\lambda_0}{\lambda_p}, \quad (1.4)$$

where  $c$  is the velocity of light and  $v$  the phase velocity in the medium. When plasma is formed the detector will measure a phase change

$$\Delta\varphi = \varphi_0 - \varphi_p = 2\pi L \left( \frac{1}{\lambda_0} - \frac{1}{\lambda_p} \right) = \frac{2\pi L}{\lambda_0} (1 - \mu). \quad (1.5)$$

If the probing beam of the interferometer propagates through a magnetized cold plasma and the propagation is perpendicular to an externally applied magnetic field  $\mathbf{B}_T$ , with its  $\mathbf{E}$ -vector parallel to  $\mathbf{B}_T$  (ordinary wave propagation), and if collisional effects can be assumed to be negligibly small, the refractive index [e.g. Heal-65] can be simply formulated as

$$\mu = \sqrt{1 - \frac{f_p^2}{f^2}}, \quad (1.6)$$

where  $f$  is the frequency of the probing beam and  $f_p$  is the electron plasma frequency with

$$f_p = \sqrt{\frac{e^2 n_e(r)}{4\pi^2 \epsilon_0 m_e}} = 8.98 \sqrt{n_e(r)}, \quad (1.7)$$

where  $e$  is the electronic charge,  $n_e(r)$  is the local electron density, which may vary in space,  $\epsilon_0$  is the permittivity of the free space and  $m_e$  is the electron mass \*). From Eq. (1.6) it is clear that for a particular probing frequency there is a critical density,  $n_e(r) = n_c$ , above which the probing beam will not propagate through the plasma. From Eq. (1.7) the critical density,  $n_c$ , becomes

$$n_c = \frac{4\pi^2 \epsilon_0 m_e}{e^2} f^2 \approx \frac{f^2}{80.6}, \quad (1.8)$$

and Eq. (1.6) can then be rewritten as

$$\mu = \sqrt{1 - \frac{n_e(r)}{n_c}}. \quad (1.9)$$

---

\*) Rationalized MKS units are used throughout this thesis, unless mentioned otherwise.

Due to the presence of the plasma the phase difference,  $\Delta\phi$ , between the working path and the reference path of the interferometer will be

$$\Delta\phi = \frac{2\pi}{\lambda_0} \int_0^L [1 - \mu(n_e(r))] dL . \quad (1.10)$$

In most practical cases the frequency at which the interferometer is operated will be chosen far higher than the plasma frequency:  $n_e \ll n_c$ . It is clear that then Eq. 1.10 may be simplified and that the binomial expression of  $\mu$  to first order can be used

$$\mu \approx 1 - \frac{1}{2} \frac{n_e(r)}{n_c} , \quad (1.11)$$

which yields

$$\Delta\phi \approx \frac{0.845 \times 10^{-6}}{f} \int_0^L n_e(r) dL = \frac{0.845 \times 10^{-6}}{f} \langle n_e \rangle L \text{ rad} , \quad (1.12)$$

where  $\langle n_e \rangle$  is defined as the density averaged over the beam path through the plasma, 'line-density'. Equation (1.12) written in practical form gives

$$F = \frac{\Delta\phi}{2\pi} = \frac{1.345 \times 10^{-16}}{f} \int_0^L n_e(r) dL = \frac{1.345 \times 10^{-16}}{f} \langle n_e \rangle L \quad (f \text{ in GHz}) \quad (1.13)$$

where  $F$  is the number of complete fringes.

Obs. A more complicated situation occurs in magnetized hot plasma's where cyclotron resonance effects can not longer be neglected. This occurs when the applied frequency,  $f$ , equals the cyclotron resonance frequency,  $f_{ce}$ , at

$$f_{ce} = \frac{1}{2\pi} \frac{eB}{m_e} , \quad (1.14)$$

where  $B$  is the local magnetic field. Absorption of the waves depends on the electron temperature and on the spatial variation of the magnetic field. Since in the experimental cases the applied frequency,  $f$ , in interferometry is generally far higher than this cyclotron frequency,  $f_{ce}$ , we are not concerned with these complications. Cyclotron resonance effects will be treated in more detail in Ch. 4, Reflectometry, where it may play a more important role.

## 1.2 Refraction of electromagnetic waves

When an electromagnetic wave, with the **E**-field of the wave perpendicular to the density gradient in a cylindrical plasma, will undergo refraction effects according to Snellius' Law [Ginz-61]. It is clear that refraction must be kept small, otherwise the transmitted electromagnetic wave would miss the receiving antenna (port) (Fig. 1.2).

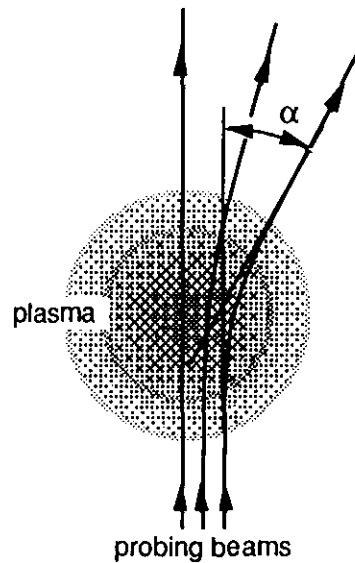


Fig. 1.2. Refraction effect of electromagnetic waves in plasma.

The angle of refraction  $\alpha$  varies with the position of the probing beam. The maximum value of  $\alpha$ , for a symmetric parabolic density profile is given by

$$\alpha_{\max} = \sin^{-1}(n_0/n_c) \approx n_0/n_c \quad (1.15)$$

where  $n_0$  is the central density [Shmo-61]. Equation (1.15) can be rewritten, with Eq. (1.8), as

$$\alpha_{\max} = 8.97 \times 10^{-16} n_0 \lambda_0^2. \quad (1.16)$$

From this it is clear that the wavelength should be chosen sufficiently small, i.e. the frequency sufficiently high, in particular for multi-channel interferometry where the entire cross-section is concerned. Note that this is the same requirement for the validity of the approximation of Eq. 1.11. An example of refraction effects for a single beam interferometer is given in Sec. 2.2 (p. 37).

### 1.3 Microwave components

Plasma densities in thermonuclear experiments range from  $\sim 5 \times 10^{18}$  to  $\sim 10^{21} \text{ m}^{-3}$ ; this corresponds with probing and cut-off frequencies of  $\sim 20 \text{ GHz}$  to  $\sim 300 \text{ GHz}$  (Eq. 1.8). A brief introduction of various components used in microwave interferometry in this frequency domain will be given here.

Sources in use in interferometer systems are:

- Backward Wave Oscillators (BWO's),
- Klystrons,
- Gunn-oscillators.

BWO's and klystrons in this frequency range were developed some decades ago, but can at present be replaced in most cases by solid-state sources, e.g. Gunn-oscillators. Gunn-oscillators, working at frequencies up to  $\sim 110 \text{ GHz}$ , can produce powers of  $250 \text{ mW}$  at the lower frequencies ( $20 \text{ GHz}$ ) to about  $15 \text{ mW}$  at the higher frequencies ( $110 \text{ GHz}$ ). Gunn-oscillators with frequency triplers can produce from over  $10 \text{ mW}$  at  $140 \text{ GHz}$  to about  $1 \text{ mW}$  at  $300 \text{ GHz}$ . The convenience of using Gunn-oscillators rather than BWO's and klystrons is evident: good frequency-stability, long life, small size, and simpler power supplies may be used.

Metal waveguides are used to guide microwave energy from one point to another. To avoid transmission of higher order modes, which travel at different phase velocities and would give spurious interference effects, the dimensions are chosen such that only the dominant  $\text{TE}_{10}$  mode can propagate (Fig. 1.3).

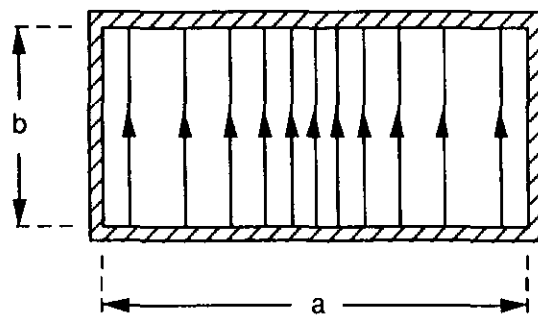


*Fig. 1.3. The electric field of the  $\text{TE}_{10}$  mode in a rectangular metal waveguide, where  $a$  and  $b$  are the inner dimensions of the waveguide.*

The wavelength in the guide,  $\lambda_g$ , is given by

$$\lambda_g = \frac{\lambda}{\sqrt{1 - \left(\frac{\lambda}{\lambda_c}\right)^2}}, \quad (1.17)$$

where  $\lambda$  is the free space wavelength and  $\lambda_c$  the cut-off wavelength of the guide. In rectangular metal waveguides the cut-off wavelength for propagation of the TE<sub>10</sub> mode is:

$$\lambda_c = 2a, \quad (1.18)$$

where  $a$  is the inner dimension of the longer side of the waveguide. The attenuation in a rectangular copper air-filled waveguide operating in the TE<sub>10</sub> mode is given by

$$\alpha = \frac{1.47 \times 10^{-4}}{a^{1.5}} \times \frac{\frac{a}{2b} \left(\frac{f}{f_c}\right)^{1.5} + \left(\frac{f}{f_c}\right)^{-0.5}}{\sqrt{\left(\frac{f}{f_c}\right)^2 - 1}} \text{ dB m}^{-1}, \quad [\text{More-48}] \quad (1.19)$$

where  $f$  is the operating frequency and  $f_c$  is the cut-off frequency ( $f_c = c/\lambda_c$ ). The inner dimensions of the guide,  $a$  and  $b$ , are in meters. A table with parameters of single-mode waveguides used in interferometry is given below (Table 1.1).

*Table 1.1. Waveguide parameters.*

Band	Frequency (in GHz)	Inner dimensions (mm)	Losses in (dB/m)	Waveguide Number		Flange number
				Europe	USA	
S	2.6 - 3.95	72.14 x 34.04	0.019	WG-10	WR-284	
X	8.2 - 12.5	22.860 x 10.160	0.11	WG-16	WR-90	UG-39/U
Ku	11.9 - 18.0	15.799 x 7.899	0.176	WG-18	WR-62	UG-419/U
K	18 - 26.5	10.668 x 4.318	0.37	WG-20	WR-42	UG-595/U
Ka	26.5 - 40	7.112 x 3.556	0.58	WG-22	WR-28	UG-599/U
U	40 - 60	4.775 x 2.388	1.06	WG-24	WR-19	UG-383/U
V	50 - 75	3.759 x 1.880	1.52	WG-25	WR-15	UG-385/U
E	60 - 90	3.099 x 1.549	2.03	WG-26	WR-12	UG-387/U
W	75 - 110	2.540 x 1.270	2.74	WG-27	WR-10	UG-387/U
F	90 - 140	2.032 x 1.016	3.82	WG-28	WR-8	UG-387/U
D	110 - 170	1.651 x 0.826	5.21	WG-29	WR-6	UG-387/U
G	140 - 220	1.295 x 0.648	7.50	WG-30	WR-5	UG-387/U
R	220 - 330	0.864 x 0.432	13.76	WG-32	WR-3	UG-357/U

Since the losses in long waveguide runs become high for the fundamental waveguide, oversized waveguides have to be used, especially at the higher frequencies. To avoid mode conversion a

gradual transition (taper) [Okre-68] from the fundamental to the oversized waveguide is necessary. A loss of  $\sim 5$  dB/m in fundamental waveguide, D-band, (at a frequency of 140 GHz) may be reduced to  $\sim 0.3$  dB/m when an X-band waveguide is used. Special care must be taken to avoid mode-conversion (other modes can travel at a different phase velocity) when bends are made in oversized waveguides. The simplest way is to use mitre-bends (Sec. 2.4, p. 49). An other way is to use tapers from oversized to single-mode waveguide and to make the bend in the single-mode waveguide (Sec. 5.2, p. 93).

Beside waveguides (straight sections and bends) other frequently used passive microwave components are:

- horn antennae,
- directional couplers,
- phase shifters,
- variable shorts,
- detectors.
- ferrite isolators,
- variable attenuators,
- terminations (microwave dump),
- sliding screw tuners,

Horn antennae, transmitting Gaussian beams, are available with different gains over an omnidirectional antenna. Isolators, based on the Faraday effect, work as a microwave diode and are used to block unwanted reflected power. Directional couplers can be used to split off power. They are available with different coupling factors to handle the microwave power in an economical way. Attenuators are to be avoided if possible since they only consume power but they have to be used e.g. to set the local oscillator power of mixers or in test set ups. Phase shifters are not needed in modern interferometers: the phase off-sets at the start of measurements can be corrected in the computer program. Terminations (dumps) are used to absorb the microwave signal. The variable short consists of a piece of waveguide containing a movable plunger to give 100% reflection. The sliding screw tuner can be used to tune out an unwanted signal (reflection).

Signal detection can be carried out in two ways:

- crystal diode detection,
- heterodyne detection using balanced mixers.

Schottky diodes are mostly used as detectors because of their excellent RF characteristics. The sensitivity is in the order of 1 mV/ $\mu$ W at 40 GHz to about 0.2 mV/ $\mu$ W at 150 GHz. High sensitivity can be obtained with heterodyne detection: the RF signal to be detected is mixed with a signal from a local oscillator (LO) operating at an only slightly different frequency. Mixing then produces an output proportional to the input signal at the difference frequency (IF). A conversion loss in the order of 5 dB at 40 GHz to about 10 dB at 150 GHz is acceptable, where conversion loss,  $L$ , is defined as

$$L = 10 \times 10 \log \frac{P_{\text{RF in}}}{P_{\text{IF out}}} \text{ dB} . \quad (1.20)$$

### 1.4 Phase modulation techniques

Simple interferometers (Fig. 1.1) have unavoidable drawbacks as far as accurate measurement of the phase-shift is concerned. The low-frequency interference signal from the detector is proportional to  $\cos\phi(t)$ , so it is impossible to determine whether phase is increasing or decreasing \*). Furthermore, the signal is dependent on the product of the amplitudes of the reference beam and the plasma beam; thus, variations in these quantities can be interpreted wrongly as a time varying phase-shift. These difficulties can be avoided by using polar interferometers or by using phase-modulation techniques.

A polar interferometer uses double reference arms with  $\frac{\pi}{2}$  phase difference and one common work path to produce, with the aid of two mixers, signals with  $\cos\phi(t)$  and  $\sin\phi(t)$  dependences. There is always a difficulty to stabilize the  $\frac{\pi}{2}$  phase difference between the two reference arms and, secondly, the sensitivities of the two mixers has to be matched. These two requirements are hard to meet. Furthermore, this system requires a large number of microwave components. Another polar interferometer, not suffering from the above mentioned weaknesses, with only one reference arm where the  $\frac{\pi}{2}$  phase difference is obtained by using phase-switch technique is described in appendix A (p. 75) [Huge-70a].

There are a number of ways to construct interferometers using phase modulation techniques. In the early days of microwave interferometry on plasmas the Wharton 'Zebra-stripe' interferometer [Heal-65] was frequently used. The modern version of the Wharton interferometer is the JET 2-mm interferometer (Ch. 2) [Huge-81, Fess-87]. The principle is given in Fig. 1.4. The interferometer provides a continuous fringe train on the output of the detector in the absence of plasma. This is achieved by using a Mach-Zehnder configuration with unequal lengths of the plasma and the reference paths, in combination with sweeping of the source frequency.

---

\*) The two waves are represented by

$$S = a \sin(\omega t - \phi(t)),$$

$$R = b \sin\omega t,$$

where S represents the signal transmitted through the plasma and R the reference signal. The result of mixing of the two waves on the square-law detector is

$$(a \sin(\omega t - \phi(t)) + b \sin\omega t)^2.$$

The detector will only produce the component of the intermediate frequency

$$ab \cos \phi(t)$$

as the detector does not respond to any of the high frequencies.

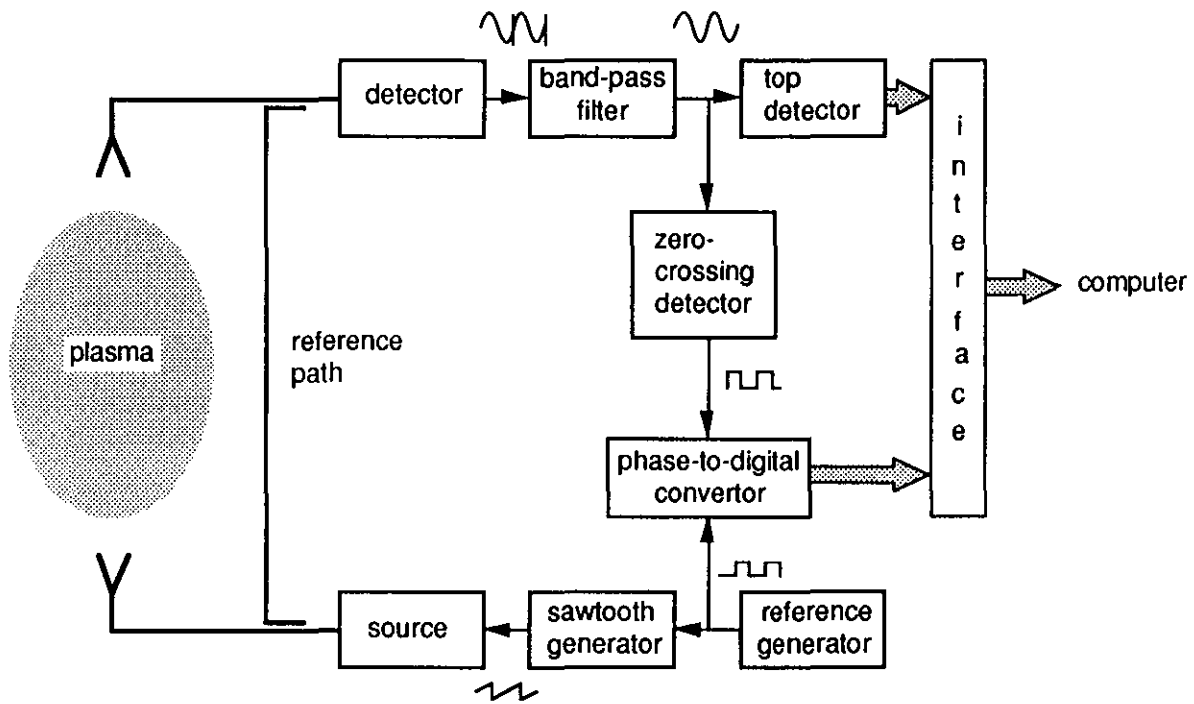


Fig. 1.4. Swept frequency interferometer with unequal reference and signal path.

The amplitude of the electric field of the waves arriving at the detector via the two paths can be expressed as

$$E_p = \hat{E}_p \cos\{2\pi ft + \Delta\phi(t)\} \quad \text{plasma path,} \quad (1.21)$$

and

$$E_r = \hat{E}_r \cos\left\{2\pi t\left(f + \frac{df}{dt} \Delta t\right)\right\} \quad \text{reference path,} \quad (1.22)$$

where  $E_p$  and  $E_r$  represent the amplitudes of the beams and  $\frac{df}{dt} \Delta t$  represents the frequency shift of the reference arm due to the combination of the frequency sweep rate of the source,  $\frac{df}{dt}$ , and the transit time delay between the two paths,  $\Delta t$ . The frequency sweep is linear with time.  $\Delta t$  is simply the time delay, i.e. the difference in the plasma and reference path lengths,  $\Delta L$ , divided by the wave velocity which is close to the velocity of light (thus  $\lambda_g \approx \lambda_0$ ). The result of mixing the two waves on the square-law detector is a time-varying output signal

$$I_s = \hat{E}_p \hat{E}_r \cos\left(2\pi t \frac{df}{dt} \Delta t - \Delta\phi(t)\right). \quad (1.23)$$

This signal is subsequently compared to the signal of an intermediate frequency reference generator to yield the phase-shift caused by the presence of the plasma. The reference generator

(Fig. 1.5a) is the clock of the interferometer electronics. By carefully setting the amplitude (Fig. 1.5b) of the sawtooth modulation of the microwave source, the maximum value of its frequency excursion,  $\Delta f$ , is arranged to give, in the absence of plasma, a phase difference between the two interferometer arms varying from 0 to exactly  $2\pi$  during the sawtooth ramp time, i.e. one 'fringe' (Fig. 1.5c); this is equivalent to  $\Delta f \approx c/\Delta L$ . In this way a sine wave output is produced, in the absence of plasma (i.e.  $\Delta\phi=0$ ), with a frequency of  $f_i = \frac{df}{dt} \Delta t$ .

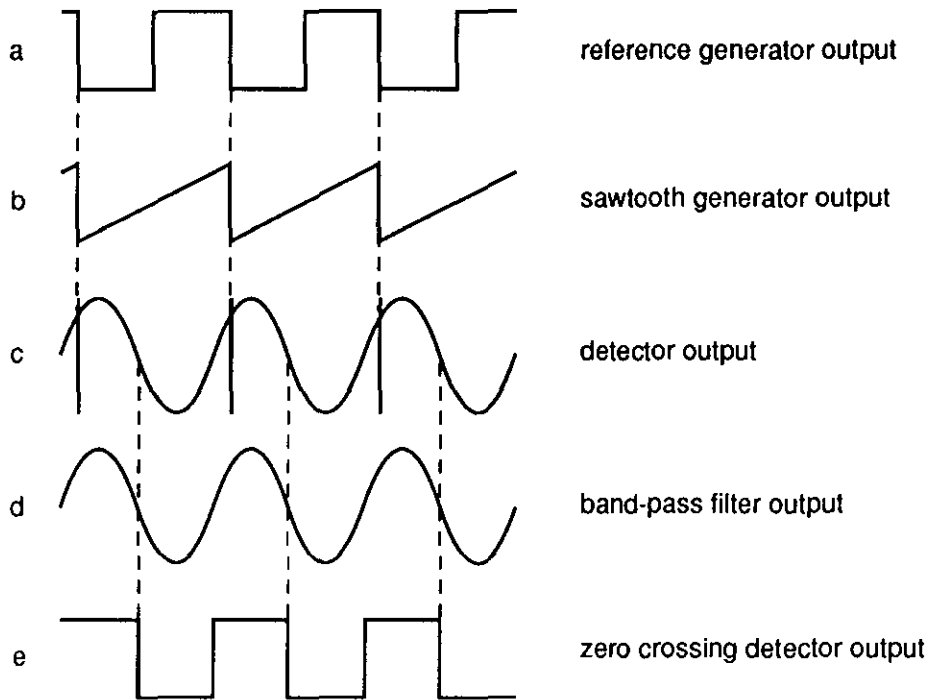


Fig. 1.5. Frequency swept interferometer waveforms.

The effect of the flyback of the sawtooth waveform is suppressed by passing the signal through a band-pass filter centred at  $f_i$  (Fig. 1.5d). The amplitude variations are taken out with the zero crossing detector and in this way a square wave train of frequency  $f_i$  is produced (Fig. 1.5e)\*. To be able to follow reliably the rapid phase changes induced by the plasma, the condition  $f_i \gg \Delta\phi/2\pi$  should be met. The signal from the detector is now compared in a counting network, the phase-to-digital convertor (Sec. 2.4, p. 51). The accumulated phase difference,  $\Delta\phi(t)$  at any moment in time, gives the evolution of the plasma electron density.

\*) Obs. Determination of the phase difference from the analog output is possible but would lead to an accuracy of a few percent. Digital processing can improve the accuracy appreciably. To be able to use digital data-handling systems it is necessary to take all amplitude variations out by converting the analog signal into square wave trains.

Another way of getting an unambiguous phase output is to use two oscillators, a source and a local oscillator at slightly different frequencies (Fig. 1.6). The incoming signal, a  $\sin\{\omega_1 t - \phi(t)\}$ , is mixed with the local oscillator signal,  $b \sin\omega_2 t$ , (heterodyne detection) to yield an intermediate frequency signal,  $ab \cos\{(\omega_1 - \omega_2)t + \phi(t)\}$ , with the advantage that the phase change data is not folded around DC but the shift-up or shift-down information is kept with the sign of the phase-shift. Another advantage of heterodyne detection is the high sensitivity. Moreover, as the local oscillator power is much larger than the signal power,  $P_o \gg P_s$ , the mixer output is only proportional to the incoming signal. In the microwave bands the frequency off-set can simply be generated by using an up-converter \*) or by using two sources oscillating at slightly different frequencies held together with a frequency discriminator (Appendix C) or with the more recently developed phase-lock loop (PLL) circuit (Sec. 5.3). The drawback of the up-converter is the high conversion loss and the poor carrier and unwanted sideband suppression ( $\sim 20$  dB). With the PLL system a clean frequency off-set signal can be obtained with an out-of-band suppression of over 60 dB (Sec. 5.3, p. 102).

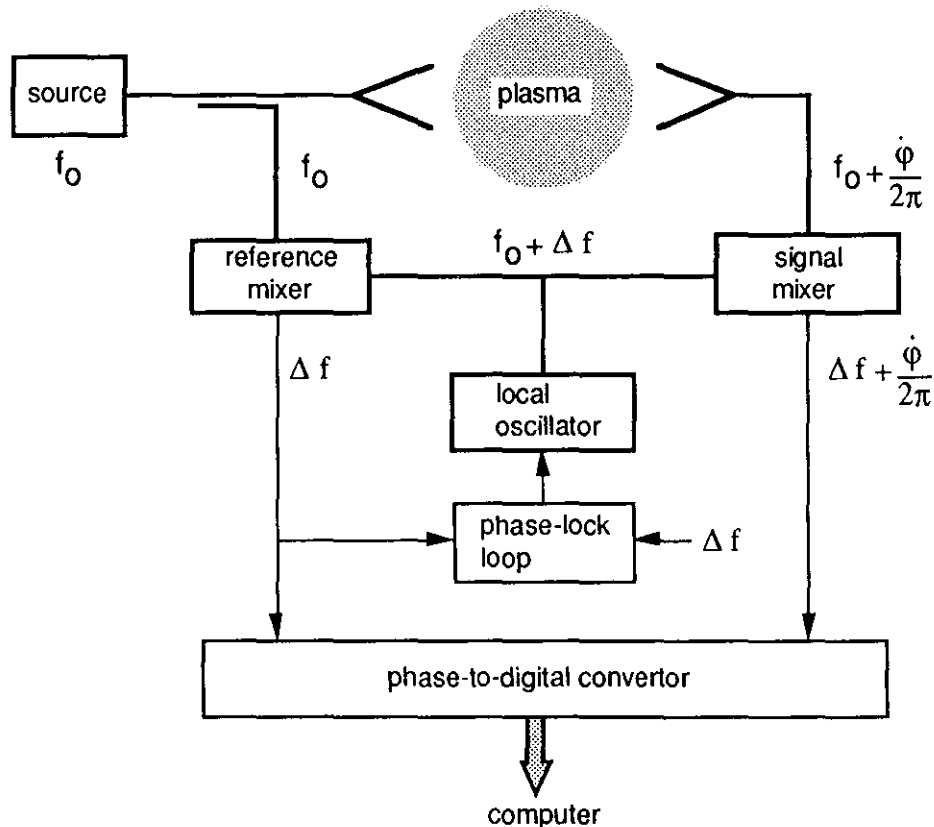


Fig. 1.6. Interferometer using heterodyne detection.

\*) an up-converter is a generator where a low frequency signal,  $f_m$ , is mixed with a RF frequency,  $f_o$ , to produce only one sideband with a frequency  $f_o + f_m$  (or  $f_o - f_m$ ).

## 1.5 Phase detectors

### Phase detectors with operational ranges of a single fringe

The simplest digital phase detector (PD) is the so-called exclusive-OR gate (Fig. 1.7). The two signals (reference and signal) of the interferometer are converted to square wave trains with a duty-cycle of 50%, for instance with a zero-crossing detector (comparator circuit), before they are fed to the exclusive-OR gate.

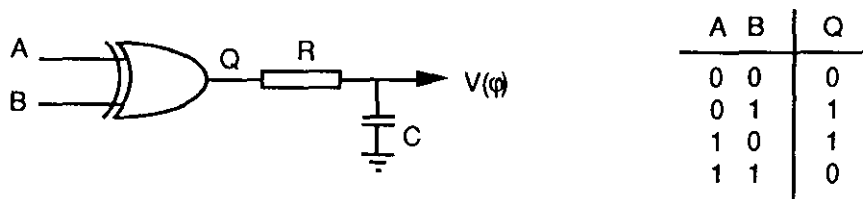


Fig. 1.7. Exclusive-OR gate phase detector and its truth table.

The output of the gate can be found from the truth table: the output is only high (binary 1) when the inputs are different (Fig. 1.8).

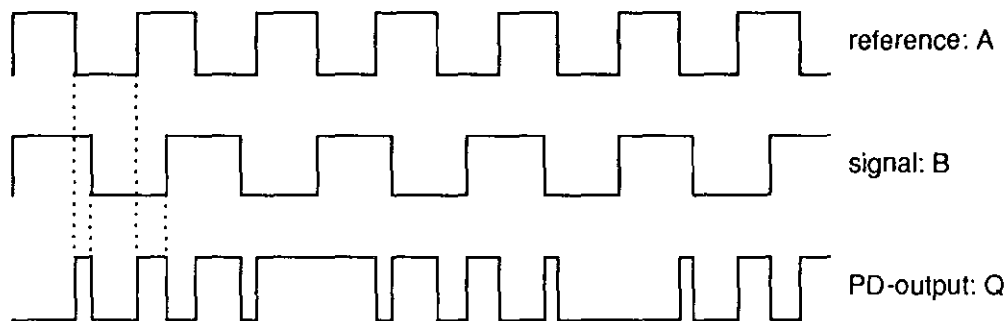


Fig. 1.8. Exclusive-OR gate phase detector waveforms.

The phase differences in Fig. 1.8 are exaggerated to show the principle. In actual interferometry smaller relative phase differences occur. The PD-output from the exclusive-OR gate is a square wave train with varying duty-cycle. The PD output has to be filtered with a low-pass filter with a cut-off frequency lower than the modulation frequency and still high with respect to the phase variations. After filtering the output  $V(\phi)$  (Fig. 1.7) corresponds to the phase difference, as can be read from the characteristic of the PD: Fig. 1.9.

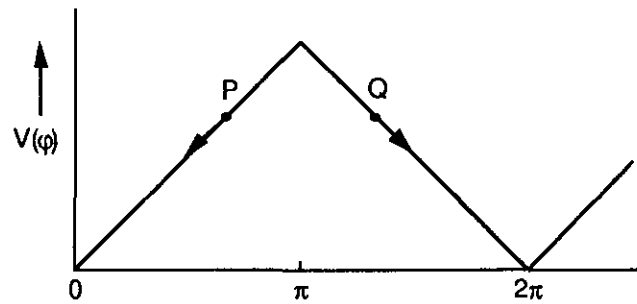


Fig. 1.9. Characteristic of the exclusive-OR gate phase detector.

This system does not yield unambiguously the sense of phase variations as may be seen from Fig. 1.9: if a decrease in  $V(\varphi)$  is observed it could be caused by a phase decrease at point P as well as by a phase increase at point Q. The PD based on an exclusive-OR gate is for this reason not attractive for phase measurements in interferometers \*). The other disadvantage is the need for an exact 50% duty-cycle for the input square wave signals.

Another group of PD's are sequential phase detectors operating on the edges (falling or rising) of the two square wave trains. The simplest form is the set-reset flip-flop [Horo-83]. Falling voltage edges on one input to set the flip-flop to a true state (binary 1) and falling voltage edges on the other input to reset the flip-flop to the false state (binary 0). An example is given in Fig. 1.10.

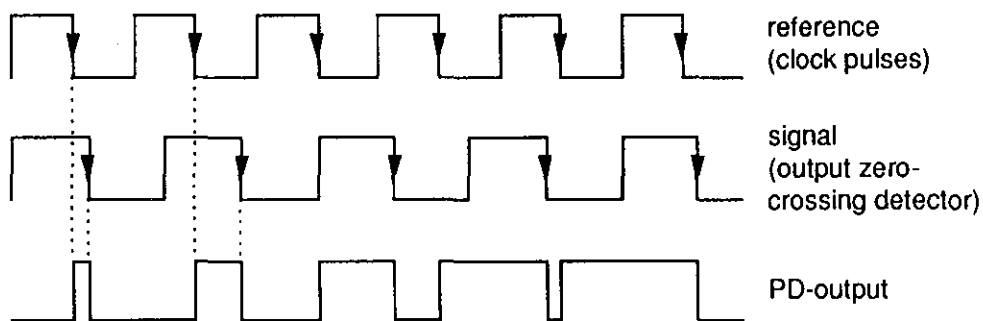


Fig. 1.10. Set-reset phase detector waveforms.

\*) A similar system operating in an analog way, using double-balanced mixers was used earlier: its drawback was the same ambiguity in the sense of  $\cos \varphi$ . A quadrature phase comparator producing two phase output signals with  $\frac{\pi}{2}$  phase difference can give unambiguous phase results [Gowe-82]; however, two data acquisition channels are necessary in this set up.

The output is again filtered; to yield a voltage  $V(\varphi)$  which corresponds to the phase difference: cf. the characteristic of Fig. 1.11.

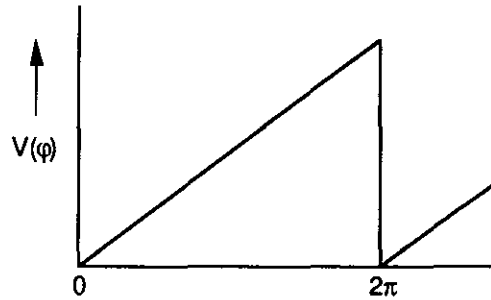


Fig. 1.11. Characteristic of the set-reset phase detector.

It is clear that the output  $V(\varphi)$  of the set-reset PD, which varies monotonously with  $\Delta\varphi$  between 0 and  $2\pi$ , is suitable for interferometric measurements because the response is now unambiguous. An other advantage of the set-reset PD, operating on the (positive or negative) edges only, is the insensibility of the input signals for the duty-cycle. But the output voltage of the PD may become noisy and unreliable when the phase difference is jittering around the  $2\pi$  (or  $N \times 2\pi$ ) phase point. A system that can tackle this problem is described below.

A PD that does not suffer from the above mentioned jittering is the phase-frequency PD [Gard-79] which has recently been built for the JET multi-channel reflectometer (Ch. 5) [Huge-86], (Fig. 1.12). At the rising edge of the clock pulse the information on the D input is transferred to the Q output (the D inputs are kept on logic '1').

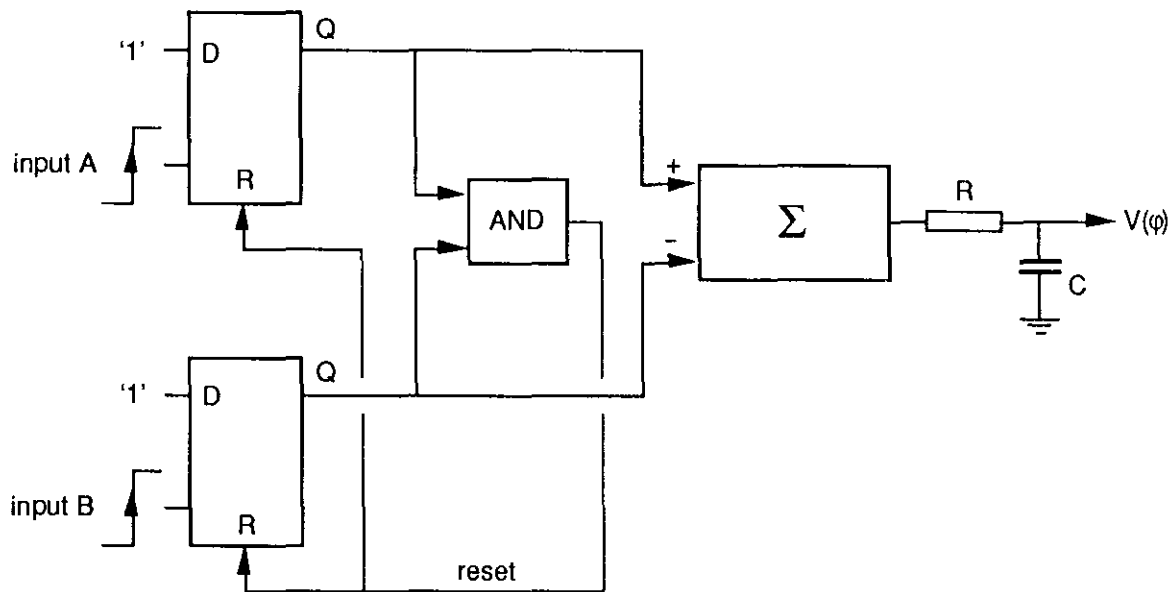


Fig. 1.12. Phase-frequency phase detector.

The outputs (Q's) of the two D-flip-flops are subtracted and then again filtered. The PD output  $V(\varphi)$  corresponds to the phase difference according to the characteristic of Fig. 1.13.

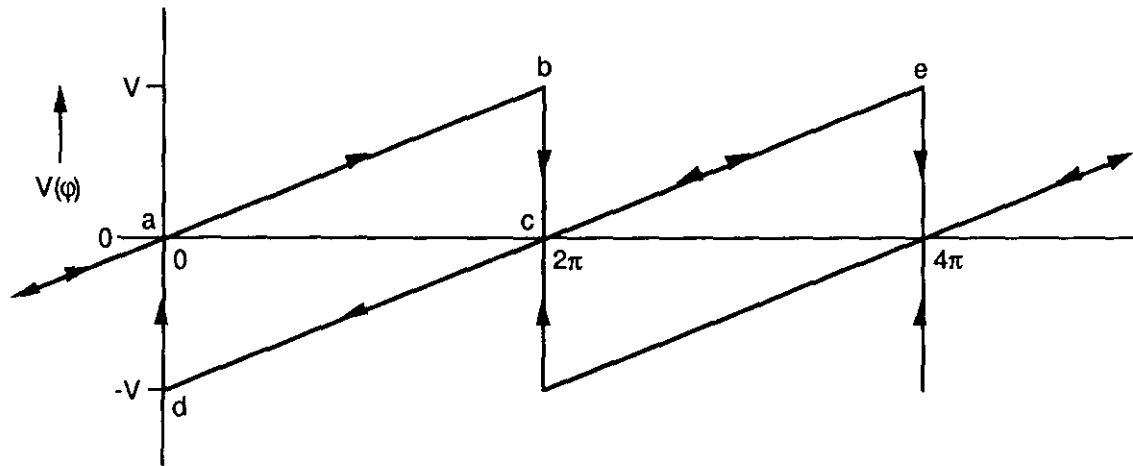


Fig. 1.13. Characteristic of the phase-frequency phase detector.

If the phase change is positive and varies e.g. from a to b and when the phase change reaches the  $2\pi$  point, the output voltage  $V(\varphi)$  of the PD will drop from  $V$  to 0. If the phase change is still positive the output will proceed along the line c to e, when the phase starts to decrease the output follows the line e to d. So, there is no jitter in the output voltage when the phase passes  $(N \times) 2\pi$ .

A totally different approach can be followed by measuring the time delay between the rising (or falling) edges of the two signals by means of counter pulses (Fig. 1.14). The counter starts at the rising edge of the reference square wave and stops at the rising edge of the signal square wave. The time delay measurement can be translated into a phase measurement when the reference frequency is measured as well, or when the reference and the counter frequency are in a fixed relation to each other. The counter frequency has to be high with respect to the reference frequency in order to obtain an accurate measurement of the phase difference; the ratio of the counter to the reference frequency determines the accuracy. For instance; if the counter frequency is 100 MHz and the reference frequency 1 MHz, each pulse from the counter will represent a  $3.6^\circ$  phase difference between the two signals. The drawback here is that the error accumulates over the course of the measurement (plasma shot).

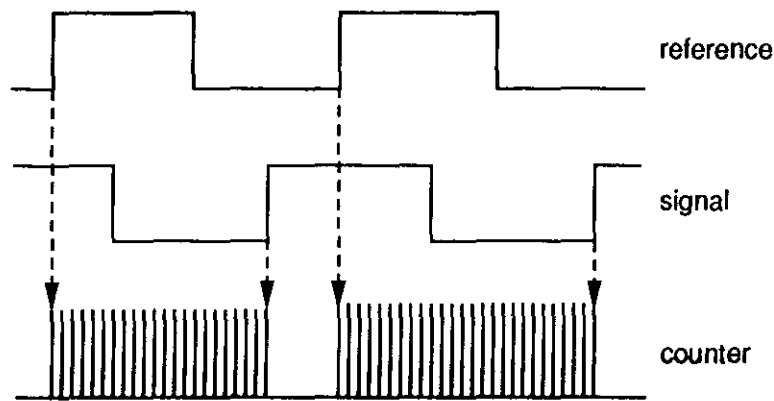


Fig. 1.14. Time delay measurement waveforms.

### Phase detectors working over many fringes (fringe counters)

The previously described PD's can work over many fringes  $F$  when the frequencies of the input signals are divided by  $N$ , where  $N \approx F$ . The range of the PD's then becomes  $N \times 2\pi$ . The drawback is that the low-pass filter cut-off frequency must scale down with increased  $N$ . This will lead to a rather low response time. A fringe counter that does not suffer from this degradation is described here [Medd-74].

A phase detector, based on the set-reset flip-flop gate, which can work over many fringes, is given in Fig. 1.15. One counter is counting forwards, the other counter backwards and the outputs are added digitally. This output is then fed into a digital-to-analog convertor (DA-convertor) and filtered with a low-pass filter to get an analog output proportional to the phase-shift.

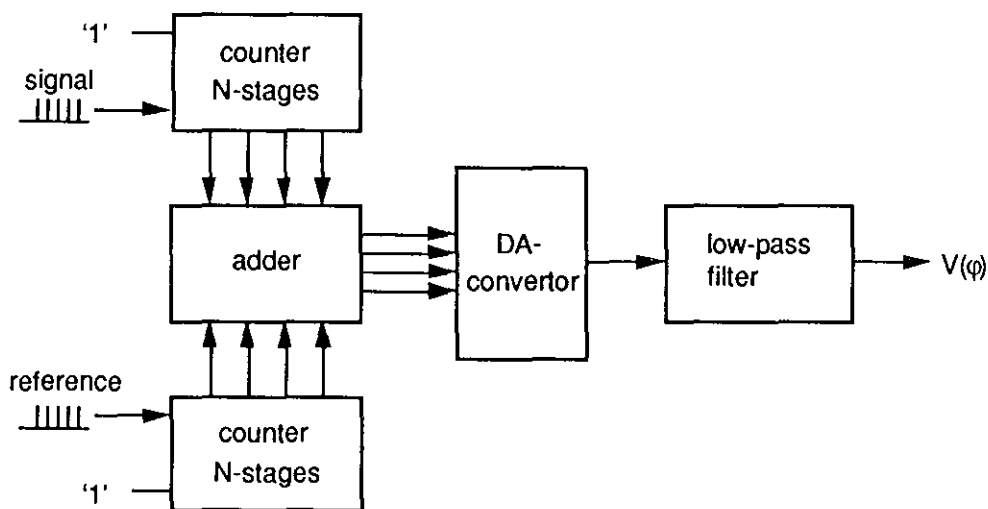


Fig. 1.15. Fringe counter using up-down counters.

The waveforms of this PD are given in Fig. 1.16. The merit of this fringe counter is that the filter cut-off frequency of the low-pass filter does not scale down with the number  $N$ .

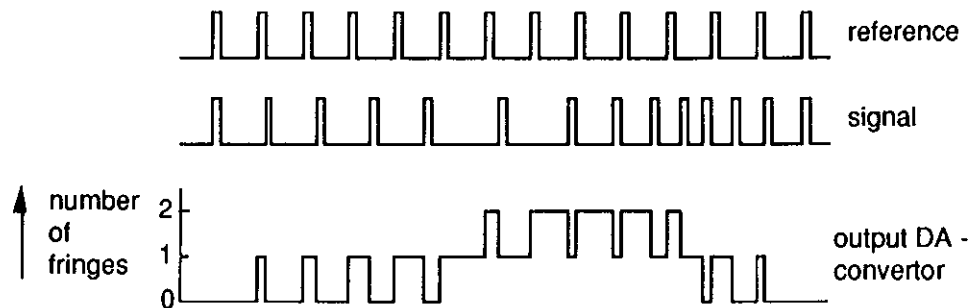


Fig. 1.16. Fringe counter input- and output waveforms.

The filtered output voltage  $V(\phi)$  against the phase difference is given in Fig. 1.17.

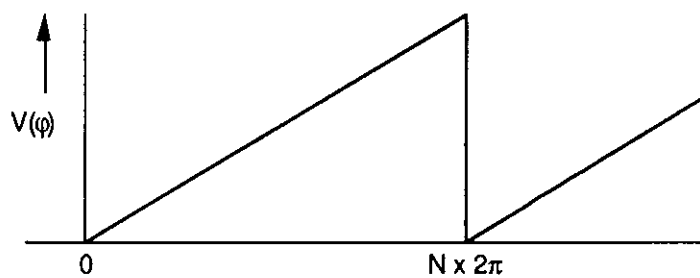


Fig. 1.17. Characteristic of the fringe counter.

Phase detectors of this type are used in the  $\text{CO}_2$ -laser interferometer described in Ch. 3. For highly accurate phase difference measurements, this type of PD still poses problems as the accuracy scales down with  $N$ .

A digital fringe counter with high accuracy is shown in Fig. 1.18 [Putt-84]. The clock frequency is fed to a counter and furthermore divided by  $K$ , the output of which is used to drive the reference generator of the interferometer (Fig. 1.4, p. 23). The signal output of the interferometer will, on each rising edge, cause the subtraction of the number  $K$  in the counter. Thus, the number in the counter returns to the previous value at each rising edge of the signal when the phase does not change. An example for  $K=100$  is given in Fig. 1.19. At the arrival of the sample pulse, the accumulated number of the counter is written in the memory (in the example of Fig. 1.19, 40). The sample pulse is held up till the end of a signal period, leading to a statistical error of a few degrees. Results from this type of fringe counter can be found in Sec. 2.4 (p. 53-56). There is of course an electronic upper limit of the clock frequency and a lower limit of the reference frequency (1 MHz is chosen for the JET 2-mm interferometer; cf. Ch. 2) to ensure a proper performance of the interferometer.

**Advantages** of the digital fringe counter described here above the other phase detectors are:

- a high accuracy, independent of the number of fringes (no accumulation of errors),
- rapid response: the phase can be measured in each period of the signal,
- no delay due to filtering on the output signal,
- totally digital system and therefore easy integrated into data-handling systems,
- no calibration required.

**Disadvantage** is:

- the reference signal frequency has to be chosen as an rational fraction ( $1/K$ ) of the clock frequency.

An other approach to phase measurements is chosen for the multi-channel FIR-laser (far-infra-red laser) interferometer and the multi-channel reflectometer being developed for the RTP-experiment \*). When a high sample pulse rate is used and the phase change per sample is less than  $\pi$ , a totally different approach may be followed. The fringe counter can then be composed with a fractional phase detector, e.g. the phase-frequency PD, and a high resolution analog-to-digital convertor (ADC). Absolute phase accuracy in the order of  $0.2^\circ$  is possible. A software check must be made to see if the integrated phase passes  $2\pi$ . If so, one fringe must be added to (subtracted from) the integral value. An accurate system will be possible with the fast data acquisition system being developed at the FOM Instituut voor Plasmafysica Rijnhuizen.

---

\*) RTP is an acronym for: Rijnhuizen Tokamak Project at the FOM Instituut voor Plasmafysica Rijnhuizen, Nieuwegein, the Netherlands.

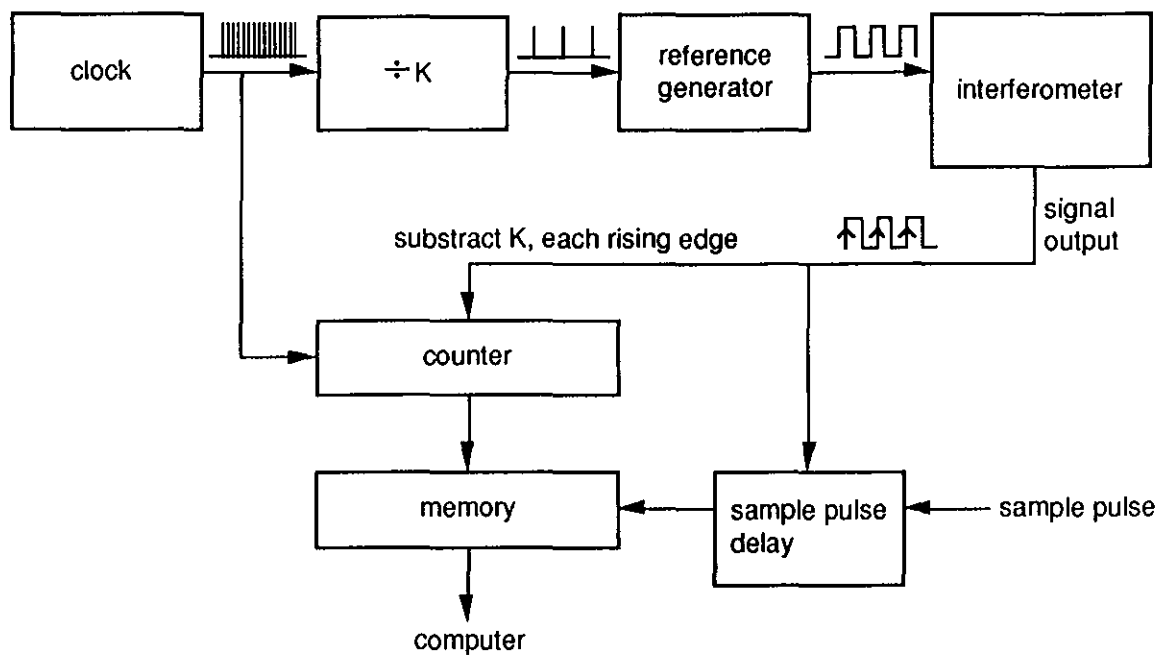


Fig. 1.18. Digital fringe counter.

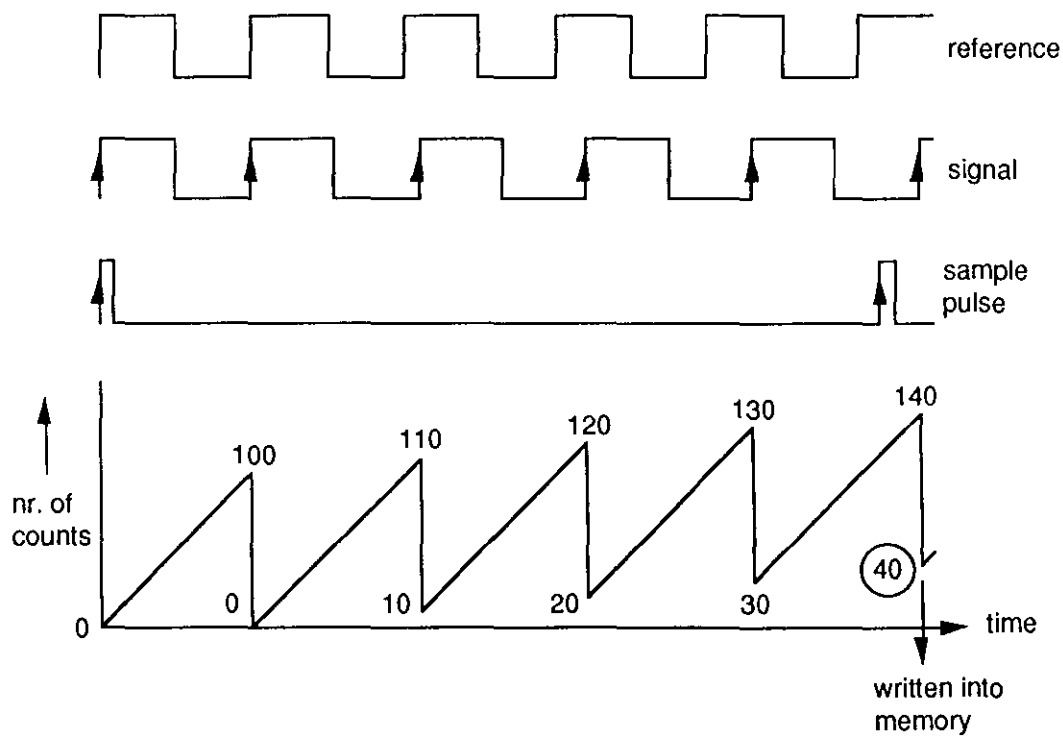


Fig. 1.19. Digital fringe counter waveforms.



## Chapter 2

### MULTI-RADIAN 2-MM INTERFEROMETER FOR JET

#### 2.1 Introduction

The Joint European Torus, JET, was built as a European collaboration under the auspices of Euratom, with the aim of testing the feasibility of producing plasmas with properties close to those under which controlled thermonuclear reactions may occur [Rebu-84, Bick-87]. The experimental parameters presently achieved in JET are listed below:

Plasma major radius	3.0	m
Plasma minor radius (horizontal)	1.25	m
Plasma minor radius (vertical)	2.1	m
Toroidal field	3.4	T
Plasma current,		
limiter bounded	7.0	MA
single null X-point	4.0	MA
Neutral beam injection power	20	MW
ICRH heating power	20	MW

JET is the largest magnetic plasma-confinement experiment in the world both in physical size and in the magnitude of the plasma current ( $7 \times 10^6$  A). Ion and electron temperatures  $T_e$  and  $T_i \geq 10$  keV have been obtained (by the end of 1989) in a pure deuterium plasma with a corresponding fusion product,  $n_e \tau T_i$  of about  $7 \times 10^{20} \text{ m}^{-3} \text{ s keV}$  (where  $\tau$  is the energy confinement time). This would give, if a deuterium-tritium mixture had been used, a ratio of thermonuclear power output to the heating power input,  $Q$ , of 0.7. It is expected that with further technical improvements of JET the proof of feasibility ( $Q=1$ ) can be given.

A single chord 2-mm interferometer to measure the electron density along a vertical line through the centre of the plasma has been proposed and built in 1981 by the author \*) [Huge-81, Huge-82a]. The applicability of the proposed interferometer ranges approximately from  $3 \times 10^{16}$  electrons per  $\text{m}^3$ , as determined by the minimum detectable phase-shift of 0.1 fringe, to  $7 \times 10^{19}$  electrons per  $\text{m}^3$ , i.e. the refraction limit (Sec. 1.2, p. 18). Calculations of the expected losses and the sensitivity of the interferometer are given in Sec. 2.2; the antennae and windows fitting in the vacuum vessel are treated in Sec. 2.3.

---

\*) This work was performed under the JET contract JB2/9003 (1980) between the JET Joint Undertaking and the FOM-Instituut voor Plasmafysica Rijnhuizen, Nieuwegein, the Netherlands.

## 2.2 Proposal for the 2-mm interferometer

### Description of the circuit

The principle of the interferometer is given in Fig. 1.4 (p. 23). Again, the reference path and the plasma path are chosen unequal in length to make use of the frequency dependency as described earlier. The ramp voltage (frequency 1 MHz) is adjusted in such a way (Fig. 1.5, trace b, p. 24) that in the absence of plasma a sine-wave signal with a frequency of 1 MHz will appear at the detector (Fig. 1.5, trace c). A selective amplifier rejects the fly-back fringe. When the plasma is formed, the detected signal will shift in phase. The detector and the 1 MHz reference signal are compared in the phase-to-digital convertor resulting in a phase-shift as a function of time [Putt-84]. To be able to follow the expected initial density rise of  $10^{22} \text{ m}^{-3} \text{ s}^{-1}$ , yielding a maximum fringe frequency of 20 kHz, and to cope with the expected density fluctuations in the order of  $10^{21} \text{ m}^{-3} \text{ s}^{-1}$  a bandwidth of 200 kHz was chosen.

### Calculation of the expected losses and sensitivity of the interferometer

#### Propagation loss in free space

When a power,  $P_t$ , is transmitted towards the plasma chamber the power at the receiving antenna,  $P_r$ , is given by

$$\frac{P_r}{P_t} = G_t \cdot G_r \frac{\lambda^2}{(4\pi R)^2} \quad [\text{Sout-61}], \quad (2.1)$$

where  $G_t$  and  $G_r$  are the gains of the transmitting and the receiving antennae, respectively, and  $R$  is the distance between the antennae. The angle at which the radiation intensity drops to 3 dB is related to the gain as:

$$\Theta_{3\text{dB}} = \sqrt{3 \times 10^4 / G} \text{ degrees} \quad [\text{Heal-65}]. \quad (2.2)$$

For horn antennae with an aperture of  $33 \times 33 \text{ mm}^2$  (beam-width  $5^\circ$ ) the propagation loss over 4 m becomes 26 dB.

The refraction calculations done by Koechlin [Koeec-80] indicate that it is preferable to use an antenna with a not too narrow beam-angle (Fig. 2.1), as can be understood from the following.

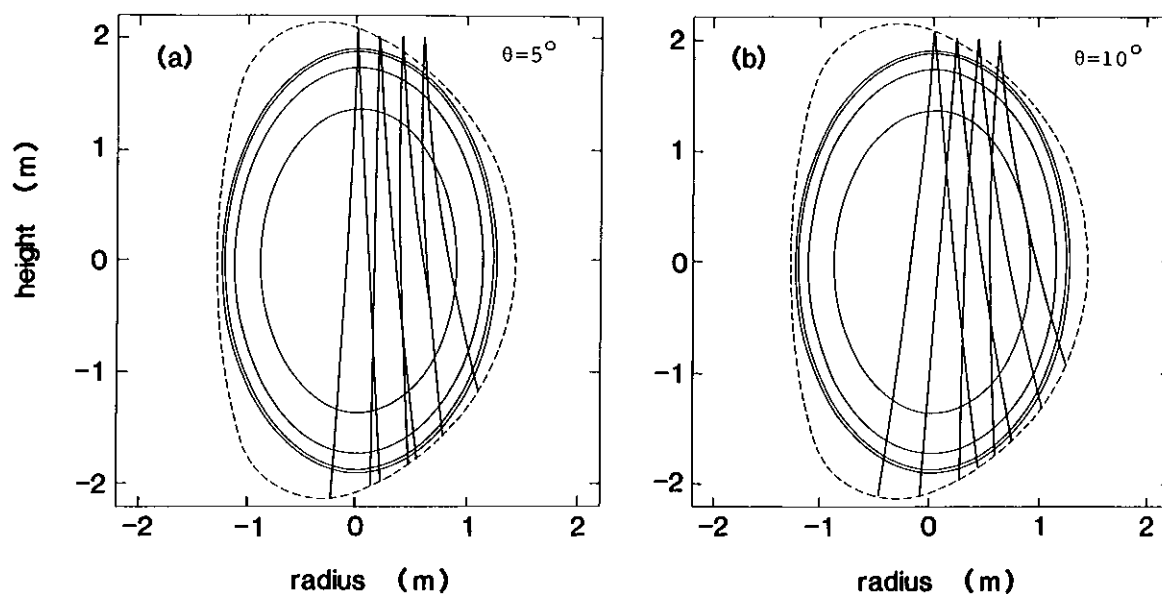


*Fig. 2.1. Refraction of 2-mm waves in the JET plasma.  
Contour lines of equal density are indicated.*

The rays starting from a height above the mid-plane of  $Y = 2$  m with beam-widths of  $5^\circ$  (Fig. 2.1a) and  $10^\circ$  (Fig. 2.1b) at radial locations  $X = 0, +0.2, +0.4, +0.6$  m are shown; these figures illustrate the refraction when the plasma is off-centre with respect to the rays. The calculations are done with a rather flat density profile with a maximum density of  $5 \times 10^{19} \text{ m}^{-3}$ . The choice of an antenna with  $5^\circ$  beam-width is a compromise between the refraction losses shown and propagation losses calculated from Eqs 2.1 and 2.2. The antenna is located at  $X = 0.06$  m. A wider beam, of  $10^\circ$ , would certainly give a reduced chance losing the beam by refraction in the highest density regimes, but it also implies additional propagation losses of 12 dB. Some work had to be done to find out whether oversized horn antennae, without mode-filter, could be used instead of tapers and conventional 2-mm horns. The high-vacuum quality requirements of the JET experiment forced us to have all components inside the discharge chamber executed in plain or copper plated inconel. The advantages of making the antenna system matched to oversized waveguide will be explained in Sec. 2.3.

**Estimate of the total loss in the interferometer**

The losses in the various microwave components calculated and/or estimated (in dB) are given in Table 2.1.

*Table 2.1. Estimated losses in the various components of the interferometer (in dB).*

directional coupler	2 x 1.5	3.0
isolators	2 x 1.3	2.6
50 m S-band waveguide (copper)	50 x 0.15	7.5
3 m X-band waveguide (inconel)	3 x 2	6.0
bends in S-band	14 x 0.2	2.8
tapers 2 mm to S-band	2 x 1	2.0
quartz windows	2 x 1.0	2.0
propagation loss between the antennae in the vacuum vessel		26.0
	total loss	51.9 dB

The power output of the Varian 2-mm klystron is 100 mW (20 dBm) \*). With a total loss of 51.9 dB the received power at the detector will be  $P_r = -31.9 \text{ dBm} = 0.65 \times 10^{-6} \text{ W}$ . This power is far above the detection limit as will be shown later.

\*) Power given in dBm are related to milliwatts (20 dBm is 20 dB above 1 mW).

**Estimate of the minimum detectable signal**

The noise figure of a receiver [Sout-61] is given by

$$F_r = F_c + L(F_{amp}-1), \quad (2.3)$$

where  $F_c$  and  $L$  are the noise figure and conversion loss ratio of the detector and  $F_{amp}$  is the noise figure of the amplifier. The noise figure can also be expressed by

$$F_r = \frac{P_i}{kT\Delta f} \times \frac{N}{S}, \quad (2.4)$$

where  $N$  and  $S$  represent the noise and signal outputs of the amplifier and  $P_i$  is the available signal power. The properties of the detector (TRG D925) are: conversion loss  $L= 13$  dB and noise figure  $F_c= 10.5$ . The noise figure of the amplifier is measured as  $F_{amp}= 1.2$ . With this, the noise figure of the receiver becomes  $F_r= 14.5$ . Thus the signal-to-noise (S/N) ratio at the input will be 14.5 times that at the amplifier output. With a desired signal-to-noise ratio at the output of 10 and a bandwidth of 200 kHz we get for the minimum input power  $P_i= 1.2 \times 10^{-13}$  W. This theoretical value is 67 dB below the estimated incoming power. A measurement carried out on a test bench with a detector (Baytron 1T5/X) which was found to have a very high conversion loss (50 dB) resulted in a minimum detectable signal (S/N is 10) of  $1.6 \times 10^{-10}$  W, which is still 36 dB above the expected signal. Therefore, the power output of 100 mW of the 2-mm klystron (Varian VRT-2121A) was expected to be sufficient. With the expected power of  $0.65 \times 10^{-6}$  W at the detector an amplifier gain of 80 dB is sufficient to obtain an output signal of 500 mV to drive the phase-to-digital convertor described later.

**Data handling and control**

A block diagram of the electronics and the interface to the JET computer system, CODAS \*), is given in Fig. 2.2. The 1 MHz pre-amplifier has a gain of 40 dB and a bandwidth of 100 kHz. The pre-amplifier is followed by a second 1 MHz amplifier (40 dB gain) and an amplitude detector to give a continuous check on the performance of the interferometer; it can also be used for tuning the interferometer. The top detector gives an indication of the refraction during the discharge. The system uses a conventional Varian klystron source. The power supply with remote controls from CODAS is developed by the UKAEA Culham Laboratories; all the other electronics, like the fast phase-to-digital convertor CPD1, by the electronic department of the FOM-Instituut voor Plasmafysica Rijnhuizen [Putt-85]. The reference generator and the driver-ramp generator CRG1, the top-detector with light-to-digital convertor CLE1, and the phase-to-digital convertor will be described in Sec. 2.4. All connections between the Faraday box and the outside electronics are done with fibre optics.

---

\*) CODAS is the name of the JET computer system; **C**ontrol and **D**ata Acquisition Systems.

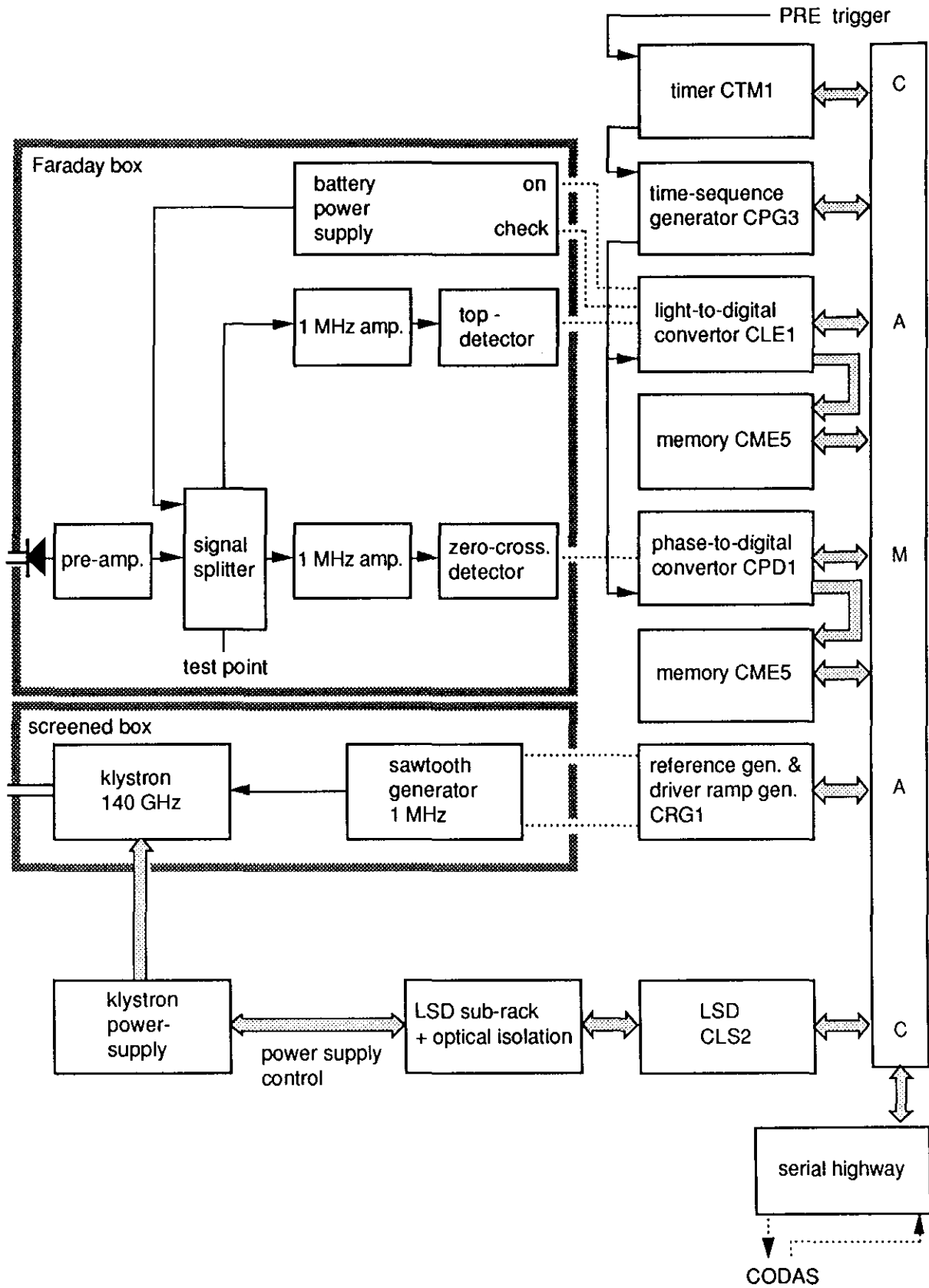


Fig. 2.2. Block diagram of the electronics and data-handling system.

### 2.3 Horn antenna matched to oversized waveguide and vacuum window

#### The test bench

A test bench shown in Fig. 2.3 was set up to measure field patterns of the antenna; all tests were performed at a frequency of 140 GHz.

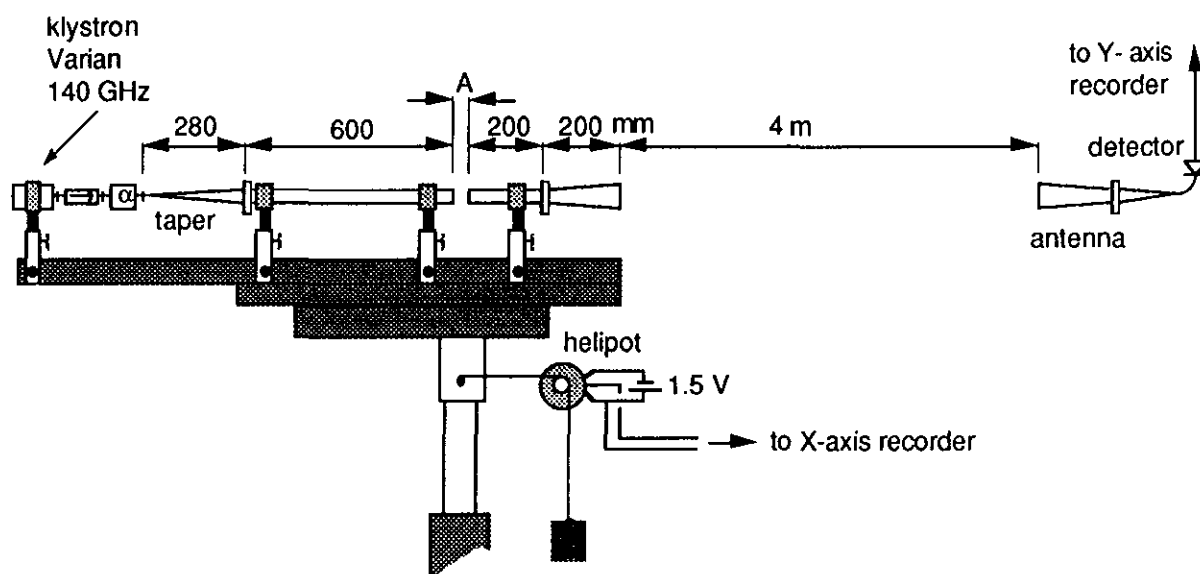


Fig. 2.3. Microwave test bench.

The klystron (Varian VRT-2121A), the waveguide system and the antenna under test are mounted on a revolving support. The angle of rotation is translated to the X-axis of a XY-recorder via a single-turn helipot.

### Losses and reflections at the vacuum window

Different measurements were carried out to determine the best arrangement to transmit the microwave power through the quartz vacuum window of the JET experiment. The measured losses between two oversized open-ended waveguides (X-band) facing each other with a variable separation (gap width  $A$ ) are shown in Fig. 2.4.

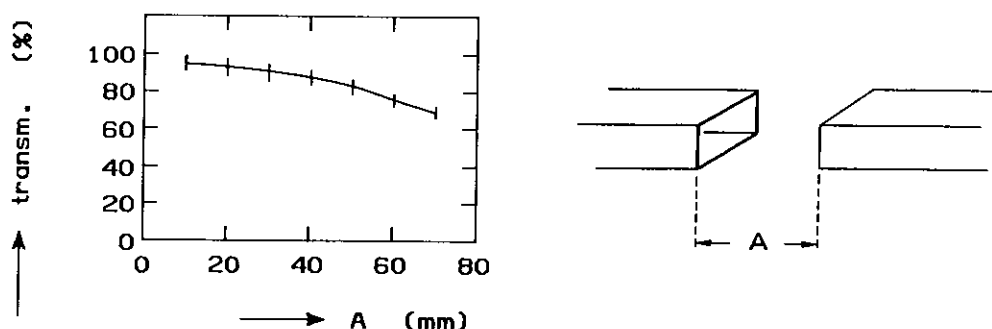


Fig. 2.4. Transmitted power as a function of gap width.

The vertical bars in Fig. 2.4 indicate the maximum and minimum values caused by standing waves. The measurement shows that a distance of 20 mm will give an average loss of only 7% (0.3 dB). A gap of 20 mm is sufficient for the vacuum window; it will also provide a thermal break.

A measurement with a diaphragm between oversized waveguides placed 20 mm apart, is given in Fig. 2.5. From this measurement we see that a mount of the quartz window with an aperture larger than 25 mm will not affect the microwave beam at all; in fact a mount of 36 mm is available.

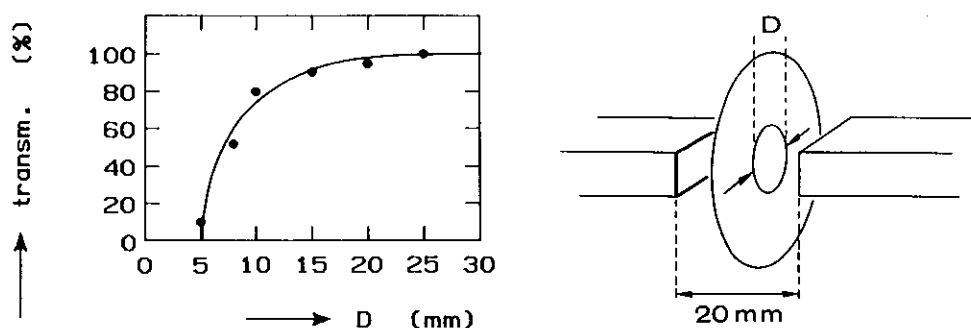
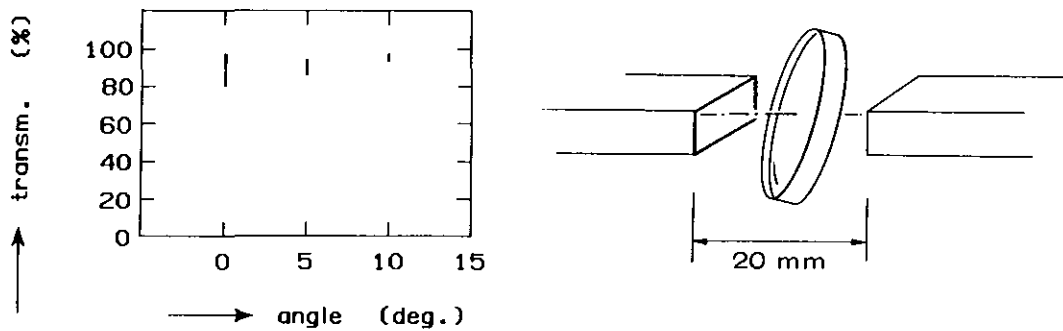


Fig. 2.5. Transmitted power as a function of the aperture of a diaphragm.

Measurements of reflection on a 5.0 mm thick fused quartz window are carried out at different angles (Fig. 2.6).



*Fig. 2.6. Transmitted power as a function of tilting angle  $\alpha$ .*

With the window fitted to an angle of  $5^\circ$  in both directions, perpendicular to the direction of the oversized waveguides, reflection becomes negligible. The vertical bars in Fig. 2.6 again give the maximum and minimum values caused by standing waves.

Obs. To get a minimum of reflections the thickness of the window must be a multiple of half a wavelength. The fused quartz window ( $\epsilon = 3.78$  at 140 GHz) is 4.5 wavelengths thick. A test with a 5.1 mm thick Z-cut crystal quartz window ( $\epsilon = 4.437$  at 140 GHz) gave the same results as the fused quartz one.

#### **A 2-mm horn antenna matched to an X-band oversized waveguide**

The shape of the oversized horn antenna is selected in the following empirical way. Two test antennae are made, each one consisting of two parallel copper plates with one end fixed at the 3-cm waveguide flange (X-band) and the other end adjustable in separation,  $A$ , (Fig. 2.7). There is one set, called 'E-plates', with the electrical field lines parallel to the copper plates and another, called 'H-plates', with the electrical field perpendicular to the copper plates.

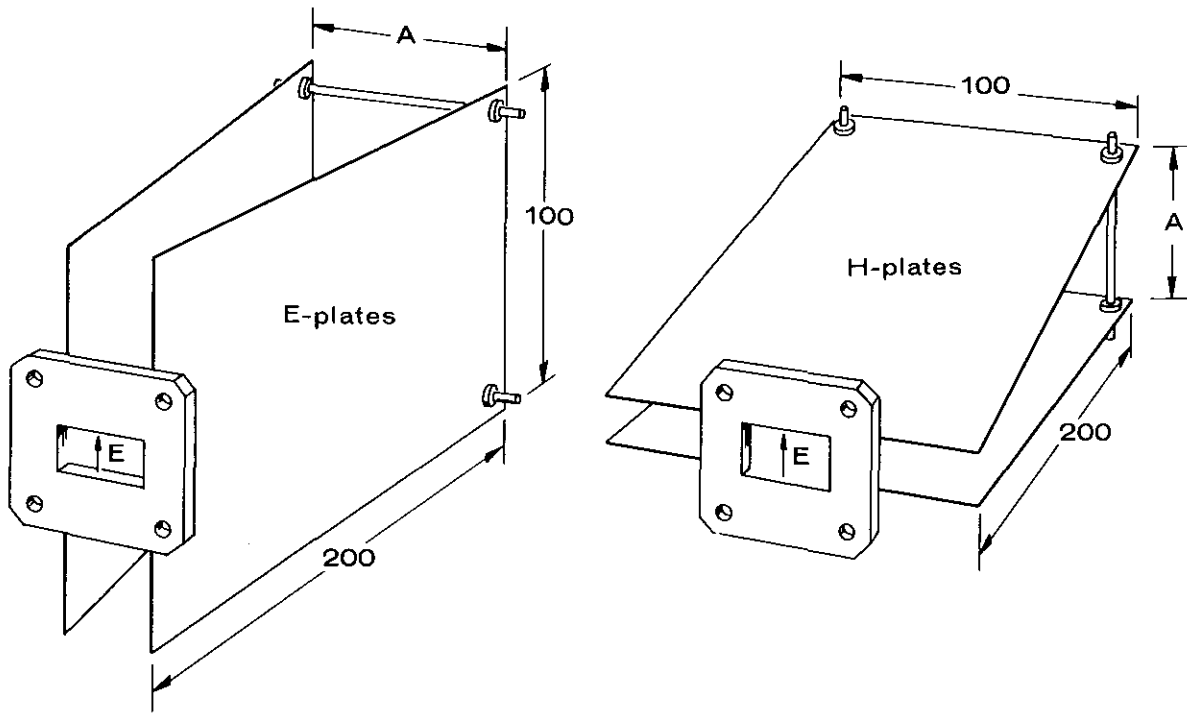


Fig. 2.7. 'Plate antennae'.

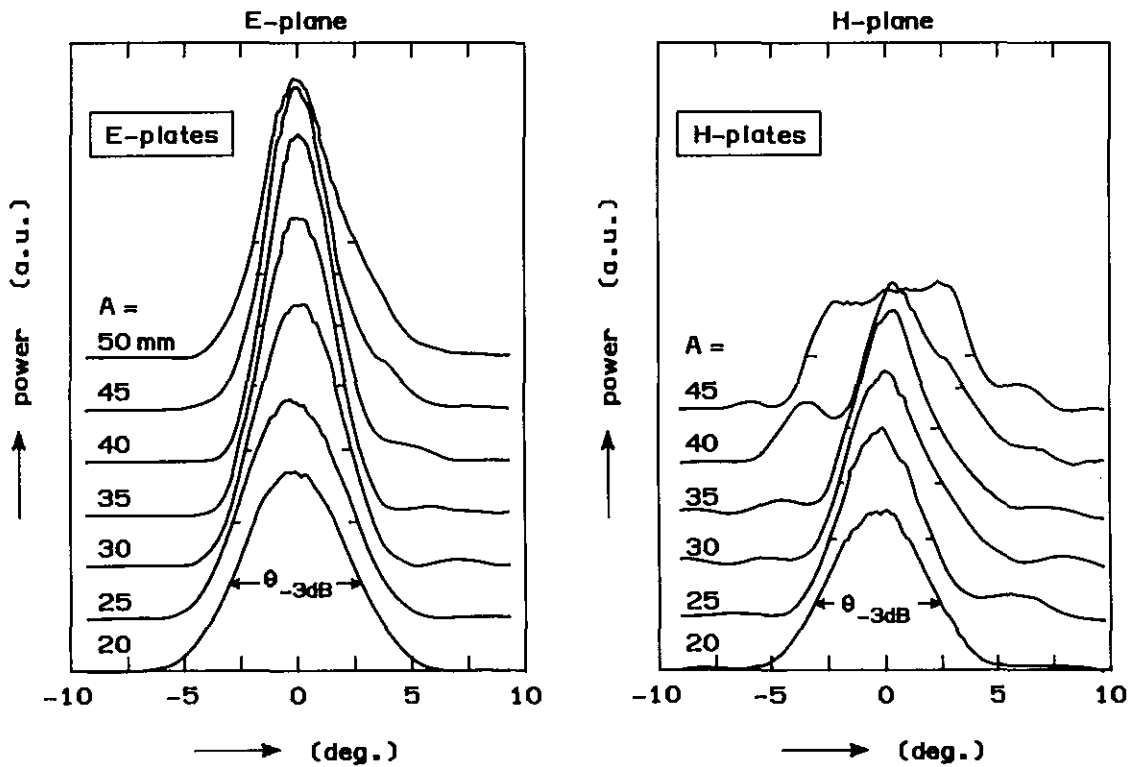


Fig. 2.8. Field patterns of the 'plate antennae' measured with a slightly non-linearly responding detector; the markers indicate the half-power points determined at - 3 dB of the maximum by means of a calibrated attenuator.

From the field patterns measured at different separations, the aperture of the final horn antenna was selected. The length of the antenna, which must be large compared to the wavelength  $\lambda = 2$  mm, was chosen arbitrarily. The two sets of field patterns with the aperture 'A' as a parameter are given in Fig. 2.8. The aperture of the 200 mm long horn antenna is selected from these measurements. In the E-plane, where the field patterns are found to be non-critical, 30 mm is chosen, corresponding to a  $5^\circ$  half-power beam width. In the H-plane A = 25 mm had to be selected to fit in the JET port, though A = 30 mm would have been preferable. The resulting field patterns of the horn antenna are given in Fig. 2.9; where the influence of the vacuum-window is negligible. The measured beam widths correspond very well with the measurements done with the 'plate antennae'.

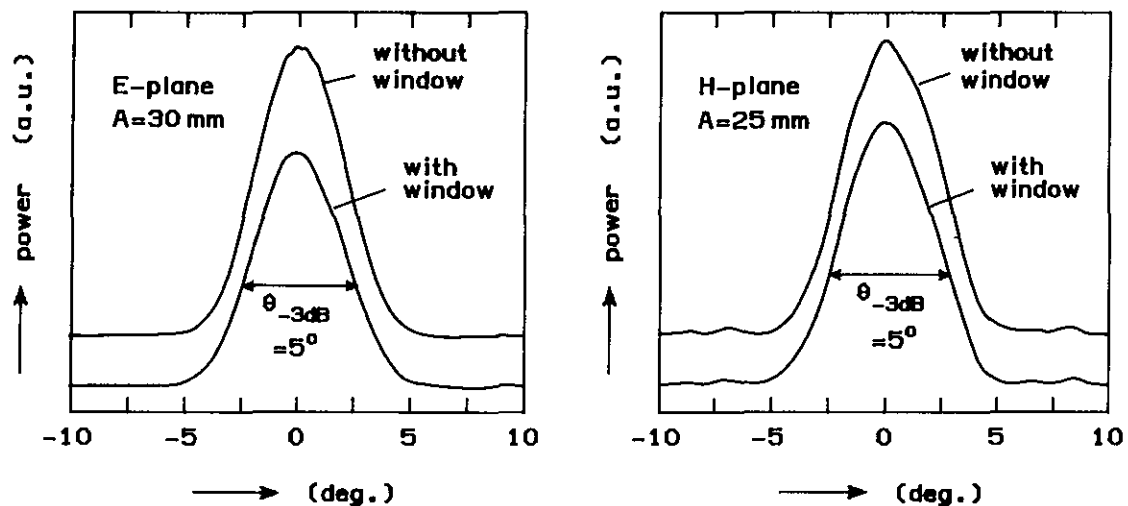


Fig. 2.9. Field pattern of horn antenna with and without window.

A test with the antenna situated in a diagnostic mock-up port showed no disturbance of the field patterns when the antenna was withdrawn over 20 mm back into the observation-port of the JET experiment. The influence of the metal sides of the port became perceptible only when the antenna was withdrawn as far as 100 to 150 mm.

Misalignment, where the horn antenna is placed with its axis at  $2^\circ$  with respect to the incoming oversized waveguide, showed side-lobes 7 dB below the maximum signal.

## 2.4 Plasma electron density measurements in JET with the 2-mm microwave interferometer

### Introduction

The simple 2-mm microwave interferometer described here has been used as the primary density monitor throughout the ohmic heating phase of the JET programme [Fess-83, Fess-85]. In addition, it provides the control signal for the plasma density feedback system. It measures the line-integrated electron density along a single vertical plasma chord located at  $R=3.14$  m, i.e. nearly through the centre of the discharge chamber. Access to the JET experimental device is restricted during an experimental period and all the non-passive components of the interferometer have to be positioned outside the biological shield. This results in a very long transmission path length of 76 m for the plasma ‘arm’ of the interferometer. More than 70 m of this transmission path is an oversized waveguide with a total of 24 low-loss mitre bends (Fig. 2.10). The total measured attenuation is  $65 \pm 3$  dB. A 150 mW, 140 GHz reflex klystron is used as microwave source and a high-sensitivity liquid-helium-cooled InSb detector has to be used to compensate for the high attenuation (QMC Instruments, estimated noise equivalent power (NEP) of  $2 \times 10^{-12}$  W Hz<sup>1/2</sup>). The maximum density achieved on JET caused a total phase excursion of  $\sim 125$  fringes in the interferometer. This was recorded without difficulty by the instrument with a phase resolution of 0.02 fringes. The high density resolution which is achieved makes the system, in addition to its basic density monitoring role, a powerful diagnostic for the study of density oscillations. It has been demonstrated that plasma density fluctuations, which represent a variation of only 0.1% of the maximum line-integrated density, can be studied with this interferometer. The details of the interferometer, and examples of the density measurements and the magnetohydrodynamic (MHD) phenomena detectable on the signals are presented below.

### Principle and limitations of the measurement

As explained in the introduction (Sec. 1.1) variations of optical path length are measured with the interferometer. These variations are caused by the change in refractive index of the plasma as its electron density grows and decays during the JET pulse. For the 140 GHz probing beam the critical density is  $2.43 \times 10^{20}$  m<sup>-3</sup>. However, before this density limit is reached the approximation underlying Eq. (1.13)

$$F = \frac{1.345 \times 10^{-16}}{f} \langle n_e \rangle L, \quad (f \text{ in GHz})$$

will not be valid any more. For example, for cases in which the density profile is flat and  $n_e/n_c = \frac{1}{4}$  or  $\frac{1}{2}$ , the approximation will lead to systematic overestimates of  $n_e$  by 1% or 6%, respectively.

Although the beam is not cut off at these densities it may be refracted away from the receiving antenna if the plasma is not well centred with respect to the probing path.

The effects of refraction have been computed by a number of authors [Heal-65, Vero-83]. For a parabolic density distribution in JET an approximate limit has been estimated by setting the maximum acceptable refraction angle of the beam equal to the divergence angle of the launching antenna. This leads to the requirement that for  $\frac{n_e(0)}{n_c} = \frac{1}{2}$  (where  $n_e(0)$  is the central density) the plasma should be centred to within  $\sim 100$  mm of the probing beam path. This is normally the case and thus the 140 GHz interferometer can be used up to a density of about  $10^{20} \text{ m}^{-3}$ . The maximum average density in JET at present is  $\sim 4 \times 10^{19} \text{ m}^{-3}$  which creates 125 fringes in the interferometer, which can be measured routinely and without difficulties.

The minimum resolvable phase change is limited to 0.02 fringes by digital noise and detection system noise, which are about equal. Since the instrument measures the line-integrated electron density,  $\int n_e dL$ , along a nearly central vertical chord through the plasma, this minimum corresponds to an average electron density variation along the chord of only  $7 \times 10^{15} \text{ m}^{-3}$  for a typical plasma with a vertical dimension,  $L$ , of 3 m.

### Description of the system

A sketch of the interferometer is given in Fig. 2.10.

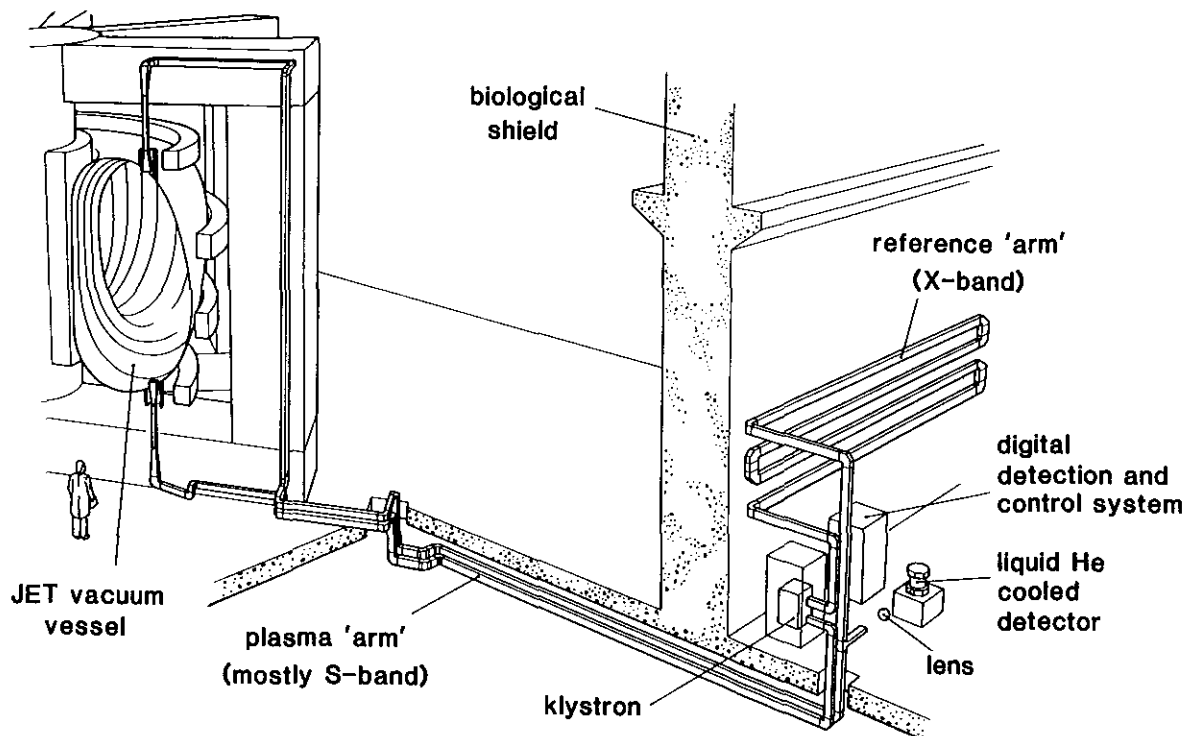


Fig. 2.10. Scheme of the 2-mm microwave interferometer on JET.

A block diagram of the electronics of the interferometer is given in Fig. 2.2 (p. 41) and the microwave part in Fig. 2.11.

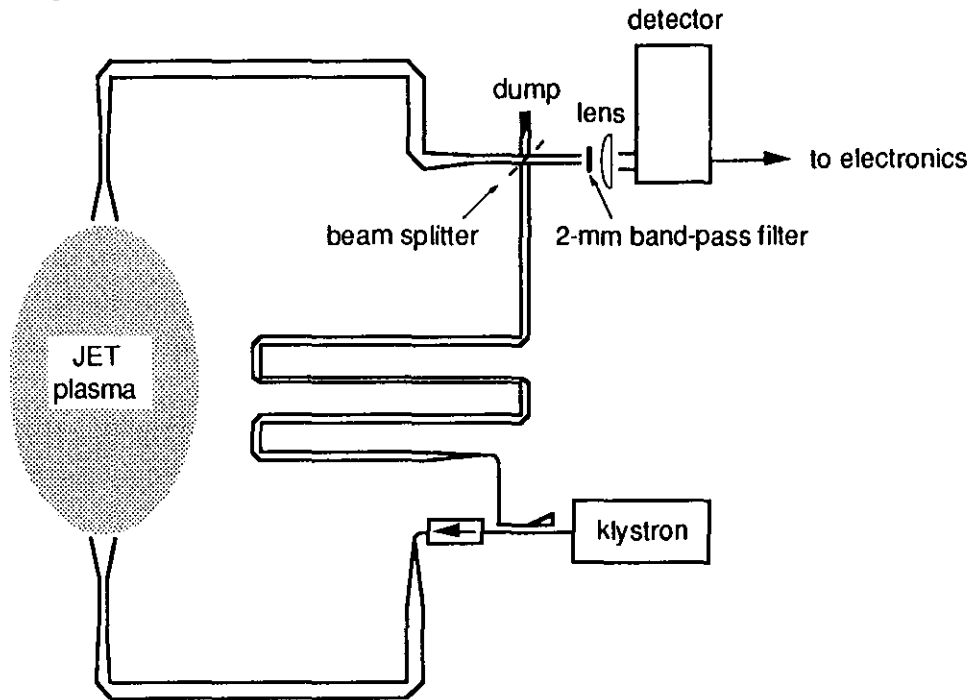


Fig. 2.11. Diagram of the microwave components of the 2-mm interferometer.

The path length difference in the JET 2-mm interferometer is approximately  $\Delta L = 12$  m. This leads with the condition  $\Delta f = c/\Delta L$  to a  $\Delta f$  of 25 MHz and  $V_{\text{mod}} \approx 3$  V for the klystron sawtooth modulation. For the interferometer to be able to follow all plasma induced phase changes reliably, the condition  $f_i \gg \Delta\phi/2\pi$ , where  $f_i = 1$  MHz, should be met. The choice of 100 kHz as the bandwidth for filtering ensures that all but the extremely rapid phase changes, associated with major disruptions of the plasma, can be followed accurately.

By comparing the approximately 1 MHz signal from the detector with the 1 MHz reference signal used to drive the sawtooth modulator, the phase difference,  $\Delta\phi$ , due to the plasma is measured and the evolution of the plasma electron density is determined from that.

It is normal practice to use oversized waveguides to avoid the unacceptable attenuation of single mode waveguide at millimetre wavelengths. The theoretically lowest obtainable loss in a D-band waveguide is  $5.2 \text{ dB m}^{-1}$  at a frequency of 140 GHz. The attenuation of the  $\text{TE}_{01}$  mode in an oversized waveguide ( $\lambda \ll a$  or  $b$ , where  $a$  and  $b$  are the dimensions of the rectangular waveguide) is inversely proportional to the height of the waveguide wall parallel to the electric vector. A pure aluminium WG10 guide ( $a = 34$  mm and  $b = 72$  mm) has been used in the interferometer with the electric vector parallel to the longer wall. The measured attenuation at  $\lambda = 2.2$  mm was less than  $0.06 \text{ dB m}^{-1}$  which was acceptably close to the calculated value of  $0.04 \text{ dB m}^{-1}$ .

For low mode conversion losses and compactness in such an oversized system, so-called mitre bends are used. The loss for a perfect bend of this type is  $1.96(\lambda/b \sin\Theta)^{1/2}$  dB for an E-plane bend and  $2.05(\lambda/a \sin\Theta)^{3/2}$  dB for an H-plane bend where  $\Theta$  is the angle of the bend. The minimum attenuation for 90° E-plane and H-plane bends is 0.33 dB and 0.03 dB, respectively. In addition, the tilt between the axis of the guide and the connecting flange face will give rise to serious losses. Thus, for a low attenuation oversized waveguide system the total number of bends should be minimized, H-plane bends should be used in preference to E-plane bends and the manufacturing and installation tolerance should be better than 0.1° [Okre-68]. These requirements have been met wherever possible, but the routing of the waveguide between the active part of the interferometer and the JET-experiment still necessitates the use of 24 high precision mitre bends and of about 70 m of waveguide. The total attenuation, including the losses in the torus between the horn antennae, was measured to be  $65 \pm 3$  dB (cf. the estimated 51.9 dB of table 2.1, p. 38).

### Electronics \*)

Below a description is given of the three CAMAC \*\*) modules especially built for the JET 2-mm interferometer system:

- a phase-to-digital convertor module to digitize the phase-shift difference of the 1 MHz interferometer signal,
- a ramp-reference module to supply the necessary timing signals for the ramp generator and the phase-to-digital convertor,
- a light-to-digital convertor module to read the amplitude of the detected interference signal to check the performance of the interferometer during a plasma pulse.

A block diagram of the electronics and the interface to CODAS, the JET computer system, is given in Fig. 2.2 (p. 41). In addition to the CAMAC modules special signal conditioning units were developed and incorporated in the interferometer. The connections between the signal conditioning units in the Faraday cage and the CAMAC modules are made by fibre optics to guarantee interference free operation. In the absence of plasma, the frequency shift is adjusted to produce a phase-shift of  $2\pi$  between the reference and plasma arm for each cycle (1  $\mu$ s) of the sawtooth modulation voltage. The chosen intermediate frequency of 1 MHz is derived from a 100 MHz reference clock. The detector is followed by an amplifier with a

---

\*) This work was performed under the JET contract JB2/0620 (1981) between the JET Joint Undertaking and the FOM-Instituut voor Plasmafysica Rijhuizen, Nieuwegein, the Netherlands.

---

\*\*) CAMAC is an acronym for: Computer Aided Measurement And Control, and is a modular system.

bandwidth of 100 kHz centred at 1 MHz to reduce the noise and to filter out the fly-back pulse. The resultant 1 MHz signal is then compared with a reference signal in a phase-to-digital convertor.

### Phase-to-digital convertor

With the phase-to-digital convertor the phase-shift variation of the 1 MHz interferometer signal can be measured (Fig. 2.12).

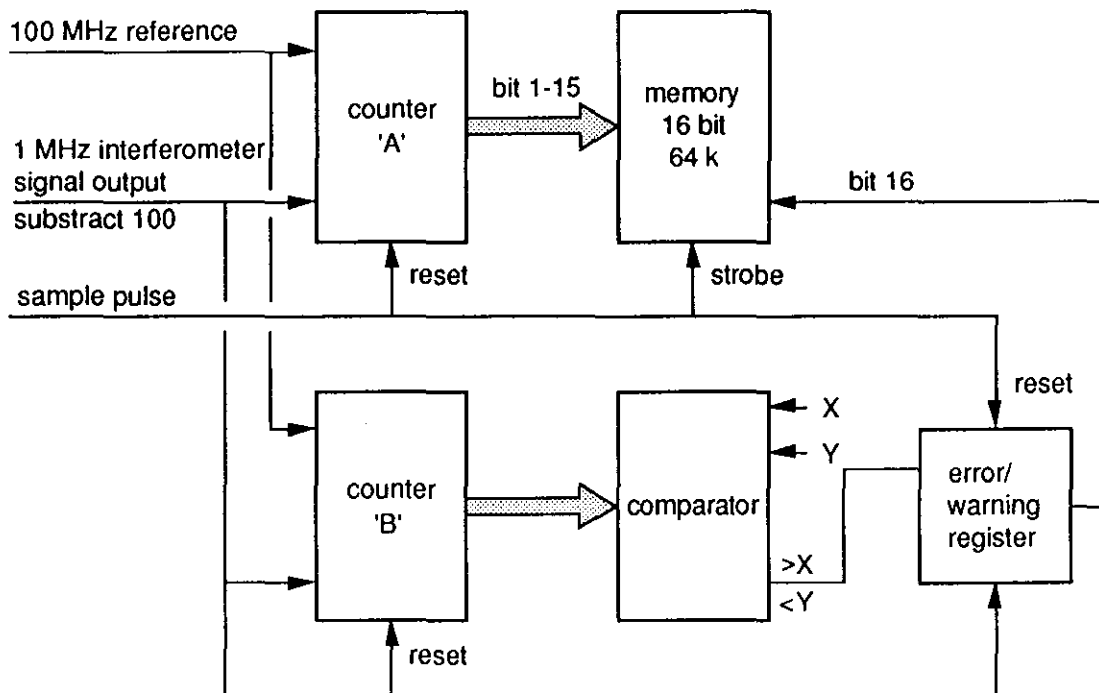


Fig. 2.12. Phase-to-digital convertor.

Counter 'A', counts the 100 MHz reference signal; the number 100 will be subtracted at the end of each input signal period. So, if the phase in the plasma path does not vary, the subtraction of 100 will bring the counter number back to zero after each signal period. If the phase varies, the reference counter will accumulate the phase-shift of each period until the sample pulse is given (sample pulse rate for instance 1 ms). The counter value will now be given out as a 15 bit word together with a strobe pulse and the counter will be reset. The data is written into a standard 16 bit, 64 k memory module (LeCroy MM8806). Bit D1-D8 contains the fraction of  $360^\circ$  in BCD (binary coded decimal) and bit D9-D15 the number of fringes in 2's complement. This strange format is derived from the reference counter set up where 2 BCD counters are used to be able to subtract 100 and to reach the high speed of 100 MHz requested. The BCD, 2's complement format is converted to degrees phase-shift in a simple software subroutine.

The error/warning bit addition works as follows. At the end of each input signal period (a number of) 100 is subtracted from counter 'B'. The remainder is given out to the comparator and the counter is reset. If the remainder is above an pre-set upper value or below a pre-set lower value an error/warning bit is passed onto the error bit register. Thus if the limits are set to  $+36^\circ$  and  $-36^\circ$ , a phase change  $> 136^\circ$  in  $1 \mu\text{s}$  will stimulate the error/warning. At the sample pulse the error/warning bit will be added as bit 16 to the phase sample and the error bit register will be reset. The error/warning bit can be used for control and for automatic data correction (Fig. 2.16, p. 56)

The phase-to-digital convertor does not require any 'reset' or 'calibration' pulse. The phase sample resolution is  $3.6^\circ$ .

### **Ramp-reference generator**

This CAMAC module provides the amplitude control and frequency (1 MHz) of the sawtooth generator. The module is coupled to the sawtooth generator by means of light fibres (Fig. 2.2, p. 41). The transmission is with pulse width modulation at 1 MHz. The 1 MHz sawtooth modulates the 2-mm klystron in frequency. The frequency deviation is proportional to the amplitude of the sawtooth. The sawtooth generator is built in the klystron compartment and is kept floating at the high voltage of the klystron supply; the DC powering of the sawtooth generator originates from the klystron filament supply.

The reference generator is a 100 MHz pulse signal (emitter coupled logic, ECL) for the phase-to-digital convertor.

### **Light-to-digital convertor**

With this CAMAC module and the amplitude-to-light convertor, located in the signal conditioning Faraday cage, the envelope of the linearly amplified 1 MHz output signal of the microwave detector can be followed (Fig. 2.2, p. 41). The two units are coupled with light fibres. The transmission uses pulse-width modulation at 10 kHz. The amplitude is passed onto the dataway and on a trigger command (sample clock) to the output port together with a strobe pulse and written into a standard 16 bit, 64k memory (LeCroy MM8806).

The three CAMAC modules have been in continuous use since the first day of operation of JET. The error/warning feature of the phase-to-digital convertor module has proven to be particularly useful, allowing in many cases full recovery of the complete density evolution by the use of extra off-line software (Fig. 2.16, p. 56).

## Results

Virtually all plasma measurements during the ohmic heating phase of the JET project were made using the 2-mm interferometer system [Fess-87, Tang-84]. Figure 2.13 shows an example of the electron density and signal amplitude waveforms of the JET pulse.

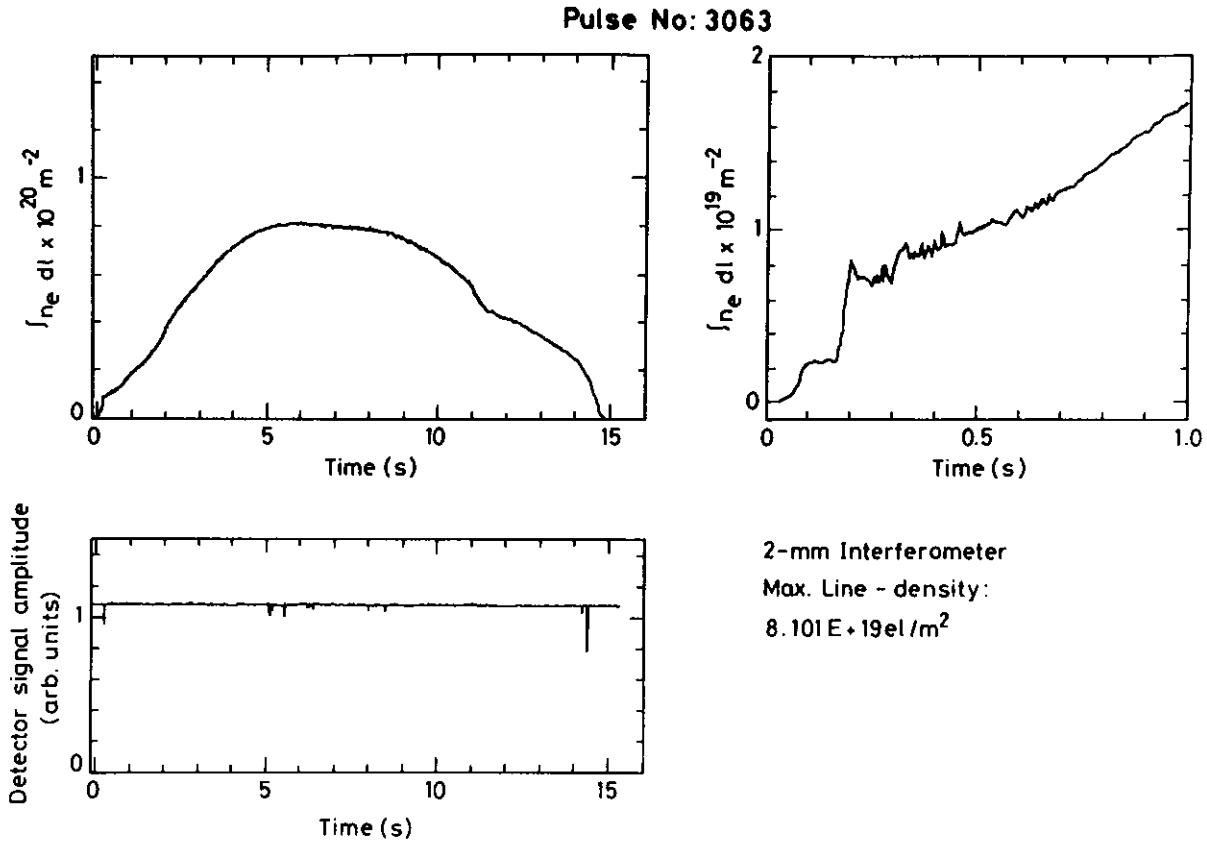


*Fig. 2.13. a) Evolution of the line-integrated density for JET pulse no. 3063.  
b) Blow up of the first second of (a).  
c) Detector signal amplitude during pulse.*

Figure 2.14 shows the density signal compared with current and voltage waveforms. A comparison of preliminary data from the JET FIR-laser interferometer [Vero-82, Vero-83] with that from the microwave instrument showed agreement to within 3% during the pulse flat-top period, thus, the assumption made in Eq. 1.12 is justified. This difference is due to: (a) noise in the FIR measurements, and (b) the fact that the two instruments measure the line-integrated density along chords at different toroidal positions and at different major radii. It has been noted, however, that at the highest densities there is some evidence that the binomial approximation used in Eq. (1.13) produces a systematic overestimation of  $\int n_e dl$ , measured by the 2-mm microwave interferometer, of  $\leq 1\%$ .

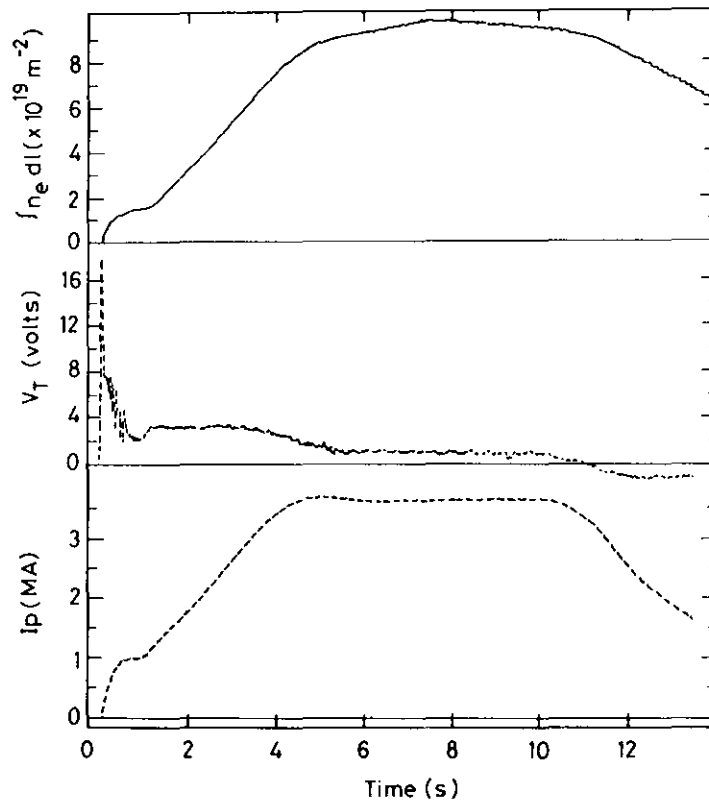


Fig. 2.14. Waveforms of: a) Line-integrated density .  
 b) Loop voltage.  
 c) Plasma current.

The resolution of the instrument at the density maximum is 1 in 5000. The value of this high resolution is illustrated in Fig. 2.15. Sawtooth oscillations corresponding to  $\sim 1\%$  variation of the  $\int n_e dl$  amplitude, are easily resolved in the expanded waveform Fig. 15b. Fast oscillations on the individual sawtooth of only  $0.1\%$  of the amplitude are also resolvable when the data are further expanded (Fig. 2.15c). In the example shown these faster oscillations can be observed since faster sampling (5 kHz) was used between 6.0 and 6.4 s for this pulse.

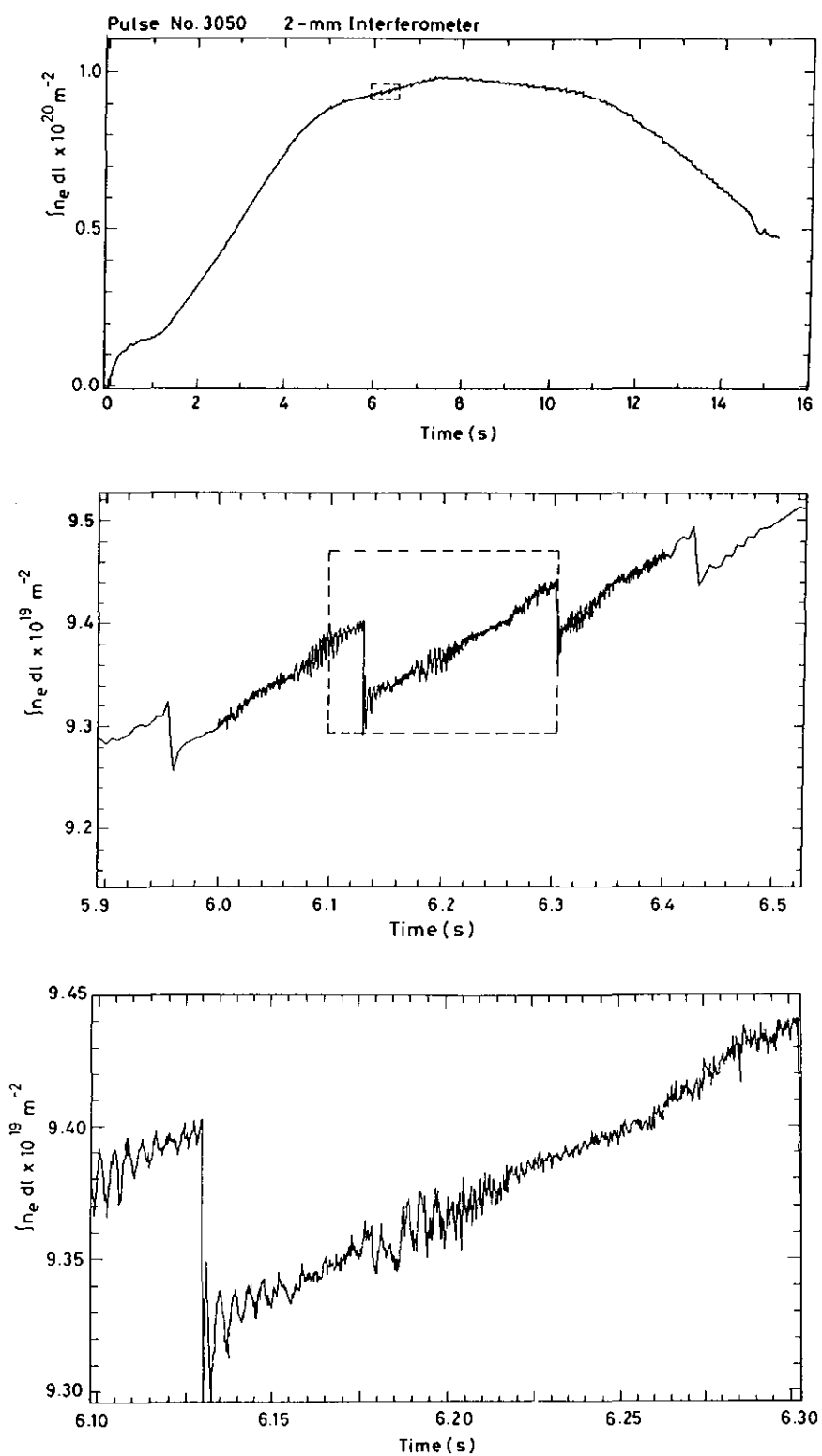


Fig. 2.15. a) Density waveform, with indication of expanded region.  
 b) Expanded waveform showing sawtooth oscillation.  
 c) Further expansion showing high frequency fluctuations on the sawteeth.

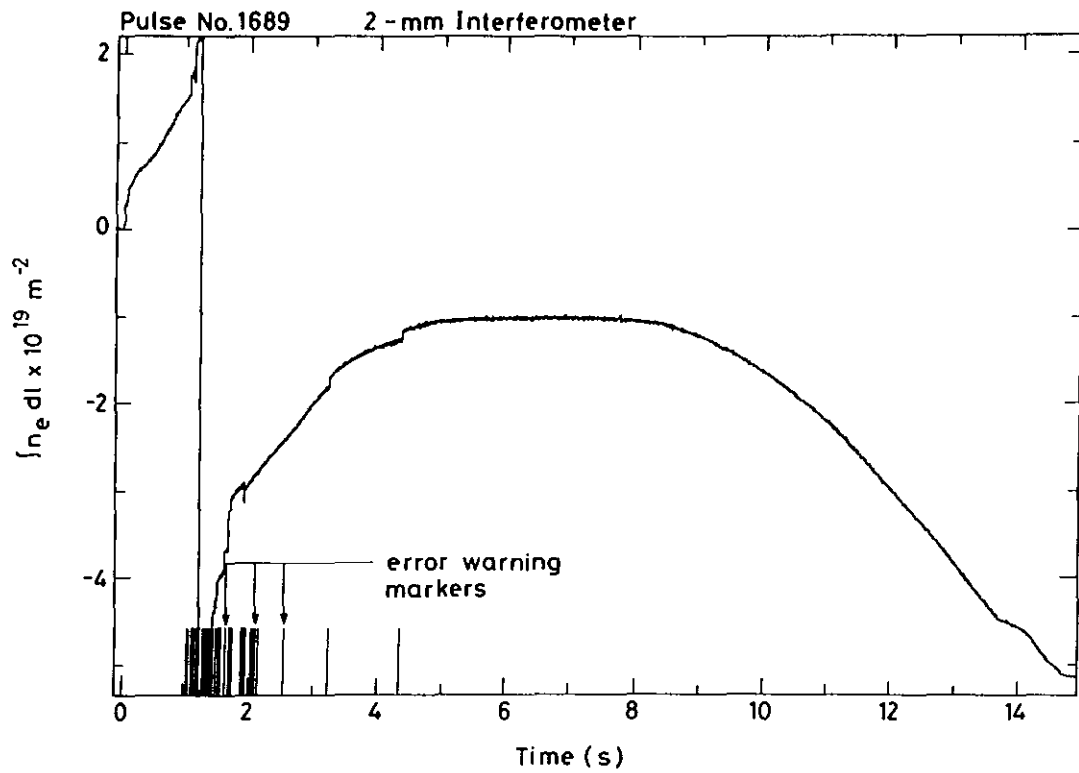


Fig. 2.16a. Corrupted density waveform caused by disruptions during plasma current rise.

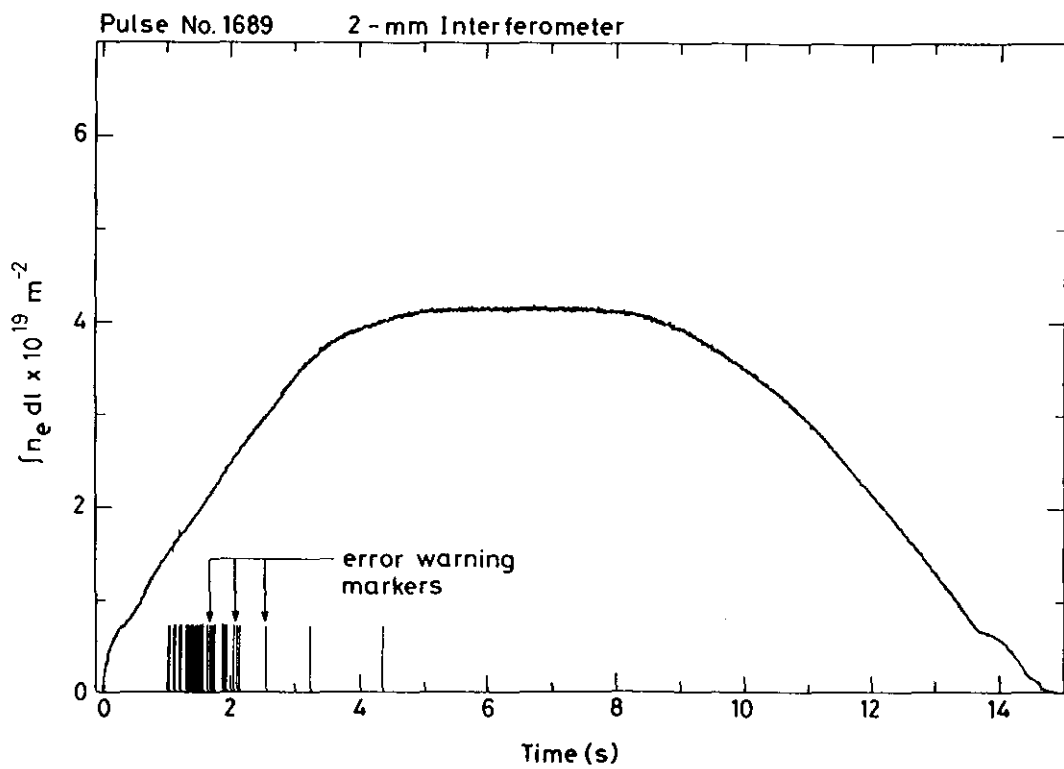


Fig. 2.16b. Waveform after processing with automatic reconstruction program.

As with many similar interferometers, rapid changes in density associated with minor and major disruptions of the plasma can cause phase sampling errors. However, when this occurs with our instrument, it is possible in many cases to re-analyse the data off-line and try to reconstruct the corrupted waveform, because the error/warnings are all flagged by the hardware. This has been done by identifying and correcting the faulty samples either manually or with an automatic correction program. For the results shown in Fig. 2.16a the error/warning bit was set wherever the phase-shift between 1  $\mu$ s samples exceeded  $136^\circ$ . All samples with error/warnings are indicated on Fig. 2.16a by a vertical bar, marking the times at which phase measuring errors may have occurred. The updated result obtained with an automatic reconstruction program is shown in Fig. 2.16b. Different procedures like forward integration until an error is met and backward integration down to the same error are used by the JET team. For minor disruptions, provided the incidence rate of error flags is not too high, the technique appears to work well, as can be judged from the fact that the phase signal returns to zero at the end of the pulse. Major disruptions, however, create a very high incidence of errors from which it has not been possible as yet to recover the complete density history. Normally the data are reliable until such an event occurs in the waveform, i.e. until the onset of a major disruption.



## Chapter 3

### HETERODYNE CO<sub>2</sub>-LASER INTERFEROMETRY

#### 3.1 Introduction

A CO<sub>2</sub>-laser interferometer,  $\lambda = 10.6 \mu\text{m}$ , can be used to measure line-integrated plasma densities in the range of  $3 \times 10^{19} \text{ m}^{-2}$  to  $3 \times 10^{23} \text{ m}^{-2}$  [Huge-76]. The CO<sub>2</sub>-laser interferometer is a reliable and convenient tool for measuring plasma densities and fluctuations thereof. The main advantage of working at the CO<sub>2</sub>-laser wavelength is that the diffraction of the waves is negligible when applied to plasmas in the density range of  $5 \times 10^{21} \text{ m}^{-3}$ . Since it is not possible to determine the increasing or decreasing character of fluctuations in the density with a simple Mach-Zehnder interferometer, systems have been built which have heterodyne detection (intermediate frequency of 300 - 500 kHz) and a direct density read-out.

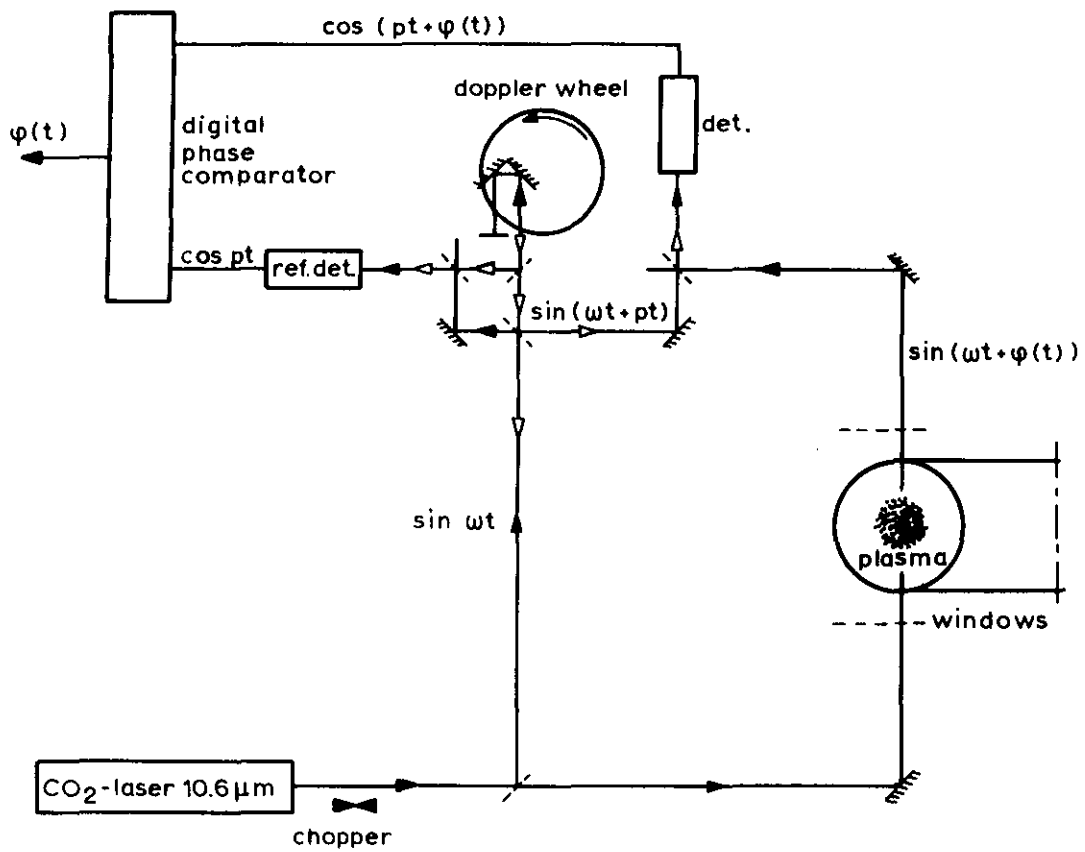


Fig. 3.1. Diagram of the interferometer.

### 3.2 CO<sub>2</sub>-laser interferometer with a Doppler-wheel \*)

A schematic diagram of the interferometer is given in Fig. 3.1. The signal in the reference path of the interferometer is frequency-shifted by means of two perpendicular reflectors mounted on a rotating wheel with a diameter of 200 mm: the so-called 'Doppler wheel'. When the wheel rotates at an angular speed of 120 r.p.m. a frequency shift of  $p = 300$  kHz is obtained (\*\*). The interference of this frequency-shifted beam,  $\sin(\omega t + pt)$ , with the beam going through the plasma,  $\sin(\omega t + \varphi(t))$ , will result in a signal,  $\cos(pt + \varphi(t))$ , after detection. Here,  $\varphi(t)$  is the phase shift caused by the plasma. The frequency-shifted signal,  $\sin(\omega t + pt)$ , is also mixed in a second branch which acts as a non-plasma interferometer, to obtain a reference signal,  $\cos pt$ . The application of this second interferometer is necessary because the frequency shift varies non-linearly with the angular position of the reflectors on the rotating wheel. In this set up a maximum measuring time of 60 ms is available, in which time interval the 300 kHz frequency shifts by about 20 kHz. The signals from both interferometers are detected and are fed to a digital phase comparator, yielding a continuous signal, representing  $\varphi(t)$ .

#### Description of some components

The interferometer has been built on a non conducting frame to prevent forces from eddy currents. The frame is mounted on a movable platform which is placed on a stiff aluminium console. The console is placed on rubber blocks to avoid mechanical vibrations. This arrangement makes it possible to measure density profiles on a shot-to-shot basis by shifting the position of the complete interferometer without the need for re-alignment.

The source is a 3 W cw, non-polarized CO<sub>2</sub>-laser with a current-stabilized power supply (20 kV at 10 mA).

---

\*) This work was published earlier as Rijnhuizen Report 76-100 (1976).

---

\*\*) In an earlier phase the interferometer was developed with an intermediate frequency of 100 kHz. Due to the rapid density fluctuations in some experiments, counting errors corresponding to steps of  $2\pi$  did occur. By increasing the intermediate frequency to 300 kHz and the bandwidth of the pre-amplifier to 200 kHz the system was made to work reliably.

Beam-splitters and windows in the interferometer consist of ZnSe. This material has convenient properties: low loss and a wide transmission range from 0.5 - 22  $\mu\text{m}$ , a feature which makes it possible to align the interferometer with a HeNe-laser. The windows have anti-reflection coatings. Most of the beam splitters have 50% reflection coatings on one side and anti-reflection coatings on the other side. The mirrors are gold-coated pyrex discs. All optical elements of the interferometer had to be mounted in holders of insulating material to avoid disturbances by magnetic forces.

A wide-band pyro-electric detector (Molelectron P3-01) is used. To avoid electrical interference from the experiment, the detector element and a selective amplifier at 300 kHz with a bandwidth of 200 kHz are shielded. The power on the detector is about 5 mW which is far above the noise level. The input stage of the pre-amplifier is designed in such a way as to have a low frequency output available as well as for alignment purposes in connection with the chopper in front of the laser.

The modulator system consists of the two perpendicular reflectors mounted on a wheel, which is driven by an air-jet (Fig. 3.3).

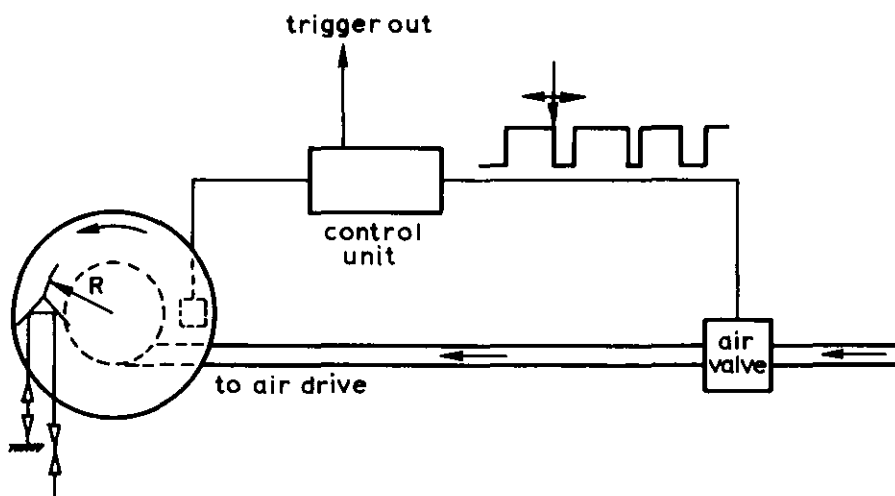


Fig. 3.3. Pneumatically driven Doppler wheel.

The frequency shift  $\Delta f$  can be calculated from:

$$f = 4 \frac{2\pi RN}{\lambda}$$

where:

R is the distance from the centre of the wheel to the centre of the reflector system,

N is the number of revolutions per second,

$\lambda$  is the wavelength of the laser (10.6  $\mu\text{m}$ ).

The Doppler wheel is carefully constructed to avoid vibrations which would disturb the interferometer. The rotation frequency is kept constant by electrical feedback from the wheel to the air valve.

The signal from the interferometer,  $\cos(pt + \varphi(t))$ , and that from the reference interferometer,  $\cos pt$ , are processed to drive two digital counters. The momentary phase shift,  $\varphi(t)$ , can be obtained by subtracting the digital output of the counters. The digital output is fed into a R-2R ladder network (Fig. 3.4). After filtering, a continuous output is obtained, which is proportional to the phase shift .

Just before the start of the measurement a short calibration pulse is generated with a prefixed amplitude, which can be set to any  $n \times 2\pi$ . As the initial phase difference of the signals from the two detectors can have any value between  $+2\pi$  and  $-2\pi$ , the phase comparator is reset to a level of  $2\pi$  above the lowest limit of the output (Fig. 3.5); this level is the zero-line of the calibration step and is followed by the zero-line of the density signal.

Description of the circuit diagram of the phase comparator (Fig. 3.4).

Both input signals are coupled to two identical input stages by ferrite core transformers with broad pass-bands. The square wave outputs are connected to the clock inputs of the counters SN74193 in such a way that the upper one counts forward and the lower one counts backward. The outputs are continuously added in a SN7483. On a trigger command the upper counter is loaded with '1' or '4' (calibration) and the lower counter is reset. After about 100  $\mu$ s the upper counter is also reset. After another 100  $\mu$ s both reset commands cease and the input pulses take over. The carry input of the adding device is kept on a logical '1' all the time to accomplish an offset of  $2\pi$  as mentioned before. The 100  $\mu$ s commands are generated by two monostable multivibrators (pulse times 100 and 200  $\mu$ s) together with gating circuits and are initiated by a positive pulse of minimum 3 V at the trigger input. If a range lower than  $15 \times 2\pi$  full-scale is desired, only part of the ladder network can be used. We use 3 parts for a  $7 \times 2\pi$  range, with a  $4 \times 2\pi$  calibration step. A buffer amplifier with a voltage gain of about 1.6 is used to feed a filter. The filter is designed to have a smooth step response and a rather steep cut-off slope. Theoretically, a cut-off frequency of 100 kHz is possible, but to be compatible with the

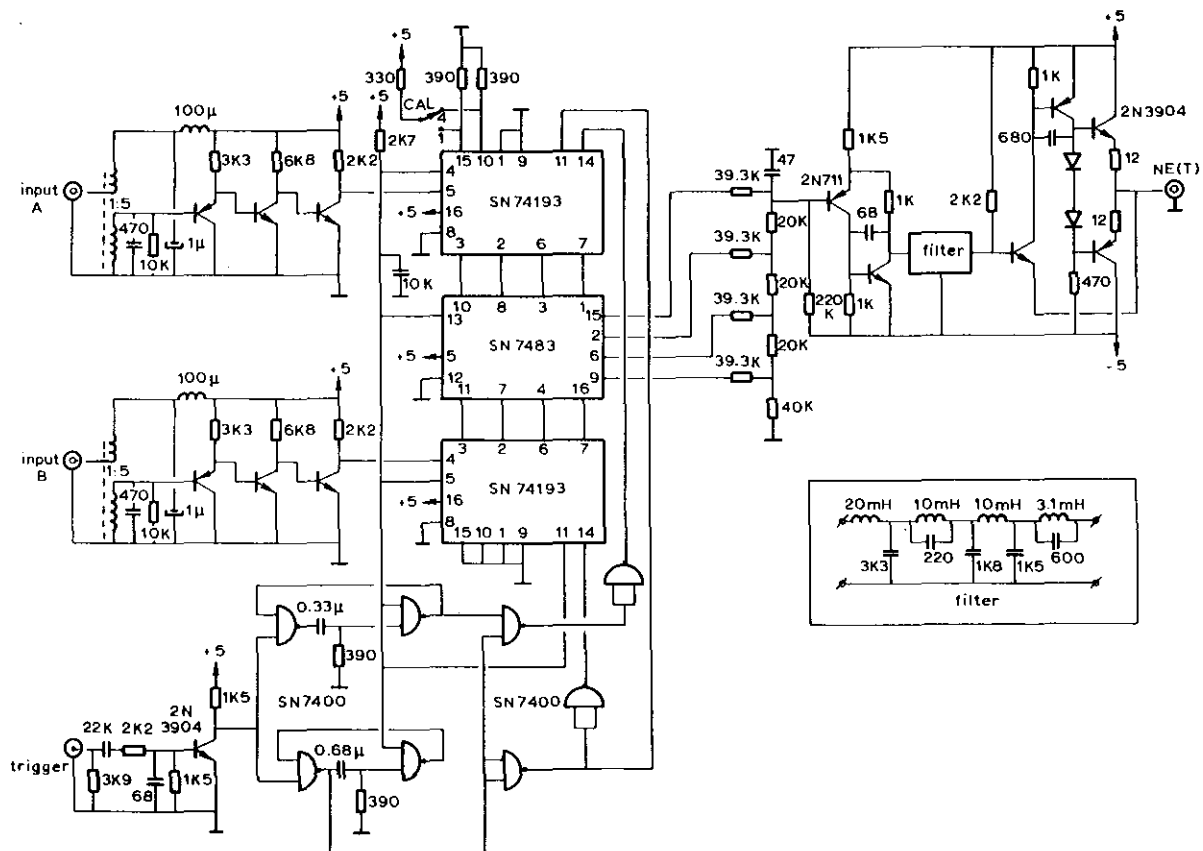
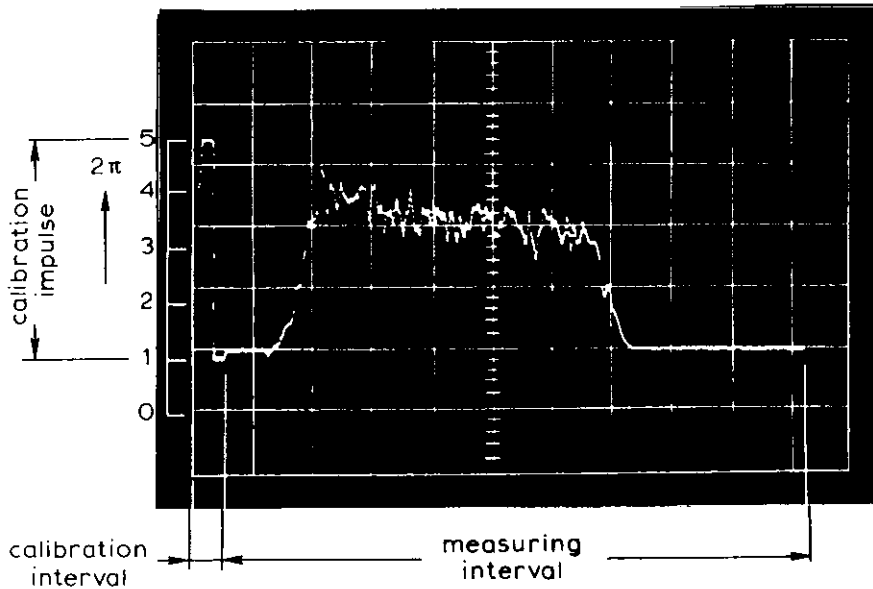


Fig. 3.4. Circuit diagram of the phase comparator.

delay in propagation of the carry-bit in the adder SN7483 this frequency is chosen as low as 20 kHz. The characteristic impedance of the filter is 2200 Ω. The output voltage ranges from -2.5V to +2.5V.

**Example of results**

The CO<sub>2</sub>- laser interferometer has been applied to the RINGBOOG-experiment of the FOM-Instituut voor Plasmafysica Rijnhuizen: a toroidal discharge experiment in which high-density, low-temperature plasmas with cold gas blankets have been studied [Orns-79]. The output from the phase comparator can be displayed on an oscilloscope (Fig. 3.5) or it can be used in a data-handling system by storing it in a transient recorder, in which case it can be readily correlated with other diagnostic datas.



*Fig. 3.5. Interferogram of a typical discharge in the RINGBOOG-experiment.  
horizontal axis: 500 μs/div.  
vertical axis: scale to be referred to the calibration step of  $4 \times 2\pi$ .*

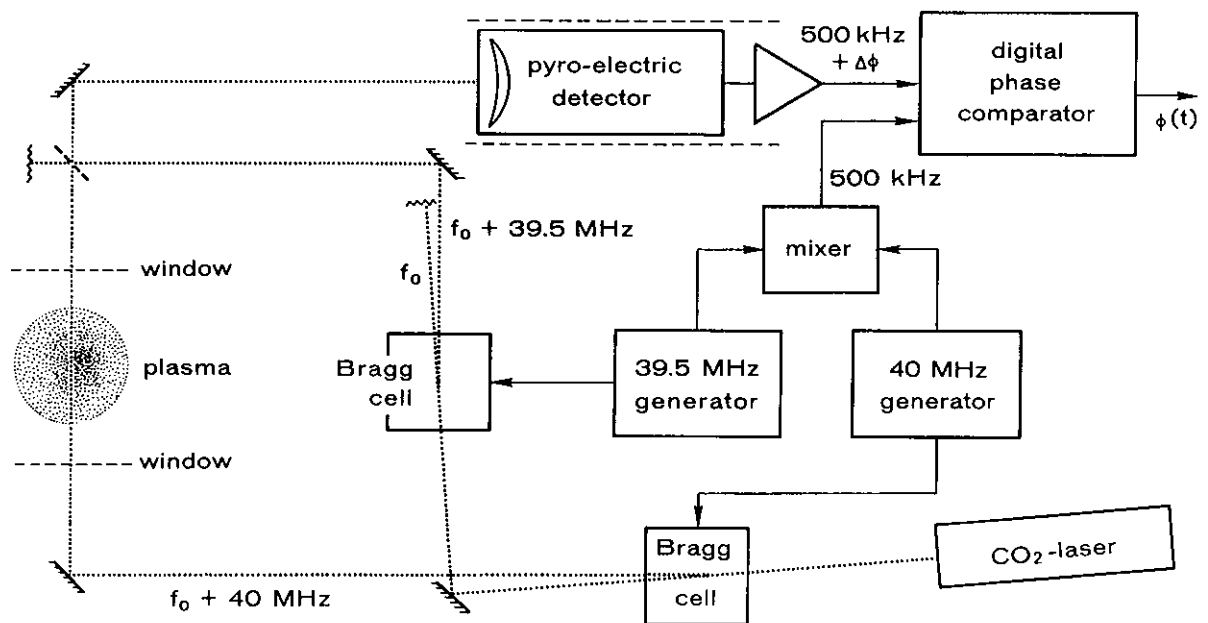


Fig. 3.6. CO<sub>2</sub>-laser interferometer with acousto-optic modulators.

### 3.3 CO<sub>2</sub>-laser interferometer with acousto-optic modulators \*)

Heterodyne operation has been accomplished in a different way by using two counteracting acousto-optic modulators at a frequency difference of 500 kHz [Huge-79]. Again, a digital phase comparator is used to obtain direct read-out of the phase shift.

The CO<sub>2</sub>-laser is a 3 W cw laser (Sylvania 941P) (Fig. 3.6). The acousto-optic modulators (Bragg cells, Isomat 1207) have been designed to work at modulation frequencies around 40 MHz. The only way to obtain a convenient frequency for the detector (500 kHz) is to use a heterodyne system with two counteracting modulators. In the reference path of the interferometer the frequency of the laser beam is shifted by 40 MHz and the shift in the work path is 39.5 MHz. The power in both beams is 200 mW.

Interference of these beams results in a beat signal at 500 kHz. The modulators are driven with two 12 W crystal controlled generators. A small part (approx. 20 mW) of the output signals of these generators is mixed to obtain a reference signal of 500 kHz. The interference signal, with an amplitude of 200 mW, is focused on a pyro-electric detector (Molelectron P3). The phase shift of the laser beam passing through the plasma causes a phase shift with respect to the 500 kHz reference frequency. This difference in phase is converted by means of a phase-to-voltage convertor. The beat frequency of 500 kHz is chosen sufficiently high to follow the density variations of the plasma (response time 3.5  $\mu$ s).

The signal-to-noise ratio is measured at the output of the detector amplifier (bandwidth 70 kHz) to be 40 dB. Obviously, this is well below the accuracy determined by the mechanical stability, which corresponds to a 2° uncertainty in phase. The non-linearity in the phase-to-voltage convertor is about 0.1% of full-scale. Full-scale can be chosen as a  $(1 \text{ to } 255) \times 2\pi$  phase shift. So, at the lowest densities measured, the inaccuracy in phase shift introduced by the electronic circuitry is negligible.

The water-cooled acousto-optic Bragg cells (frequency-shifters) have an aperture of 1 by 7 mm<sup>2</sup> and are sensitive to laser-beam polarization. The Bragg angle is 38.5 mrad and the beam separation is 77 mrad at the centre frequency of 40 MHz. The deflection efficiency is 50% with a drive power of 12 W. The advantage of an interferometer with acousto-optic modulators with respect to one with the Doppler wheel (Sec. 3.1.) is that a measurement can be taken at any trigger time, instead of only during the limited time interval in which a moving mirror is in a suitable position.

---

\*) This work was published earlier in the Rev. Sci. Instrum., 50 (1979) 1123.

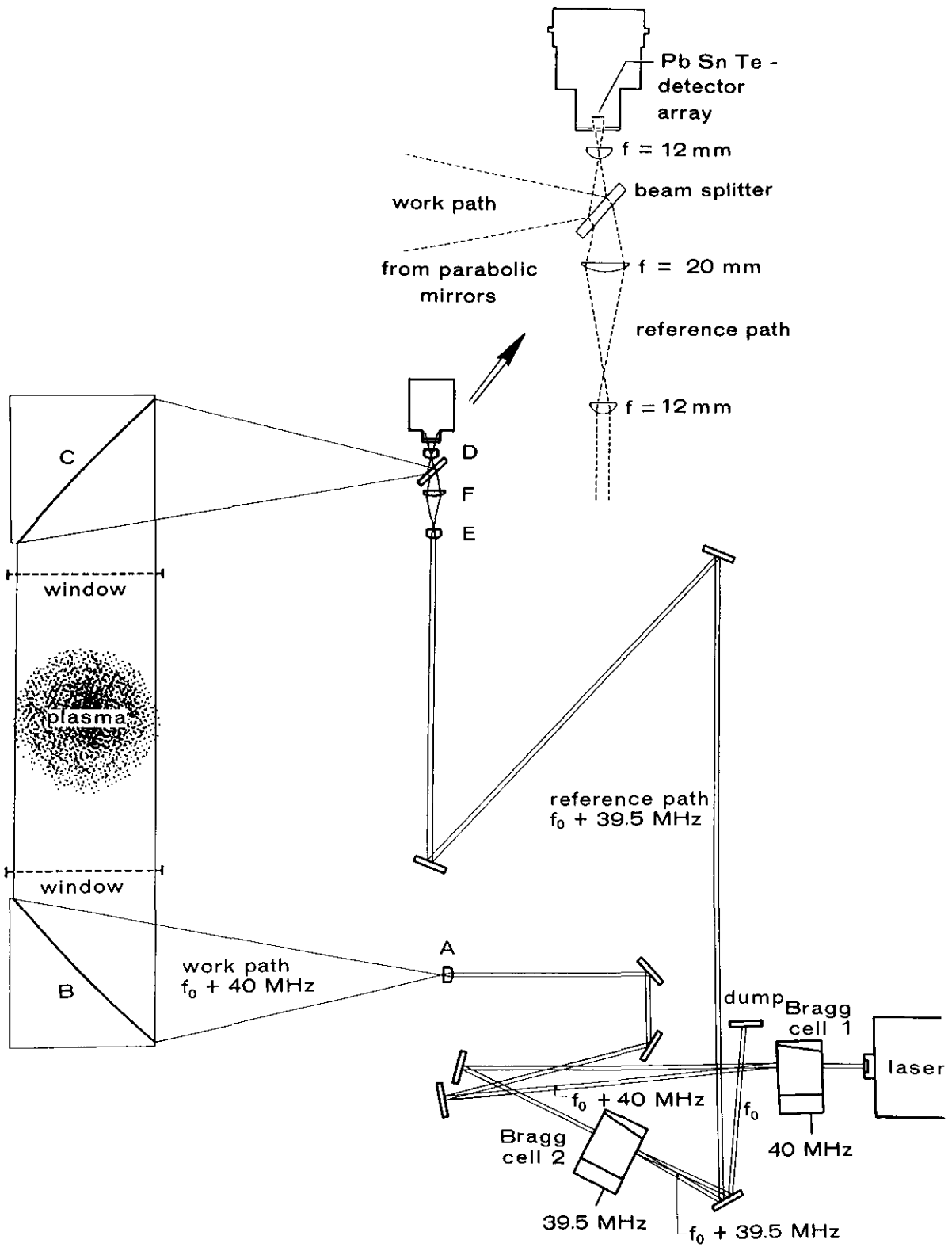


Fig. 3.7. Multi-channel CO<sub>2</sub>-laser interferometer.

### 3.4 Multi-channel CO<sub>2</sub>-laser interferometer using a PbSnTe detector array \*)

#### Introduction

With the CO<sub>2</sub>-laser interferometers described in Secs 3.2 and 3.3 density profiles could only be obtained on a shot-to-shot basis by shifting the whole instrument to different positions. To improve this situation a multi-channel CO<sub>2</sub>-laser interferometer has been built to measure electron density profiles of plasmas more reliably [Huge-82]. To this end, a sheet-like beam is transmitted in the work path over the total extension of the plasma, to be re-focussed onto a detector array, where interference with the reference beam occurs. In this way a 'phase image' of the plasma is produced on the array of detector elements. With the data acquisition system which is used, it is possible to follow the development in time of the profiles.

#### Description of the instrument

The CO<sub>2</sub>-laser is again the 3 W vertically polarized laser type (Sylvania 941S). On the wooden C-bracket, a rather simple instrument is constructed with a large number of channels (in our case 15, but this number could be increased even to 100, depending on the detector array used). A sheet-like, 200 by 7 mm<sup>2</sup> beam is made by the combination of the cylindrical ZnSe lens, A, and a gold-plated mirror, B, of parabolic shape in one direction. The beam is transmitted through the whole of the cross-section of the plasma (Fig. 3.7). The distance from the laser, with divergence 4 mrad, to lens A is 1.2 m, giving a good illumination of this 10 mm wide lens. This results in a power level difference over the entire surface of mirror B of less than 3 dB. The focal length of the lens is 12 mm. With the second parabolic mirror, C, and the cylindrical field lens, D, a 'phase image' of the plasma is focused onto a cooled (77 K), one-dimensional 15-element PbSnTe detector array. The reference beam is folded to obtain equal lengths in work and reference paths, in order to have the same beam divergences at the detector. The reference signal is also focused on the detector array with cylindrical lens, E. The cylindrical lens, F, focal length 20 mm, is added to diverge the reference beam to create enough space for the introduction of a beam splitter (cf. insert in Fig. 3.7). The plasma beam and the reference beam are shifted 40 and 39.5 MHz in frequency, respectively, by the acousto-optic modulators. The plasma causes different phase shifts over the width of the sheet-like beam. The different phase-shifts occurring at the 15 elements of the detector-array are converted by means of phase comparators yielding direct phase read-out.

---

\*) This work was published earlier in the Rev. Sci. Instrum., 53 (1982) 171.

### **Description of some components**

The gold-coated parabolic mirrors are made of 10 mm thick strain relaxed plexiglass using a milling machine with a digital read-out. The irregularities are within 1  $\mu\text{m}$  (i.e. 1/10 of the  $\text{CO}_2$ -laser wavelength). The mirrors are fixed to the C-bracket. All the mounts are again made out of non-metallic materials to avoid disturbances by eddy current forces.

The 15-element PbSnTe detector array, made by Plessey, is composed of  $250 \times 250 \mu\text{m}^2$  wide elements on a row with 50  $\mu\text{m}$  spacing. The power level measured at the detector array is 1.6  $\text{mW}/\text{mm}^2$ . The maximum allowed power level per element is about 6 mW, i.e. 100  $\text{mW}/\text{mm}^2$ . Focusing is only necessary to obtain a sufficient spatial resolution on the detector array. Since the power is high enough (signal-to-noise ratio 55 dB at a bandwidth of 70 kHz), focusing in the other direction is not necessary. Moreover, it would make the alignment more complicated.

### **Data acquisition**

The data acquisition system is shown in Fig. 3.8. The 15 signals from the detector array are fed to 15 current amplifiers and 15 different phase-to-voltage convertors. The phase comparators have a selectable measuring range from  $2\pi$  to  $255 \times 2\pi$ . An automatic calibration pulse, selectable from  $2\pi$  to  $64 \times 2\pi$ , is given 2 ms in advance of the discharge, as can be seen in Fig. 3.10b. These calibration pulses are processed to obtain the density scale of Fig. 3.10c. The data system with 16 sample-and-holds, a multiplexer, and an analog recorder (Biomation 805) can give scans with a minimum repetition time of 32  $\mu\text{s}$ . In the example given in Fig. 3.10 a repetition time of 320  $\mu\text{s}$  is used. The sample time of the multiplexer is less than 20 ns. As the data system has one unused channel, this free channel is connected to +5 V to give a marker at the beginning of each scan. A second recorder is used to follow one of the channels continuously (Fig. 3.10b).

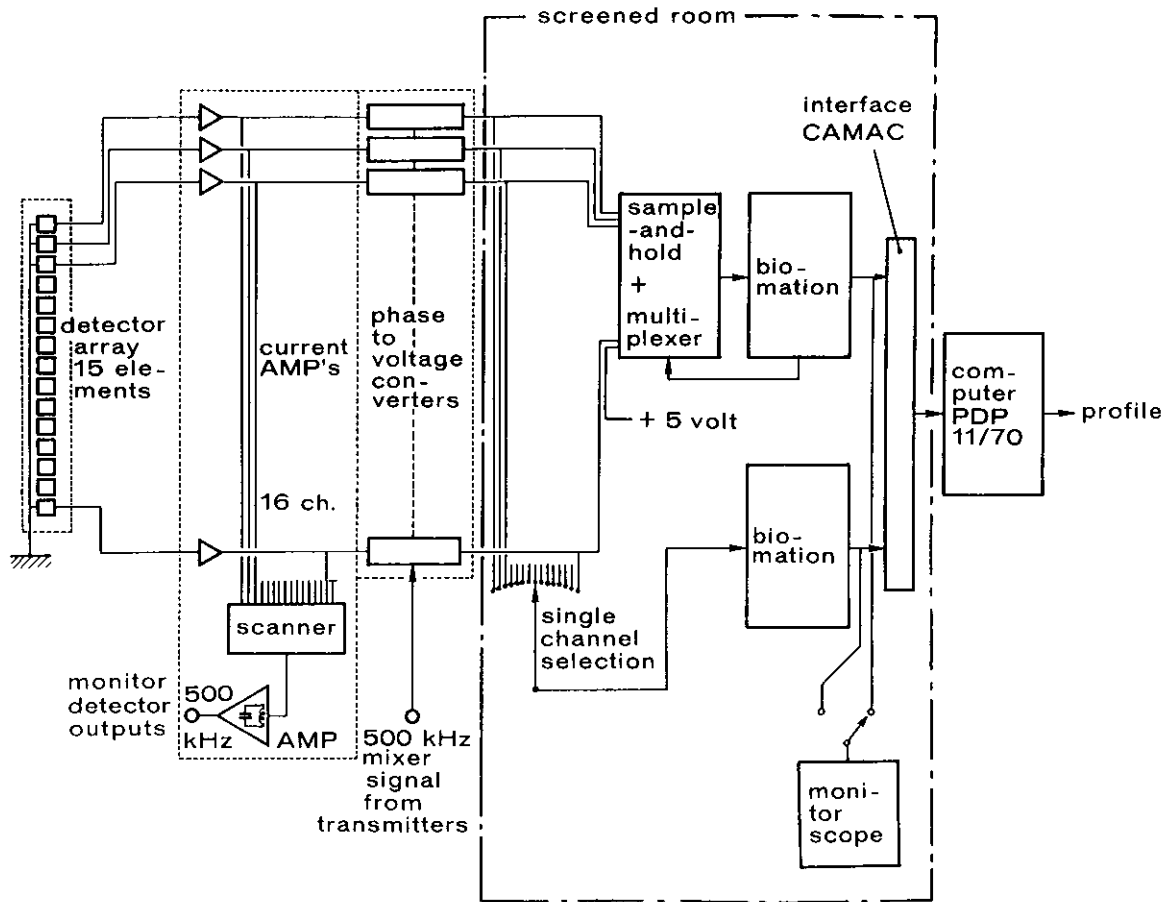
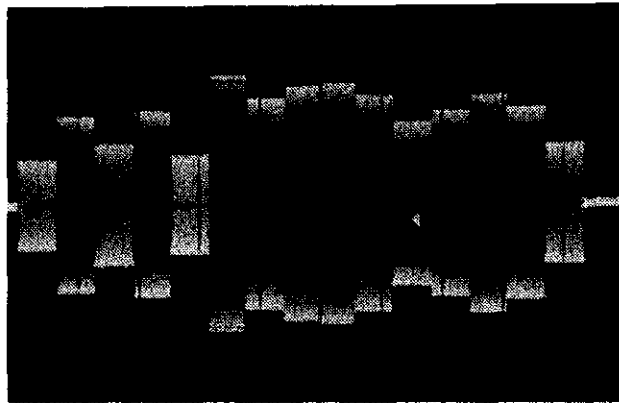


Fig. 3.8. Data acquisition system.

### Alignment

The first global alignment of laser, modulators, and mirrors was done with thermal image plates and an ultraviolet lamp. By switching the hf transmitters on/off with 500 kHz the reference or the work path can be measured separately. The 16-port scanner gives a view of the power distribution over the 15 elements of the array; the 16th channel is short-circuited to give zero output.



*Fig. 3.9. Scanner output.  
Horizontal scale: 1 ms/cm,  
vertical scale: 500 mV/cm.*

The scanner is followed by a 500 kHz selective amplifier. When the two beams are aligned the keying of the hf transmitters is switched off and the interferometer is finally adjusted for maximum interference (Fig. 3.9). There is some variation in the sensitivity of the single elements of the array. This variation is not important since the output level far exceeds the minimum input required for the phase-to-voltage convertors.

### Results

The multi-channel CO<sub>2</sub>-laser interferometer described here has been proven to be a reliable tool to measure plasma density profiles in one single shot (Fig. 3.10). After reading the output of the transient recorder with a computer, the signals are de-multiplexed and corrected for the phase offsets. The measurements of density profiles done with this system are more reliable than the measurements performed in a shot-to-shot procedure. Furthermore, the optical system described here is also well suited for other FIR (far-infra-red) lasers. The minimum line-integrated density which can be measured is of the order of  $2.5 \times 10^{17} \text{ m}^{-2}$ , corresponding to an uncertainty in phase of  $1^\circ$ .

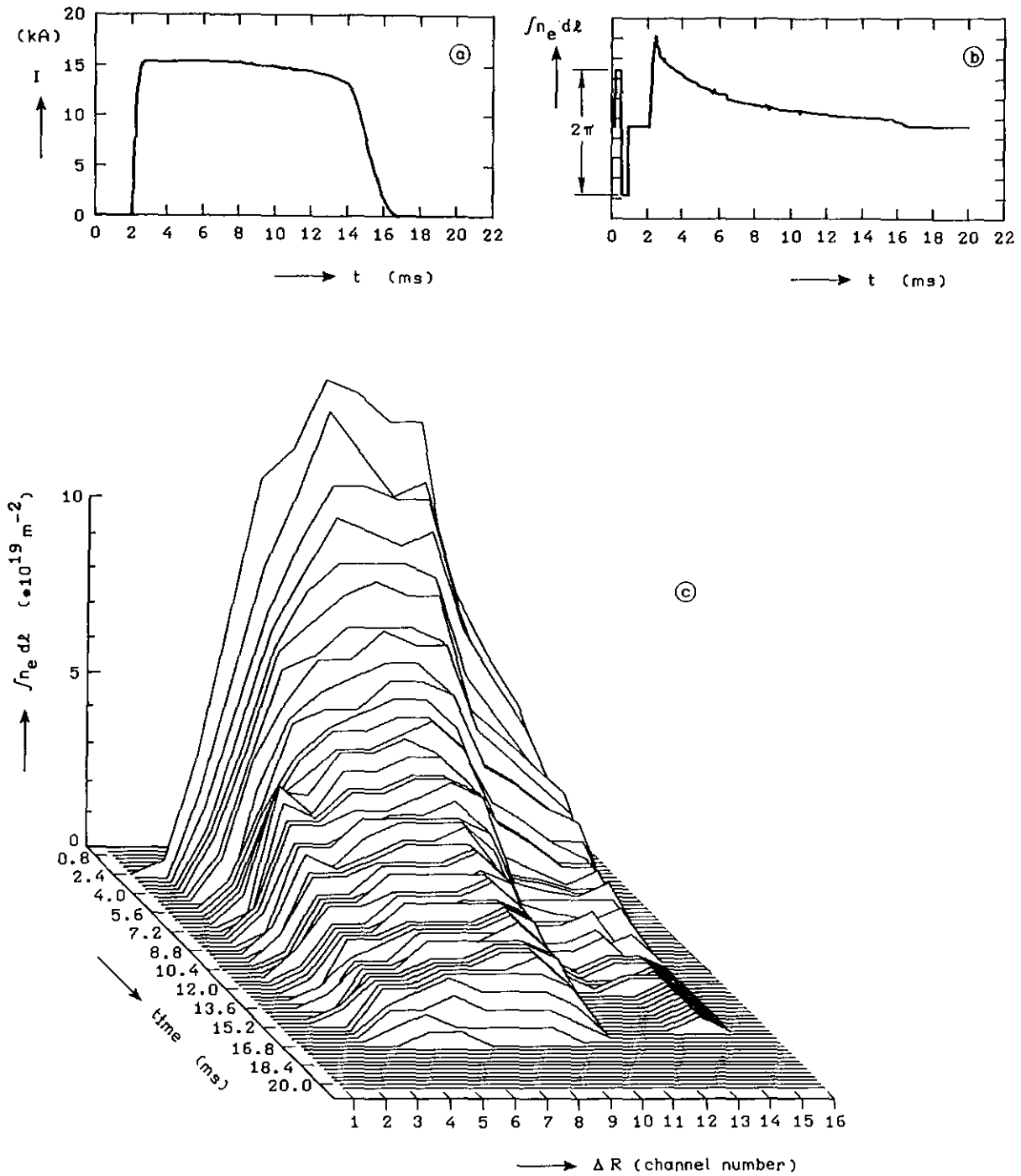


Fig. 3.10. Line-integrated density measurements in the RINGBOOG experiment.

a) Plasma current.

b) Transient recorder signal of channel 8 before processing.

Calibration pulse:  $2\pi$  is  $2.11 \times 10^{20} \text{ m}^{-2}$ .

c) Output of the 15-channel interferometer as a function of time.

Obs. In this case the diffraction could amount to maximum  $5 \times 10^{-4}$  rad.



## Appendix A

### A SIMPLE METHOD TO OBTAIN POLAR INFORMATION WITH A NORMAL MICROWAVE INTERFEROMETER \*)

#### Introduction

A simple method to obtain polar information from a microwave interferometer is described here [Huge-70]. The two paths in the microwave interferometer are made unequal in length so that the output becomes frequency dependent. Square-wave modulation of the repeller voltage of the klystron is used to obtain two signals with slightly different frequencies. An appropriate choice of the frequency difference can yield a  $\frac{\pi}{2}$  phase difference, so that a polar interferometer results. With the method described here polar information can be obtained with a good time response by means of a single null-path bridge. The economy of microwave components is obtained at the cost of only a slightly increased complexity of the low-frequency electronics.

The following considerations are fundamental for the method. In an interferometer bridge with a difference  $\Delta L$  between the work path and the null path, the phase difference  $\Delta\phi$  between the two paths is

$$\Delta\phi = \frac{2\pi\Delta L}{\lambda_g}, \quad (1)$$

where  $\lambda_g$  is the guide wavelength. If the frequency  $f$  at which the interferometer is operated is varied, one finds

$$\frac{d(\Delta\phi)}{df} = \frac{2\pi\Delta L}{c} \frac{\lambda_g}{\lambda}. \quad (2)$$

Now, if the frequency is switched from  $f$  to  $f+\Delta f$ , one obtains for  $\Delta\phi$ , corresponding to a  $\frac{\pi}{2}$  phase difference,

$$\Delta\phi = \frac{c}{4\Delta L} \frac{\lambda}{\lambda_g}. \quad (3)$$

---

\*) This work was published earlier in the Journal of Physics E: Scientific Instruments 3 (1970) 750.

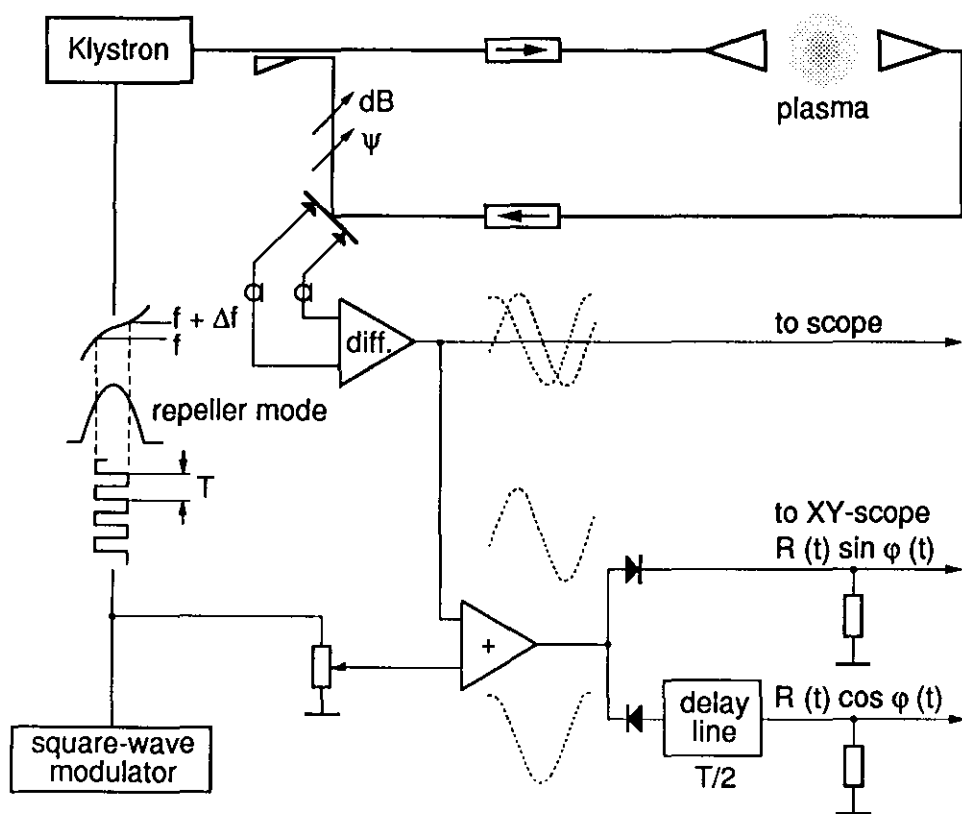


Fig. A.1. Block diagram of the interferometer.

As an example: for an interferometer with central frequency  $f= 33.750$  GHz and path difference  $\Delta L= 3.9$  m, a frequency difference  $\Delta f= 15$  MHz is required. The  $\Delta f$  chosen here is sufficiently large to neglect frequency instabilities of the klystron. An interferometer of this type (Fig. A.1) has for instance been used in connection with microwave reflection probes [Herm-66, Bobe-68].

### Description of the method

Square-wave modulation of the repeller voltage of a 80 mW cw 8 mm Klystron (Philips 41 DS) leads to the required frequency switching. The two power levels can be made equal by tuning the repeller voltage. The phase difference of the two signals at the balanced detector can be adjusted to  $\frac{\pi}{2}$  by choosing the amplitude of the square-wave voltage. The detection is done with a pair of balanced crystal detectors (1N26). The output of the differential amplifier is then alternately proportional to  $\sin\phi$  and  $\cos\phi$ . Notice that the signals have the same amplitude and the same zero-line. The complete polar information as a function of time is included in this 'chopped' signal. It is possible to separate the signals in the following way. The same square-wave voltage that modulates the klystron is added to the signal so that, for example, a positive voltage is added to the  $\sin\phi$  component and a negative voltage to the  $\cos\phi$  component. The resulting separation can be adjusted with the amplitude control of the square-wave. Two diodes connected in opposite polarity split the signals. A delay line with a delay time of half a period of the square-wave makes it possible to have  $\sin\phi$  and  $\cos\phi$  information coinciding in time. Feeding of these two signals to an XY-oscilloscope results in a polar display.

### Remarks

The adjustment of the bridge described here is simple, since only one balanced detector is used. These simplifications also facilitate polar measurements at higher frequencies (140 GHz). Moreover, this method is suitable for taking measurements of rapidly varying quantities, since the response is only limited by the modulation frequency of the repeller voltage. This can easily be as high as 10 MHz [Orns-62].

## Appendix B

**A RIGID MICROWAVE ACCESS LENS INTO COPPER-SHIELDED  
PLASMA PHYSICS EXPERIMENTS \*)**

A microwave lens is described which gives access through thick copper shells of toroidal discharge experiments without disturbing the plasma-stabilizing effect of those shells [Huge-74]. The lens consists of a number of small cylindrical holes drilled in a flat, metal disc. When the distance from the centre is increased the holes in the lens become smaller in diameter, so the phase velocity will increase towards the edge, which produces a focusing effect for waves (Fig. B.1).

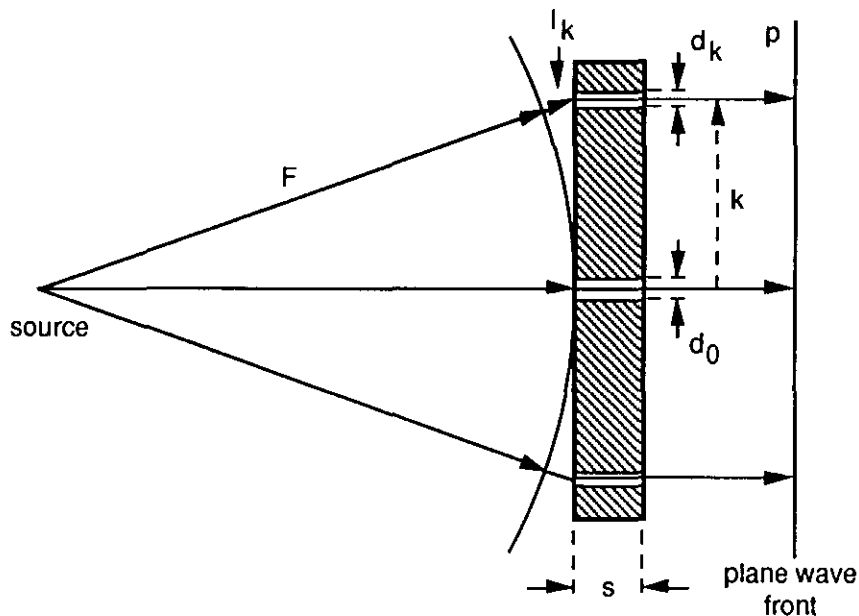


*Fig. B.1. The path lengths of all rays going from the source point to the plane p are of equal length if  $l_k/\lambda + s/\lambda_{gk} = s/\lambda_{g0}$ .*

The phase velocity  $v_p$  in an air-filled waveguide, given by the formula

$$v_g = f \lambda_g, \quad (1)$$

is greater than  $c$  by a factor  $\lambda_g/\lambda$  where  $f$  is the frequency considered.

\*) This work was published earlier by the author in the Rev. Sci. Instrum., 45 (1974) 1474.

The wavelength in the waveguide  $\lambda_g$  is given by

$$\lambda_g = \frac{\lambda}{\sqrt{1 - (\lambda/\lambda_c)^2}}, \quad (2)$$

where  $\lambda$  is the free-space wavelength and  $\lambda_c$  the cut-off wavelength. The cut-off wavelength in a circular waveguide depends on the diameter  $d$  of the guide. For the  $TE_{11}$  wave used, the cut-off wavelength is

$$\lambda_c = 1.706 \times d. \quad (3)$$

The second higher mode is the  $TM_{01}$ , with cut-off wavelength

$$\lambda_c = 1.306 \times d. \quad (4)$$

To avoid higher-order modes, the diameter of the circular waveguide must lie within the limits given by

$$\frac{\lambda}{1.706} < d < \frac{\lambda}{1.306}. \quad (5)$$

In order to focus the diverging rays from a point source into a plane wave, the path length of all rays coming from the source and going to the plane  $p$  must be made of equal length. This is accomplished when

$$\frac{l_k}{\lambda} + \frac{s}{\lambda_{gk}} = \frac{s}{\lambda_{go}}, \quad (6)$$

where  $\lambda_{go}$  is the wavelength in the centre hole,  $d_o$ , and  $\lambda_{gk}$  the wavelength in the hole,  $d_k$ , at a distance  $k$  from the centre of the lens. The path length  $l_k$  is given by

$$l_k = \sqrt{k^2 + F^2} - F, \quad (7)$$

where  $F$  is the focal length.

With a chosen centre hole just under the limit of the  $TM_{01}$  mode, one can calculate the proper diameter of the hole  $d_k$  at a distance  $k$  from the centre in the following way:

$$\lambda_{gk} = \frac{s}{s/\lambda_{go} - l_k/\lambda} = \frac{\lambda}{\sqrt{1 - (\lambda/\lambda_{ck})^2}}, \quad (8)$$

where

$$\lambda_{ck} = 1.706 d_k. \quad (9)$$

From the two formulas (8 and 9)  $d_k$  can be solved

$$d_k = \frac{0.586\lambda}{\sqrt{1 - \left( \sqrt{1 - (\lambda/\lambda_{co})^2} - l_k/s \right)^2}}, \quad (10)$$

where  $\lambda_{co} = 1.706 d_o$ .

The holes in the lens are drilled in the metal disc in a hexagonal pattern, with a precision of 0.05 mm (Fig. B.2).

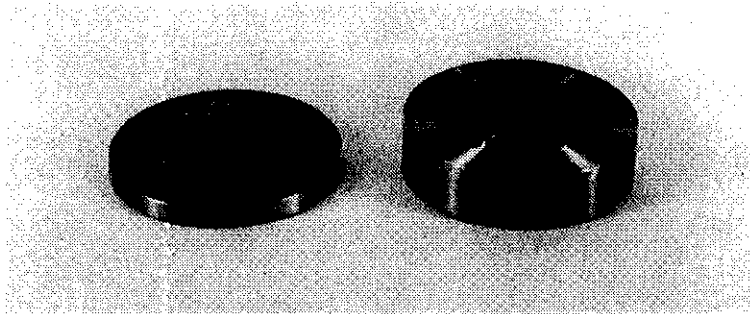


*Fig. B.2. Microwave lenses with focal lengths of 40 and 60 mm (frequency 70 GHz). The holes in the 10 mm thick copper disc lens at the right vary from 3.20 mm in the centre to 2.95 mm at the edge of the lens.*

The simplicity of the construction makes this lens favourable over lenses based on the same principle with elliptical cross-section and holes of constant diameter. The measured focal length is found to be somewhat shorter than the chosen focal length due to boundary effects of the waveguides. The lens is designed for a 70 GHz microwave interferometer used for electron density measurements in the low-density plasma regime of a screw-pinch experiment [Bobe-73].

With the lenses described here, fitted in the copper shell, the losses were 5 dB without spoiling the plasma-stabilizing effect of the copper shell. With normal horn antennae ( $3\lambda$  long) the transmission losses would have amounted to 25 dB.

**PART 2**

**REFLECTOMETRY**



## Chapter 4

### INTRODUCTION TO REFLECTOMETRY

#### 4.1 Principle of reflectometry

Reflectometry relies on the total reflection of electromagnetic waves by a plasma. When an electromagnetic wave propagates through an unmagnetized cold plasma and if non-linear effects can be neglected, the refractive index is given by:

$$\mu^2 = 1 - \frac{f_p^2}{f^2} \quad (\text{cf. Eq. 1.6, p. 16}) \quad (4.1)$$

The basic principle of a reflectometer is shown in Fig. 4.1. A microwave beam is launched from an antenna towards the plasma. As the wave propagates into the plasma, it will experience a decreasing refractive index due to the fact that the local plasma frequency increases with increasing electron density. Eventually, when the electron density is high enough, the wave will be reflected when the electron density is critical such that  $f = f_p$ , and where  $\mu^2 = 0$ . The microwave beam, reflected from this critical density layer, is received by a second antenna located outside the plasma and is consequently combined with the reference beam. The phase difference of the two signals results in an interference signal at the detector. Any change in phase is due to either the changes in the location of the critical density layer or to changes in frequency of the wave.

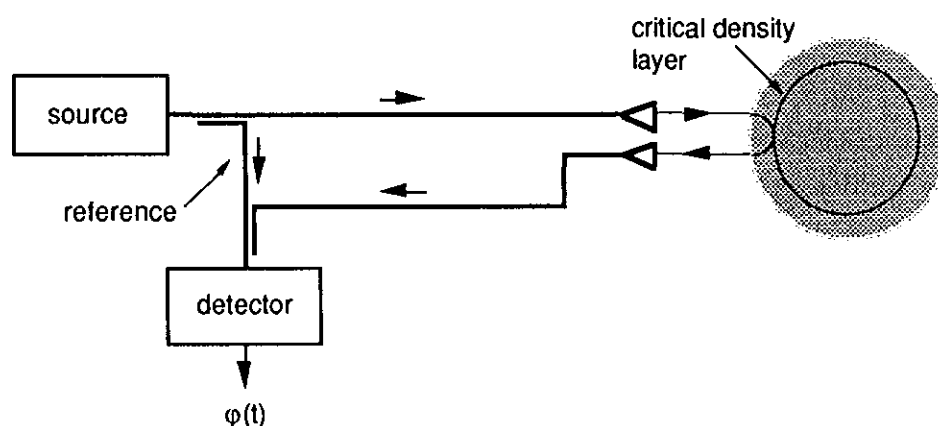


Fig. 4.1. Microwave reflectometer.

In practice, reflectometers may be operated in two different modes: at a fixed frequency and with swept frequency. The difference between the two modes of operation will be shown below.

The signal path  $L_s$  contains a number of wavelengths, a:

$$L_s = a \lambda, \text{ where } a = \frac{\varphi_s}{2\pi}, \quad (4.2)$$

and the reference path  $L_r$  contains a number of wavelengths, b:

$$L_r = b \lambda, \text{ where } b = \frac{\varphi_r}{2\pi}, \quad (4.3)$$

where  $\varphi_s$  and  $\varphi_r$  are the phases of the waves after travelling through the signal path and the reference path, respectively.

The length of the signal path may vary as a function of time  $L_s(t)$  and the reference path is always kept constant; the Eqs (4.2) and (4.3) then yield:

$$\varphi_s = L_s(t) \frac{2\pi f}{c}, \text{ and } \varphi_r = L_r \frac{2\pi f}{c}. \quad (4.4)$$

The phase difference at the detector is

$$\varphi = \varphi_s - \varphi_r = \{L_s(t) - L_r\} \frac{2\pi f}{c}. \quad (4.5)$$

Since not only the length  $L_s(t)$  may vary in time but also the frequency may be varied, any change in the phase difference becomes:

$$\delta\varphi = \delta\{L_s(t) - L_r\} \frac{2\pi f}{c} + \{L_s(t) - L_r\} \frac{2\pi}{c} \delta f. \quad (4.6)$$

In the case where the frequency of the wave is held constant  $\delta f = 0$ , changes in phase can only result from changes in  $L_s(t)$ : (Eq. 4.6), which can only be caused by movements of the reflecting layer. Thus in this mode, the fixed frequency mode, changes in the position of a critical electron density layer in the plasma are measured. To follow the effects at different density layers, several sources with different frequencies are used simultaneously.

In the other mode the frequency is swept,  $\delta f \neq 0$ . When the plasma conditions are stationary, only the frequency sweep can cause changes in the phase. When the change in phase is measured and the frequency sweep is known exactly the value of  $L_s - L_r$  is found. If  $L_r$  is known, the exact location is found at which the reflection takes place. Errors in this measurement of the absolute position will occur when the reflecting layer is moving during the course of the frequency sweep.

As an illustration a practical example will be given:

- probing frequency,  $f$  30 GHz,
- frequency sweep,  $\Delta f$  100 MHz,
- path difference,  $L_S - L_T$  6 m,
- assuming a change in the path difference,  $L_S - L_T$ , due to plasma movements during the sweep (e.g. during 5 ms) 0.5 mm.

With these numbers Eq. 4.6 gives,  $\Delta\phi = 0.1\pi + 4\pi$ . Here, the term  $4\pi$  corresponds to the path difference of 6 m and the term  $0.1\pi$  stands for the above mentioned error, corresponding to 0.15 m. It is clear that the magnitude of this error can lead to serious problems, certainly when the frequency is swept slowly over a broad band [Anab-88, Simo-85]. When the frequency sweep is narrow and fast a check on the change in path difference must still be made; this is possible when swept frequency operation is alternated with fixed frequency operation. The fixed frequency data can then be used to correct the swept frequency data. An example of this technique is given in Sec. 5.5, p. 122. To measure the location of several different density layers a number of frequencies must be applied. A twelve-channel instrument, using narrow-band sweep, is developed for the JET tokamak and is described in Ch. 5 [Boro-86, Huge-86, Pren-88].

In the description given above (Eqs 4.2 to 4.6) the presence of the plasma in front of the reflecting layer where the density reaches the critical value is ignored. Hubbard [Hubb-87] has shown that for the most common plasma density distributions the average refraction index for the plasma in front of the critical density layer becomes:

$$\langle\mu\rangle \approx 0.6. \quad (4.7)$$

The error is only 1% for parabolic profiles at the plasma edge but becomes larger at the plasma centre. A change in the position of the critical density layer,  $\Delta L$ , may be inferred from the measured phase change,  $\Delta\phi$ , by

$$\Delta L = \frac{\lambda_0}{2} \frac{\Delta\phi}{\langle\mu\rangle} \approx \frac{1}{2} \frac{\lambda_0}{0.6} \frac{\Delta\phi}{2\pi}, \quad (4.8)$$

where  $\lambda_0$  is the vacuum wavelength corresponding to the applied probing frequency.

## 4.2 Profile measurements from phase information with swept frequency

We consider again the phase difference,  $\varphi$ , between the signal transmitted on a round trip up and down the plasma path and the signal sent through the reference path. When the working frequency of the reflectometer is swept the difference in length between the two paths will cause variation in the phase difference (cf. Eq. 4.6). This leads to a beat (fringe) frequency,  $f_B$ , at the detector

$$f_B = \frac{1}{2\pi} \frac{d\varphi}{dt} = \frac{1}{2\pi} \frac{\delta\varphi}{\delta f} \frac{df}{dt}, \quad (4.9)$$

or

$$f_B = \tau(f_0) \frac{df}{dt}, \quad (4.10)$$

where

$$\tau(f_0) = \frac{1}{2\pi} \frac{\delta\varphi}{\delta f} \quad *), \quad (4.11)$$

is the difference between the time delays of the two signals propagating through the signal path and through the reference path of the reflectometer, which operates at the frequency,  $f_0$ .

The net delay,  $\tau(f_0)$ , consists of the delay occurring in the non-plasma part of the signal path,  $\tau_g(f_0)$ , in the plasma,  $\tau_p(f_0)$ , and in the reference path,  $\tau_r(f_0)$ :

$$\tau(f_0) = \tau_g(f_0) + \tau_p(f_0) - \tau_r(f_0) = \frac{1}{2\pi} \left( \frac{\delta\varphi_g(f_0)}{\delta f} + \frac{\delta\varphi_p(f_0)}{\delta f} - \frac{\delta\varphi_r(f_0)}{\delta f} \right). \quad (4.12)$$

Now,  $\tau_g(f_0)$  (waveguide, vacuum, etc.) and  $\tau_r(f_0)$  (waveguide) are determined by the construction of the reflectometer as discussed in Sec. 5.4. At this point, the only relevant term is:

$$\tau_p(f_0) = \frac{1}{2\pi} \frac{\delta\varphi_p(f_0)}{\delta f}. \quad (4.13)$$

---

\*) There is, of course, a direct relation between  $\tau$  and the path length difference ( $L_s - L_r = \Delta L$ ). Referring back to Eq. 4.6, the time delay  $\tau$  will become

$$\tau = \frac{1}{2\pi} \frac{\delta\varphi}{\delta f} = \frac{\Delta L}{c}.$$

For the typical, practical value of  $\Delta L$  is 6 m the time delay becomes 20 ns.

The phase  $\varphi_p(f_0)$  is an integral of the refractive index  $\mu(f_0, x)$  along the direction of propagation,  $x$ :

$$\varphi_p(f_0) = \frac{4\pi f_0}{c} \int_0^{x_c(f_0)} \mu(f_0, x) dx - \frac{\pi}{2} \quad *) \quad [\text{Budd-61, Ginz-61}]. \quad (4.14)$$

In this expression the edge of the plasma is at  $x=0$ , and the cut-off point is at  $x_c(f_0)$ , where  $\mu(f_0, x_c) = 0$ . Equation 4.14 can be rewritten with Eqs 4.1 and 4.13 to give the time delay,  $\tau_p(f_0)$ , as

$$\tau_p(f_0) = \frac{2}{c} \int_0^{x_c(f_0)} \frac{1}{\sqrt{1 - \frac{f_p^2}{f_0^2}}} dx \quad [\text{Doan-81}]. \quad (4.15)$$

This integral can be converted into an Abel integral equation when  $\tau_p(f_0)$  is measured in a number of different frequency bands at a number of different values of  $f_0$ . The solution is:

$$x(f_p) = \frac{c}{\pi} \int_0^{f_p} \frac{\tau_p(f_0)}{\sqrt{f_p^2 - f_0^2}} df_0. \quad (4.16)$$

Here  $x(f_p)$  is the position at which the density becomes critical for waves with frequency  $f_0 = f_p$ , and at which the reflection occurs. From Eq. 4.16 it can be understood that this means:  $x(f_p) = x(n_e)$ , and that the density profile  $n(x)$  can be inferred from  $x(f_p)$ .

In the reflectometer for JET (Ch. 5) a number of different probing frequencies are used. Each frequency is swept, but only over a small range ( $\Delta f \approx 100$  MHz) to produce phase changes. This yields values for  $\tau_p(f_0)$  at the probing frequencies. By numerical integration the values can now be inverted to find  $x(f_p)$  (Eq. 4.16); the values of  $\tau(f)$  between the measured values of  $\tau(f_0)$  are obtained by interpolation or by substitution of a simulated profile. Data below the lowest frequency must be simulated using an assumed or an independently measured density profile at the outer edge of the plasma. Hubbard [Hubb-87] demonstrated that the inversion error, when 12 probing frequencies were used, stays below 1% for a large variety of profile shapes.

---

\*) The phase integral (Eq. 4.14) neglects the breakdown of geometric optics (the WKB approximation) near the turning point  $x=x_c$  [Hubb-87]. Full wave calculations show, however, that this neglect is usually insignificant. For a linear density profile the approximation results in the term  $-\pi/2$ , regardless of the slope of the profile.

### 4.3 Complications due to external magnetic fields

It is well known that the plasmas in tokamaks are confined by means of magnetic fields. The main component is the externally applied field  $\mathbf{B}_T$ . In reflectometry waves are transmitted towards the plasma perpendicular to  $\mathbf{B}_T$ . Those waves can be decomposed into two polarizations:

- the ordinary wave (O-mode) with the electric vector of the wave  $\mathbf{E}$  parallel to the external magnetic field  $\mathbf{B}_T$  in the plasma ( $\mathbf{E} \parallel \mathbf{B}_T$ ),
- the extra-ordinary wave (X-mode) with the electric vector of the wave  $\mathbf{E}$  perpendicular to the external magnetic field  $\mathbf{B}_T$  ( $\mathbf{E} \perp \mathbf{B}_T$ ).

For O-modes, with  $\mathbf{E} \parallel \mathbf{B}_T$ , the electron motion in the waves' E-field is parallel to the magnetic field, so there is no first-order effect on electron motion and the wave propagation is the same as in an unmagnetized, cold, plasma.

Resonance effects must only be taken into account in hot magnetized plasmas. Resonance occurs when the applied frequency,  $f$ , equals  $f_{ce}$ , the electron cyclotron frequency,

$$f_{ce} = \frac{1}{2\pi} \frac{eB}{m_e} . \quad (4.17)$$

In a tokamak the magnetic field  $B_T$  varies in space as

$$B_T(R) = B_T(R_0) \frac{R_0}{R} , \quad (4.18)$$

where  $R$  is the major radius,  $R_0$  is the radius of the magnetic axis, and  $B_T(R)$  and  $B_T(R_0)$  the values of the magnetic fields at these locations. Ordinary waves propagate through the regions in the plasma where the density is below the cut-off, up to the region where the magnetic field reaches the electron cyclotron resonance value, where absorption occurs. The absorption at  $f_{ce}$  of the O-mode wave takes place in a hot plasma due to relativistic effects [Born-83]; the absorption depends on the electron temperature and on the curvature of the magnetic field. The resonant interaction of ordinary waves at the second harmonic of the cyclotron frequency,  $f = 2f_{ce}$ , is negligible.

One of the obstacles of reflectometry [Hubb-87, Pren-88a] is the possibility that the absorption of the probing wave occurs at this resonance before it reaches the reflecting layer. In Fig. 4.2 the region accessible to O-mode waves is indicated for two different density profiles with maximum densities of  $5$  and  $10 \times 10^{19} \text{ m}^{-3}$  respectively, for the external magnetic field in the centre of the plasma,  $B_T(R_0) = 3.0 \text{ T}$ . Observe: there is a narrow frequency band where the absorption can occur.

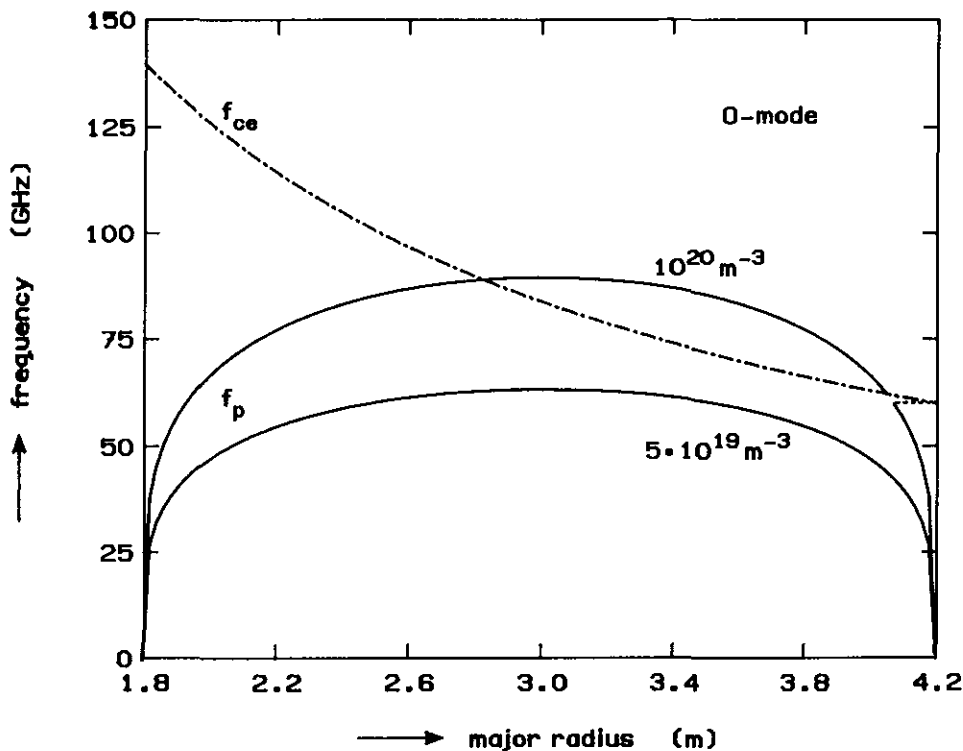


Fig. 4.2. Spatial variation of the cut-off layers, for two different density profiles in JET, for O-mode waves, propagating from the outside. Curve ' $f_{ce}$ ' gives the spatial variation of the electron cyclotron resonance frequency when  $B_T(R_0) = 3.0$  T.

The area at about 61 GHz indicates the small inaccessible part of the profile.

It is obvious that the inner half of the plasma can not be measured with O-mode waves when the reflectometer is installed at the outside of the torus; two reflectometers launching waves from both sides of the plasma are needed to measure the complete profile [Mans-88].

If the extra-ordinary wave ( $\mathbf{E} \perp \mathbf{B}_T$ ) is used, the situation becomes far more complex, since  $\mu^2$  depends not only on the local density but also on the local strength of the external magnetic field. Therefore, the X-mode was not used in the work described in this thesis. However, it should be mentioned that in some experimental facilities it is possible to make a limited use of X-mode waves in reflectometry to measure profiles at low electron densities over a rather larger extent [Anab-88, Bott-87, Doyle-89, Lehe-88]. The applicability depends on a number of conditions such as the compactness of the geometry, strength of the magnetic field, etc.



## Chapter 5

## THE MULTI-CHANNEL REFLECTOMETER FOR JET

## 5.1 Introduction

A twelve-channel reflectometer, operating in the O-mode, has been developed and constructed for the JET tokamak experiment. The objective of the reflectometer diagnostic is to measure changes of the electron density profile and electron density fluctuations, and to determine electron density profiles in the plasma. Since the distance from the JET tokamak to the diagnostic area is of the order of 30 meters, an oversized waveguide has to be used to keep the attenuation low. A drawback of oversized waveguides is that the bends, tapers and other waveguide structures can easily lead to mode-conversion and to unwanted reflections, giving resonances in the waveguide system. For this reason, an assembly of 12 different reflectometers is chosen, working at fixed frequencies, slightly tuneable (over  $\sim 300$  MHz) to avoid resonances etc. Alternatively, the reflectometers may be used in a swept frequency mode within narrow frequency bands ( $\Delta f \approx 100$  MHz). The chosen frequencies are 18, 24, 29, 34, 39, 45, 50, 57, 63, 69, 75 and 80 GHz; the corresponding critical densities are in the range of  $0.4$  to  $8.0 \times 10^{19} \text{ m}^{-3}$  (Fig. 5.1). The spacing of the frequencies of the different channels is optimized to give the best accuracy in the outer region of the plasma, where the accuracy from other electron density diagnostics is poor.

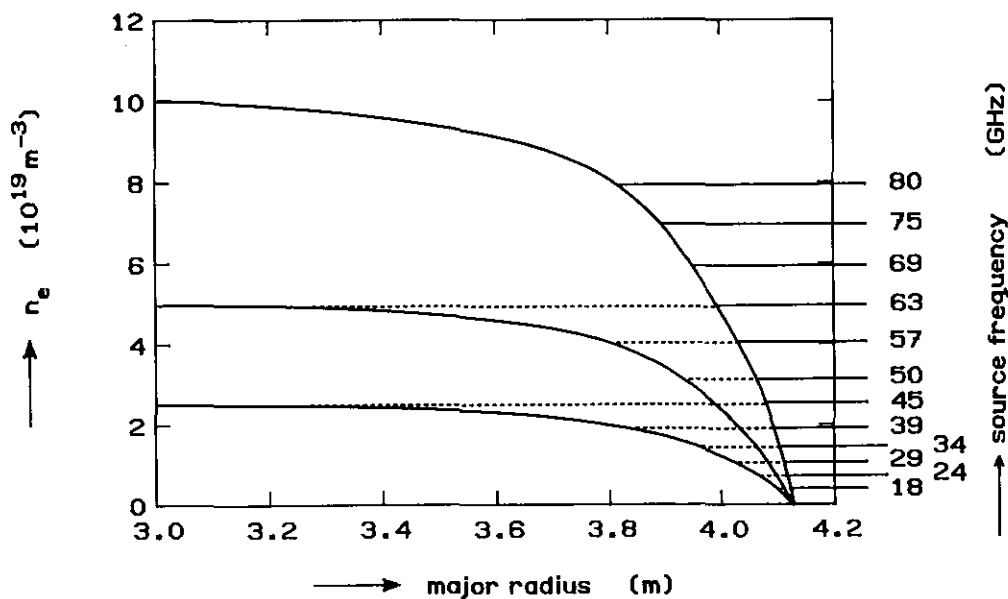


Fig. 5.1. Critical densities corresponding to the frequencies used in the multi-channel reflectometer. Schematical density profiles are shown with three different maximum values at the axis,  $R_0 = 3.0$  m.

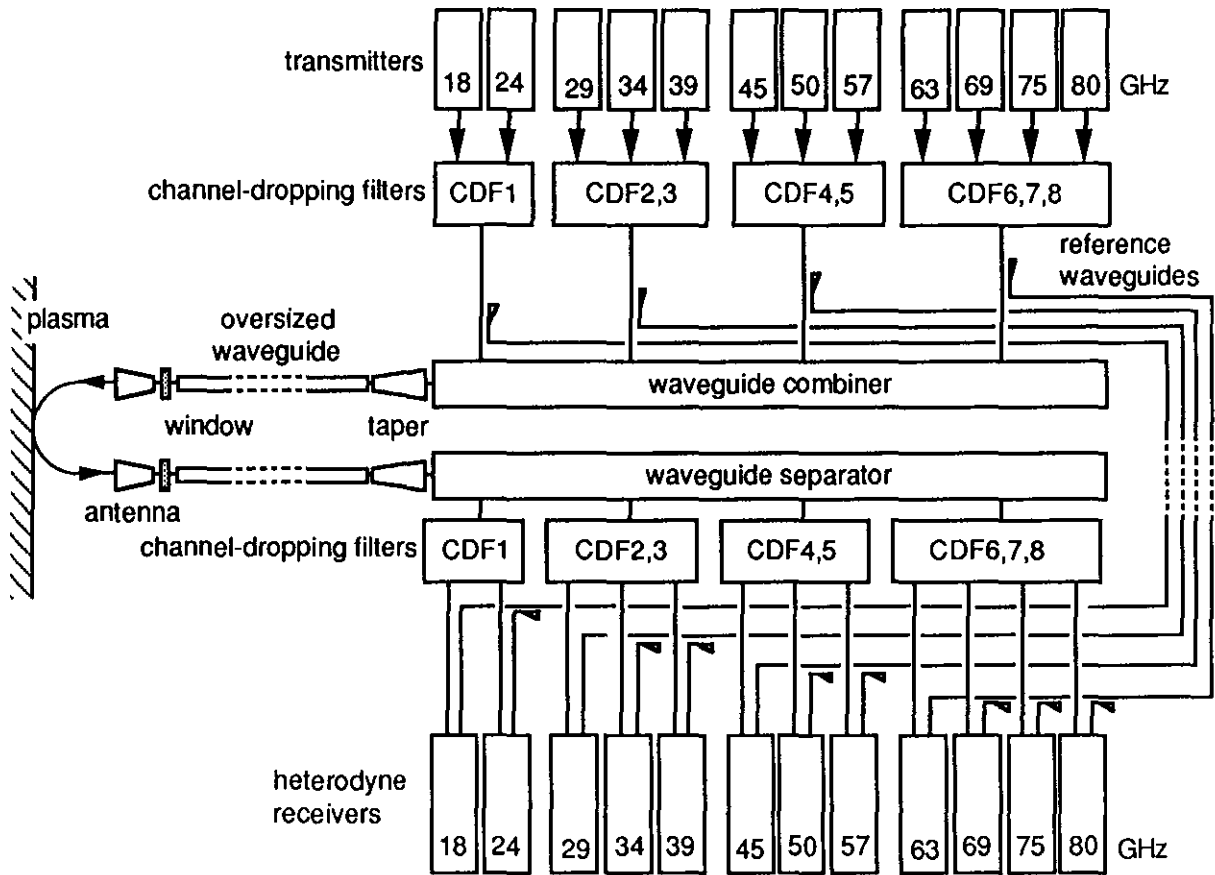


Fig. 5.2. Overview of the microwave system.

## **5.2 Construction of the multi-channel reflectometer**

An overview of the microwave set-up of the 12-channel reflectometer is given in Fig. 5.2. The combiner and separator system, the channel-dropping filters and antennae were been designed and built by ERA Technology Ltd (UK). The transmitters (Sec. 5.3, p. 104), heterodyne-receivers (Sec. 5.3, p. 105) and reference waveguides were designed and built at the FOM-Instituut voor Plasmafysica Rijnhuizen. Combiner and separator waveguide networks, developed by ERA Technology [Mede-87a], connect the 12 transmitters and 12 heterodyne receivers [Huge-86] to the oversized waveguide system which is coupled to two broad-band antennae [Mede-87b] in the vacuum vessel. The combiner/separator system is used to split the frequencies into four separate bands 18 - 26 GHz, 26 - 40 GHz, 40 - 60 GHz, and 60 - 90 GHz.

### **Reference waveguide**

In the multi-channel reflectometer four different reference waveguides are employed. The transmitters are grouped together with the channel-dropping filters using waveguides in WG20, WG22, WG24 and WG26 (Table 1.1, p. 20). The four reference guides were built in WG18. All bends are in single-mode waveguides with tapers to WG18. The signals from the four reference waveguides are split up with 3 dB directional couplers to the 12 reference mixers in the heterodyne receivers (Sec. 5.3, p. 105). The losses in the reference waveguides are below 30 dB. Thermal expansion effects of the waveguides can be neglected as shown below.

In the case of fixed frequency operation only the expansion during a short interval in time (the time of the plasma pulse) has to be considered. Since the waveguides are located in the same building, the temperature will only affect the difference in plasma and reference waveguide, which is about 10 m. The expansion of a 10 m aluminium waveguide is, at a temperature change of 1° C, approximately 0.2 mm. Thus, waveguide expansion effects are negligible.

In the case of swept frequency operation, where an absolute length measurement is made, the long term stability is important. With a 10 m long aluminium waveguide, a temperature change of 5° C will give an expansion of only 1 mm; the effect, therefore, is negligible.

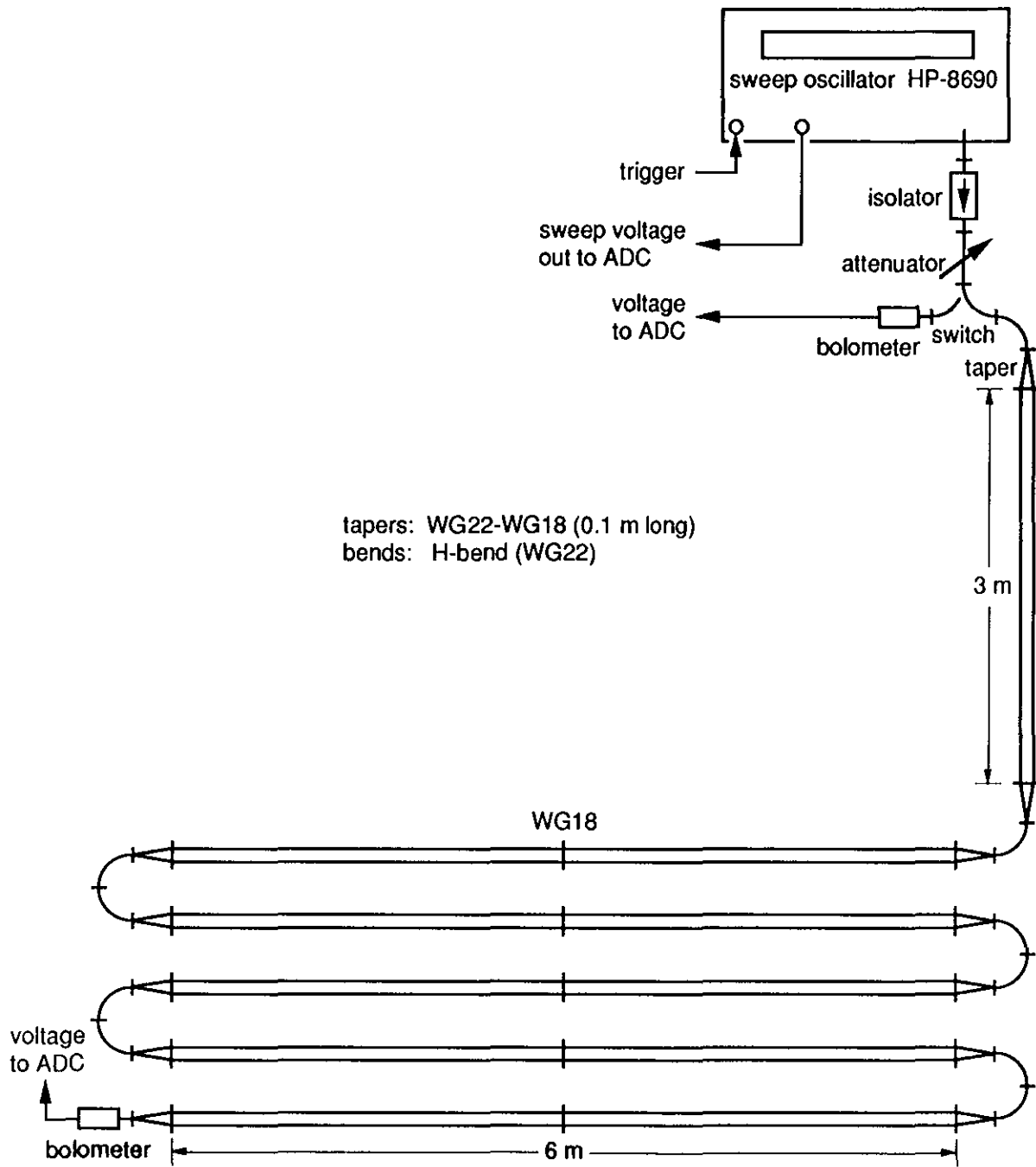


Fig. 5.3. Mock-up of reference waveguide.

**Losses in a reference waveguide mock-up**

A reference waveguide mock-up is constructed to carry out measurements of the losses and to determine possible excitation of undesirable, spurious modes. The measurements are made using a computer-controlled sweep generator (Hewlett Packard HP-8690) in the Ka-band (26.5 - 40 GHz) and an analog-to-digital convertor (ADC). The reference waveguide contains a 33 m oversized waveguide WG18 ( $15.798 \times 7.899 \text{ mm}^2$ ), 12 (0.1 m long) tapers from WG22 (single-mode waveguide) to WG18 and 13 H-bends in single-mode waveguide (Fig. 5.3).

Two runs (frequency sweeps) must be carried out to find the losses in the reference waveguide in a test. In the first run the output of the sweep oscillator is measured, since the power output as a function of frequency is far from constant; the reproducibility is within 0.1 dB. In the second run the power at the end of the reference waveguide is measured. The data of the two measurements are then divided to find the losses as a function of frequency.

The total losses in the 34 m long reference waveguide mock-up are 8.3 dB (0.24 dB/m), as measured over the frequency range of 30 - 40 GHz. Theoretically, the loss is 5.9 dB over the same frequency range. The power fluctuations are of the same order of magnitude as the accuracy of the measurement. Misalignment in the oversized waveguide by 2 mm (at one flange) gives power fluctuations of 3 dB when the frequency is changed, due to the occurrence of reflections. To avoid these losses, all the flanges (UG-419/U) of the oversized waveguide had to be modified with alignment pins. The losses in the reference waveguides in the other bands (K, U and E) are theoretically of the same order. For the configuration of Fig. 5.3 they are given in Table 5.1.

*Table 5.1. Theoretical loss (in dB) in the oversized waveguide of the reference systems for the four waveguide bands used.*

Waveguide band	K	Ka	U	E
WG18	4.9	5.4	6.2	7.2
13 bends	0.2	0.5	0.6	0.9
Total	5.1	5.9	6.8	8.1

### Reference waveguide of the JET reflectometer

The reference waveguides for the JET reflectometer system are constructed in the same way as the mock-up (Fig. 5.3). The overall length is of the order of 50 m. The estimated total losses in the oversized waveguide WG18 (plus some meters of single-mode waveguide) range from about 8 dB in the K-band to about 14 dB in the E-band. The total estimated loss, including the coupling loss in the directional couplers, can be estimated and is given in Table 5.2.

*Table 5.2. Total estimated loss in the reference waveguides (in dB).*

Waveguide band	K	Ka	U	E
Total loss (in dB)	23	28	29	35

### 5.3 Technical description of the sources, detection systems, and data acquisition systems of the multi-channel reflectometer \*)

#### Introduction

The multi-channel reflectometer [Cost-86, Hüge-86] has been designed to carry out:

- measurements of plasma movements and determination of the direction of these movements in the fixed frequency mode (insensitive to amplitude variations of the signal) i.e. a relative measurement,
- profile measurements with high resolution in the swept frequency mode (insensitive to amplitude variations of the signal) i.e. an absolute measurement.

The most important design features are:

- twelve channels in the frequency range of 18 - 80 GHz (corresponding electron densities to be probed of  $4 \times 10^{18}$  to  $8 \times 10^{19} \text{ m}^{-3}$ ) (Sec. 5.1),
- high sensitivity (max. acceptable loss 105 dB, with  $S/N = 25 \text{ dB}$ , and  $\Delta f = 1 \text{ MHz}$ ),
- distance calibration using the far wall of the discharge vessel of JET,
- mode switching from fixed to swept frequency without restraint,
- raw interference signal outputs (homodyne) which can be fed to band-pass filters, which are computer-controlled,
- automatic data recording and handling,
- modular set-up.

---

\*) This work was published earlier as Rijnhuizen Report 86-170.

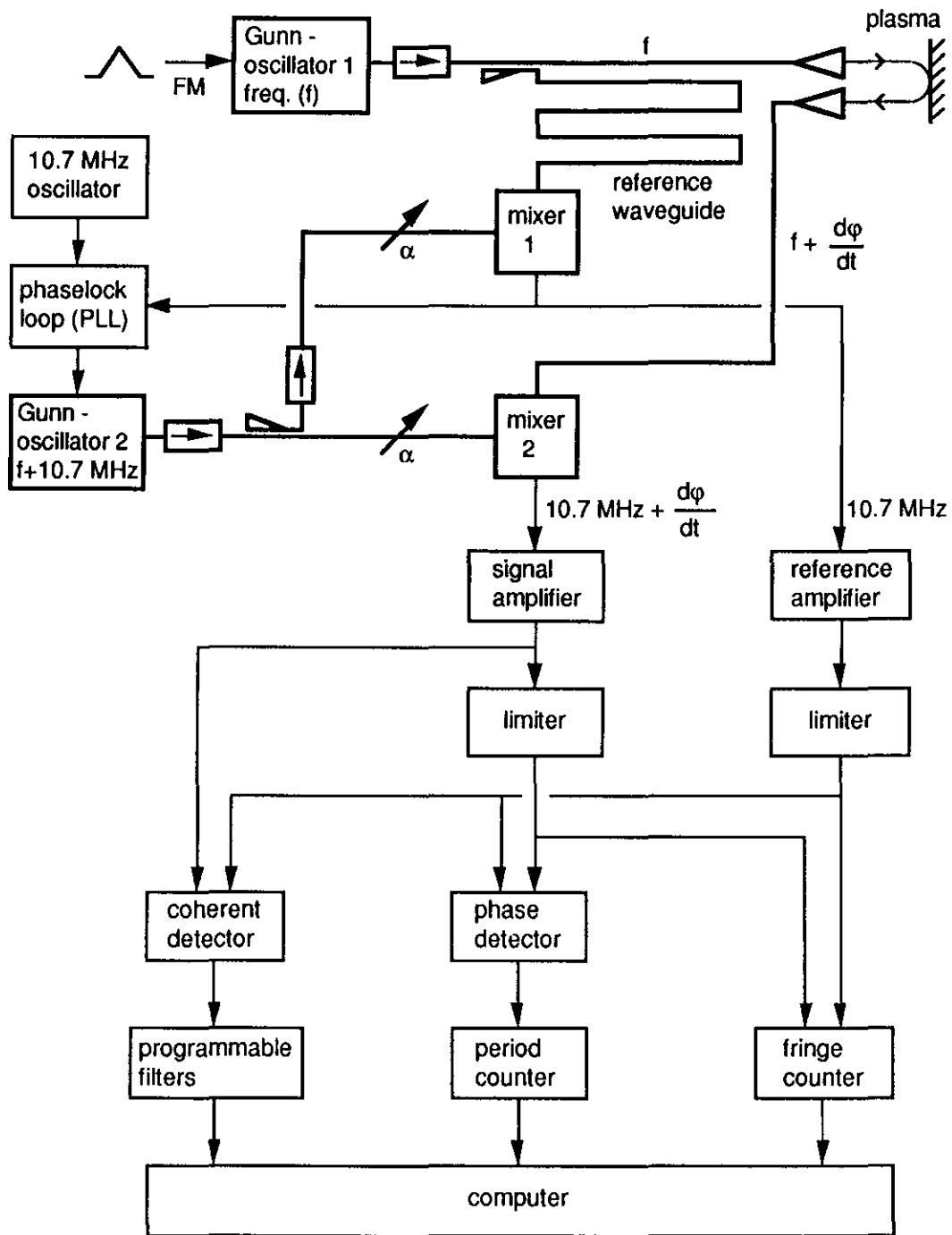


Fig. 5.4. Heterodyne reflectometer.

### **Principle of the heterodyne reflectometer**

The multi-channel reflectometer employs twelve microwave sources and twelve heterodyne detection systems in the frequency range of 18 - 80 GHz. The principle of the heterodyne reflectometer is shown in Fig. 5.4. The microwave source (Gunn-oscillator 1) transmits a wave towards the plasma, which is reflected at the critical density layer towards the antenna of the heterodyne receiver. A fraction of the transmitted signal is previously split off to be transmitted through the reference waveguide. The frequencies of the reflected signal and of the reference signal are down-converted to 10.7 MHz. This is done with a local oscillator (LO; Gunn-oscillator 2), working at a frequency of  $f+10.7$  MHz, and two mixers. A phaselock loop (PLL) [Gard-79] maintains a frequency difference (the intermediate frequency) of 10.7 MHz between the source and the local oscillator, even when the source frequency is swept to perform a density profile measurement. The maximum  $\Delta f/\Delta t$  is 9 GHz/ms. Limiters take all amplitude variations out before the two intermediate frequency signals are fed to the fringe counter and to the period counter. The input signal of the coherent detector is not limited in order to keep the amplitude variation.

The fringe counter monitors the direction and magnitude of the movements of the critical density layer. Since the signal-to-noise ratio of the heterodyne system is high, the resolution is only limited by the fringe counter configuration and is in our case  $1/32$  of the wavelength corresponding to the frequency of the channel considered.

When the source frequency ( $f$ , Fig. 5.4) is swept, a phase shift is generated which is proportional to the difference in path length of the two arms of the reflectometer. This difference in path length is measured with a resolution better than 30 mm with the help of the period counter. The difference in path length can be calibrated in a simple way if a signal reflected from the far wall of the vessel is measured in the absence of plasma.

The coherent detector will convert the signals from the two mixers to the DC intermediate frequency (homodyne). The signal from the coherent detector may be manipulated with a programmable band-pass filter to follow density fluctuations.

**Some notes on the use of Gunn-oscillators**

A Gunn-oscillator [Omar-75] is a solid-state device with which electromagnetic radiation in the millimeter wave range can be generated. The frequency range of the oscillator is set by the structure of the semiconductor (in our case GaAs) and the supplied bias voltage. As the frequency tuning by means of the bias voltage is rather limited (e.g. 100 MHz), varactor-tuned Gunn-oscillators are chosen for the reflectometers in order to be able to tune over a much wider range. A microwave isolator is necessary to reduce frequency pulling which may be caused by changes in the load impedance. A typical characteristic of the frequency and the power vs. varactor voltage of a 63 GHz Gunn-oscillator is given in Fig. 5.5. Characteristics of the current vs. bias voltage and power vs. bias voltage for a typical Gunn-oscillator (Hughes 47271H-2304) operating at 34 GHz are given in Fig. 5.6. The temperature of the Gunn-oscillator has a high influence on the power and on the frequency. For this particular Gunn-oscillator the bias voltage for maximum power (Fig. 5.6) moves from 4.1 V at 20° C to 3.8 V at 50° C. It is important to choose the bias voltage just above (e.g. 0.1 V) the point where the maximum output is obtained for the most negative varactor voltage; this point should be chosen with the body temperature at the operating temperature. The temperature controller keeps the transmitter oscillators at 50° C. The receiver oscillators, which are frequency locked with the transmitter oscillators, are mounted on the bottom plate of the receiver cabinet and kept at approximately room temperature.

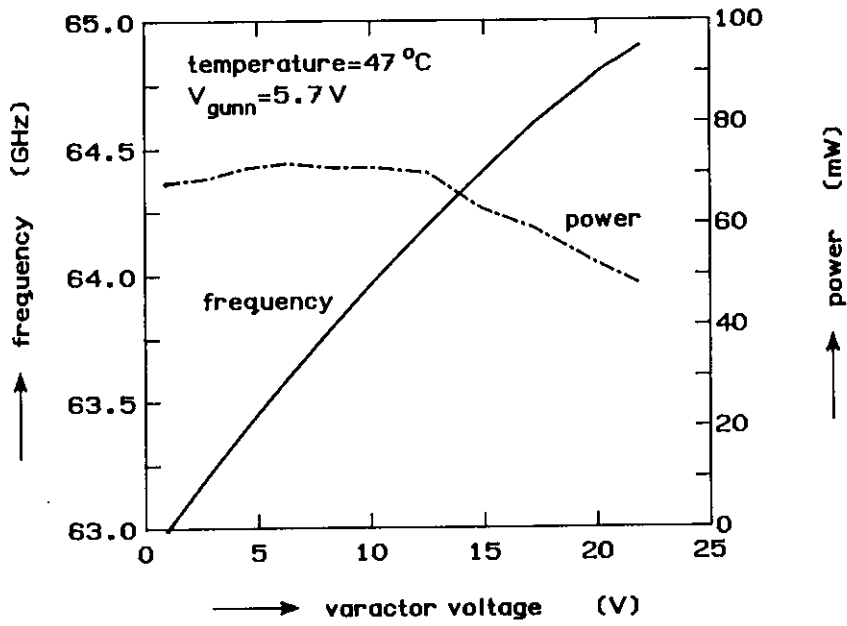


Fig. 5.5. Characteristic of the frequency and the power vs. varactor voltage.

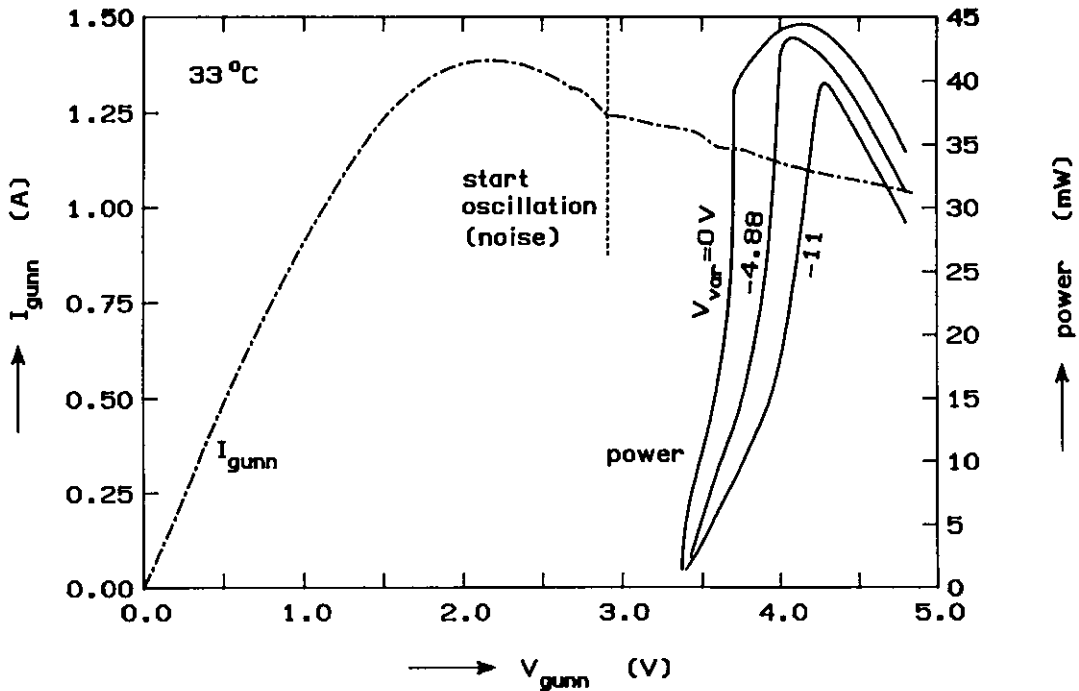


Fig. 5.6. Current vs. bias voltage characteristic and power vs. bias voltage characteristics of a 34 GHz Gunn-oscillator at three different settings of the varactor voltage.

### Some notes on the phaselock loop circuit

The phaselocked loop used in the heterodyne receiver of the reflectometer systems, is shown in more detail in Fig. 5.7 (see also Fig. 5.4, p. 98).

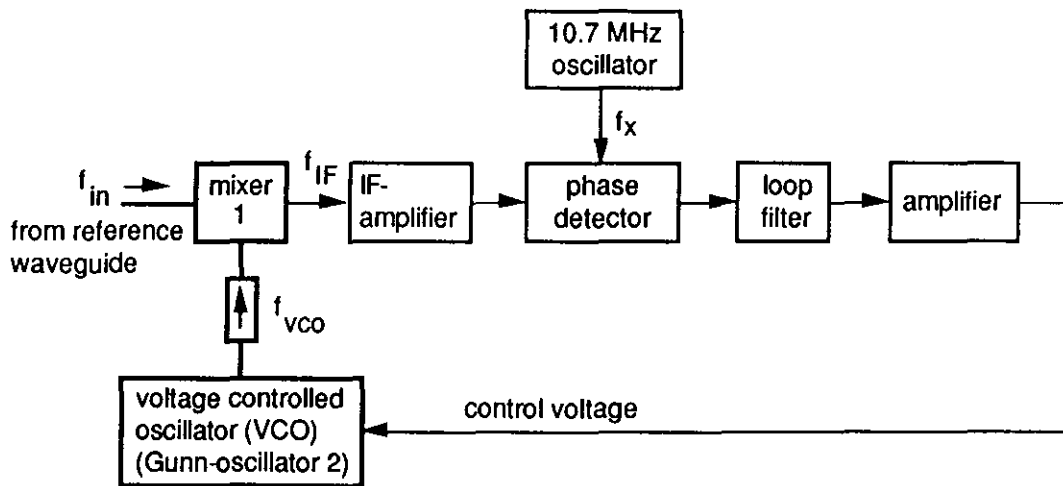
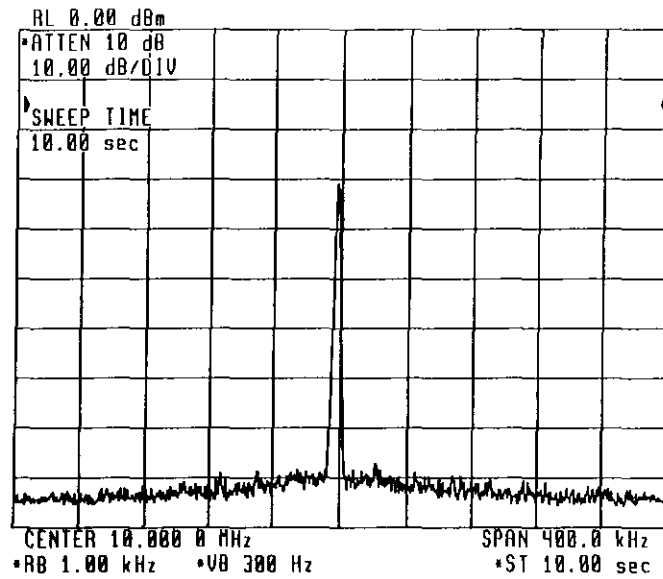


Fig. 5.7. Heterodyne receiver with phaselocking.

The difference with a basic phaselock loop system is the mixer where the two RF signal frequencies,  $f_{in}$ , from the reflectometer, and  $f_{vco}$ , from the local oscillator in the receiver, are mixed to form the difference frequency,  $f_{IF}$ . The IF signal is compared with a signal with fixed frequency, in our case a crystal-oscillator working at a frequency of 10.7 MHz. The filtered output of the phase detector controls the voltage controlled oscillator (VCO) to lock the IF signal,  $f_{IF}$ , to the 10.7 MHz oscillator,  $f_x$ . The phaselock loop uses a third order loop [Gard-79] giving optimum frequency lock when the input signal is swept. For general details and theory we refer to Gardner and Horowitz [Gard-79, Horo-83]. The IF signal in the locked state of the PLL, as measured at the reference mixer (Fig. 5.4), is given in Fig. 5.8.

To obtain the highest possible  $\Delta f/\Delta V$ , in the case of the swept frequency mode, the two oscillators are both swept in parallel. The modulation voltages of the two oscillators are tuned, with trimming potentiometers, in such a way that they oscillate over the same frequency interval (Fig. 5.9). The phaselock loop now only has to correct the dissimilarities in frequency vs. varactor-voltage characteristics of the two Gunn-oscillators. The maximum  $\Delta f/\Delta t$  is about 1 GHz/ms if only the transmitter is swept. A maximum  $\Delta f/\Delta t$  of 10 GHz/ms is possible if both the transmitter oscillator and the local oscillator in the receiver are swept. To keep the PLL in lock during swept frequency operation, triangular voltage modulation instead of sawtooth voltage modulation is used in order to avoid too sharp frequency changes. An additional advantage is given in Sec. 5.5 (p. 116).



*Fig. 5.8. IF signal in the locked state.*

The chosen IF frequency of 10.0 MHz was later changed to 10.7 MHz in view of the availability of narrow-band amplifiers (cf. Sec. 5.5, p. 118).

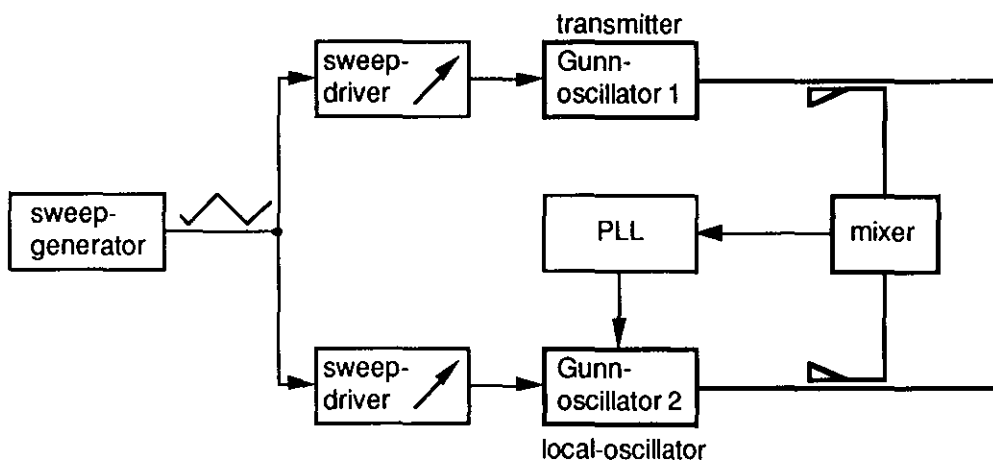


*Fig. 5.9. Parallel sweep of Gunn-oscillators.*

### Source modules

Twelve Gunn-oscillators (Hughes 4727xH) are employed as sources for the twelve different channels. Table 5.3 gives the centre frequencies of the oscillators with the employed waveguide and flange numbers.

*Table 5.3. Frequencies applied and types of waveguide and flanges employed.*

Frequency (GHz)	Waveguide nr.	Flange nr.
18.6, 24	WG20	UG-595/U
29, 34, 39	WG22	UG-599/U
45, 50, 57	WG24	UG-383/U
63, 69, 75, 80	WG26	UG-387/U

The Gunn-oscillators (Fig. 5.10) can be tuned electronically over a band of 1 GHz; the minimum output power is 40 mW. The exact frequencies can be read with the control program from the frequency/varactor voltage characteristics stored in the computer. The frequency/voltage characteristics are linear within a few percent over a frequency range of 200 MHz. Temperature controllers keep the centre frequencies of the sources stable within a few MHz.

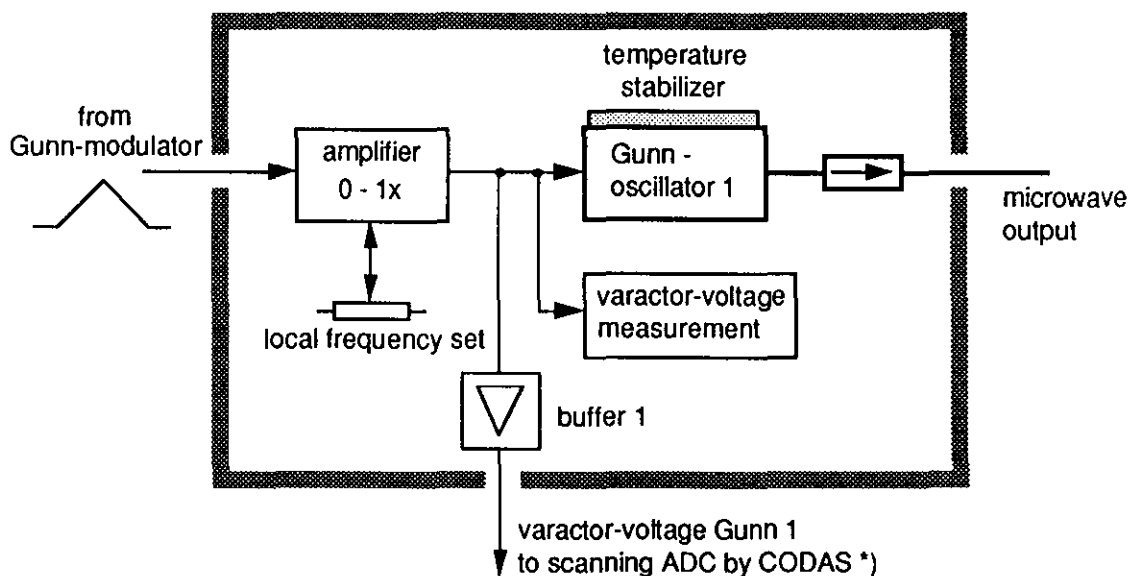


*Fig. 5.10. Source module.*

\*) CODAS is the name of the JET computer system; COnTrol and Data Acquisition Systems.

Heterodyne receiver modules

Figure 5.11 shows the heterodyne receiver module.

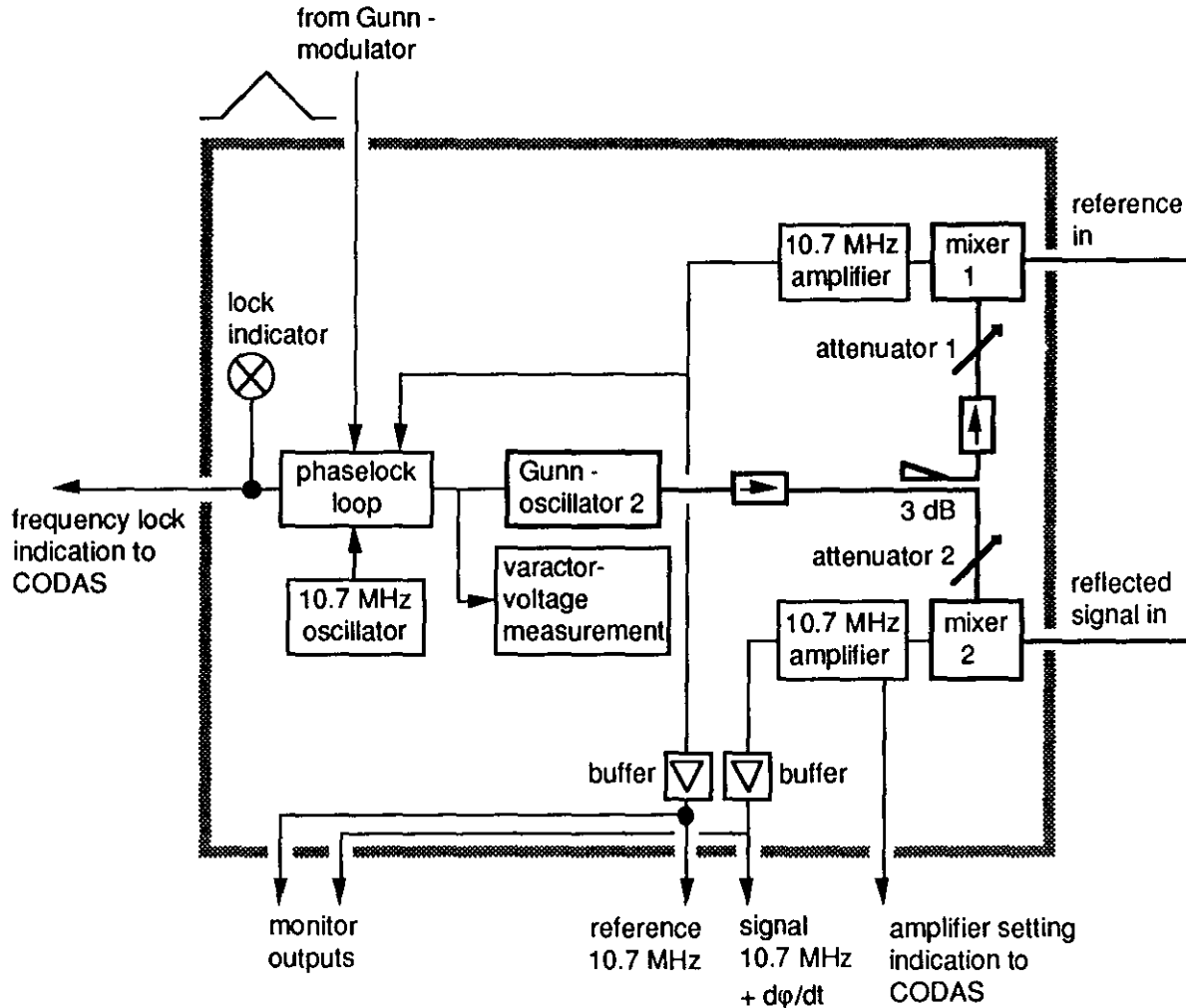


Fig. 5.11. Heterodyne receiver module.

The mixers are planar crossbar mixers (Hughes 4741xH) using GaAs beam lead diodes which yield a conversion loss of less than 6 dB. The minimum detectable power with a signal-to-noise ratio of 100 and a bandwidth of 1 MHz is  $10^{-12}$  W. This is about 105 dB under the power level of the sources. The drive power of the local oscillator for the mixers has to be set with the attenuators to about 16 mW. Two attenuators and an isolator are employed to provide optimum isolation between the reference and the reflected signal. The reference mixer 1 is followed by a wideband 40 dB amplifier with two outputs: one for the phaselock loop circuit and one for the 10.7 MHz reference. The signal detector, mixer 2, is followed by a 10.7 MHz amplifier with 2 MHz bandwidth and voltage gains of 0, 10, 20 and 30 dB, which is controlled manually but monitored remotely.

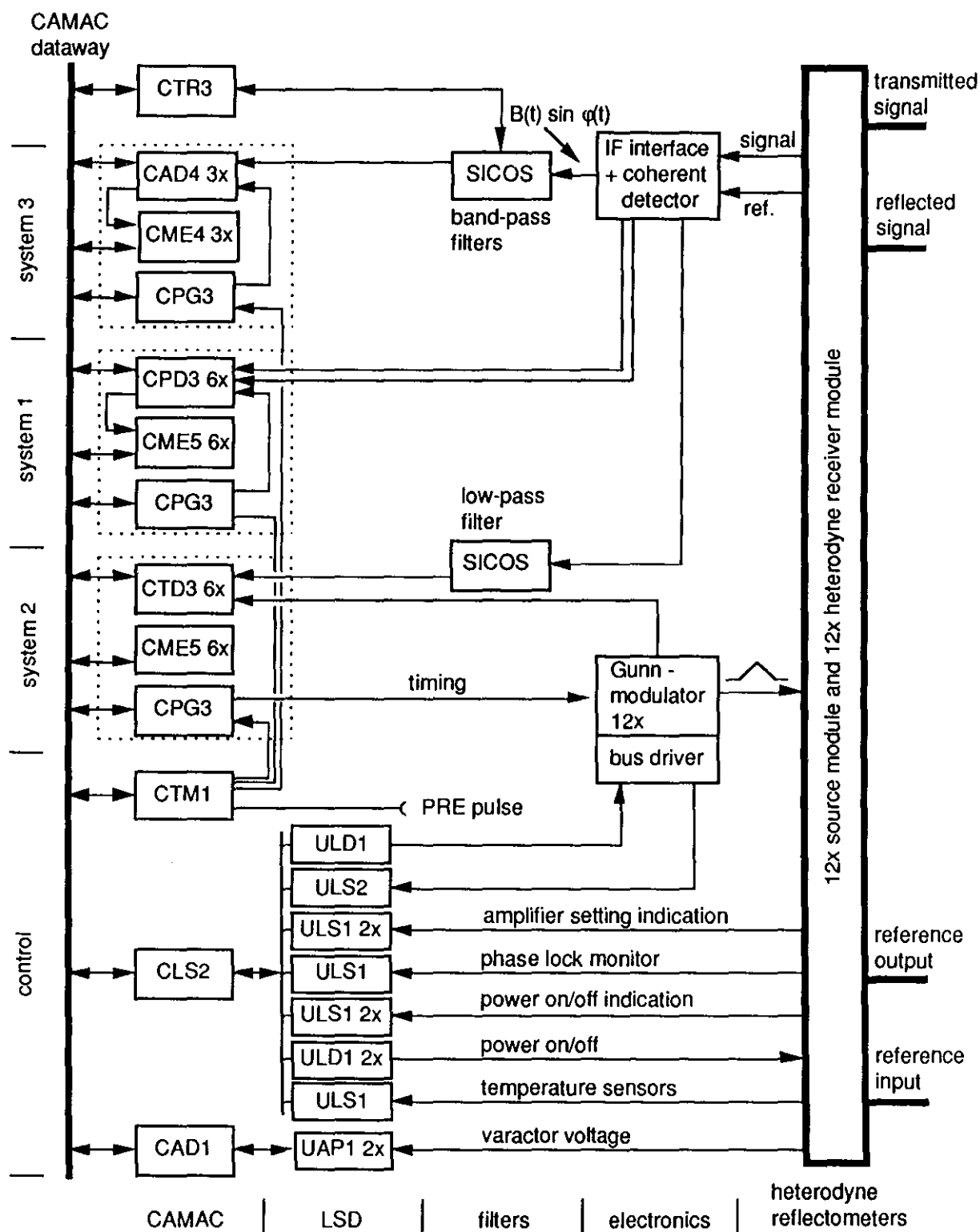


Fig. 5.12. Control and data acquisition.

**Control and data acquisition**

The scheme of the control and data acquisition is given in Fig. 5.12. All relevant functions associated with the operation of the multi-channel reflectometer are controlled and monitored through the JET computer system CODAS. Monitor signals and switches are controlled by the line surveyor/driver module CLS2 through input/output cards ULS1,2 and ULD1. The varactor voltage of the Gunn-oscillators in the transmitter modules is measured with a scanning ADC, the CAD1. The SICOS filter modules are controlled and monitored with the CTR3 interface, using the transmission signal standard RS-232.

The data acquisition system measures, digitizes, and stores all relevant settings of the multi-channel reflectometer. The three measuring systems are described below.

**Fringe counter**

The CAMAC dual fringe counters CPD3 measure the direction and amplitude of plasma movements (Fig. 5.13). Each channel (A and B) can be switched on or off individually. The phase shift, during each sample time, will be converted to two 16 bit data words (channel A and B) which will be multiplexed and written into a 64 k memory CME5 (LeCroy dual-port memory module, model MM8206/n).

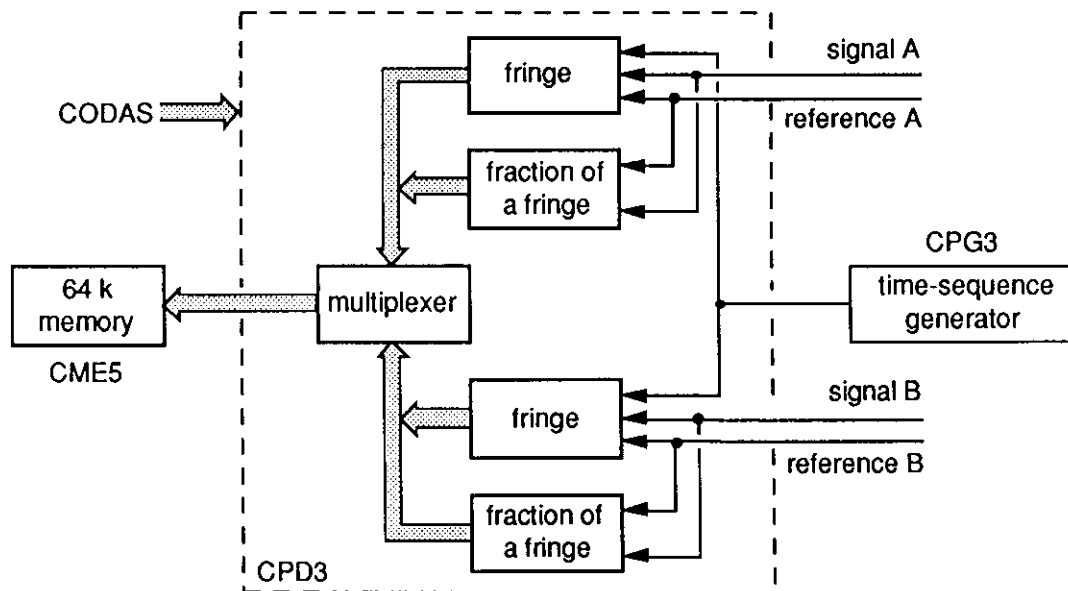


Fig. 5.13. Fringe counter system.

The fraction of the fringe, measured with an ADC, is stored in 6 bits (bit D1-D6) and the fringes in 8 bits (bit D7-D14), both in 2's complement. The most significant bit (bit D16) contains the channel information. The resolution is 1/32 of a fringe. A time-sequence generator CPG3 controls the sample rate.

### Period counter

Profile measurements can be made in the swept frequency mode using the period counter CTD3 (Figs 5.14 and 5.15). The frequency vs. voltage characteristic is presently assumed to be linear. All necessary corrections will be explained in Sec. 5.4 (p. 113).

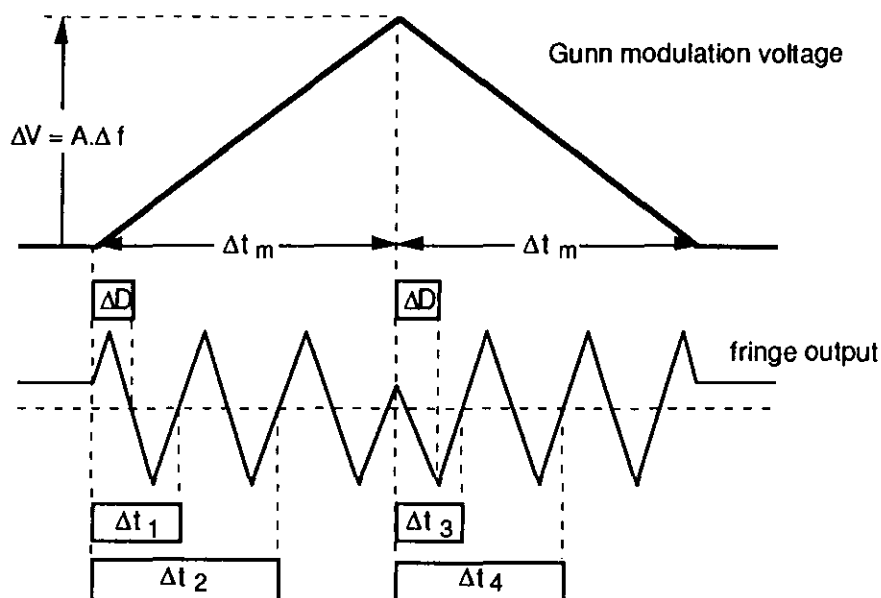


Fig. 5.14. Swept frequency mode.

In the simplified situation where the plasma density layer is an ideal mirror, the difference in length between the reference and the plasma path is given by:

$$\Delta L = A \times \frac{1}{\Delta t_2 - \Delta t_1} \times \frac{\Delta t_m}{\Delta V} \times v ,$$

where:

- $\Delta L$  = difference in length between reference and plasma path
- $A$  = calibration constant
- $\Delta t_{1,3}$  = start time of measurement period
- $\Delta t_{2,4}$  = stop time of measurement period
- $\Delta t_m$  = sweep time (set by computer)
- $\Delta V$  = amplitude sweep voltage (set by computer)
- $v$  = phase velocity \*)
- $\Delta D$  = dead time (set by computer).

\*)  $v = c$  for air and vacuum  
 $v \approx c$  for oversized waveguide  
 $v = v_{ph}$  averaged over small  $\Delta f$  for single-mode waveguide

The period counters (Fig. 5.15) are divided into two parts (period detectors and counters) with low-pass filters between the sections to filter out spurious signals which may arise from MHD instabilities in the plasma.

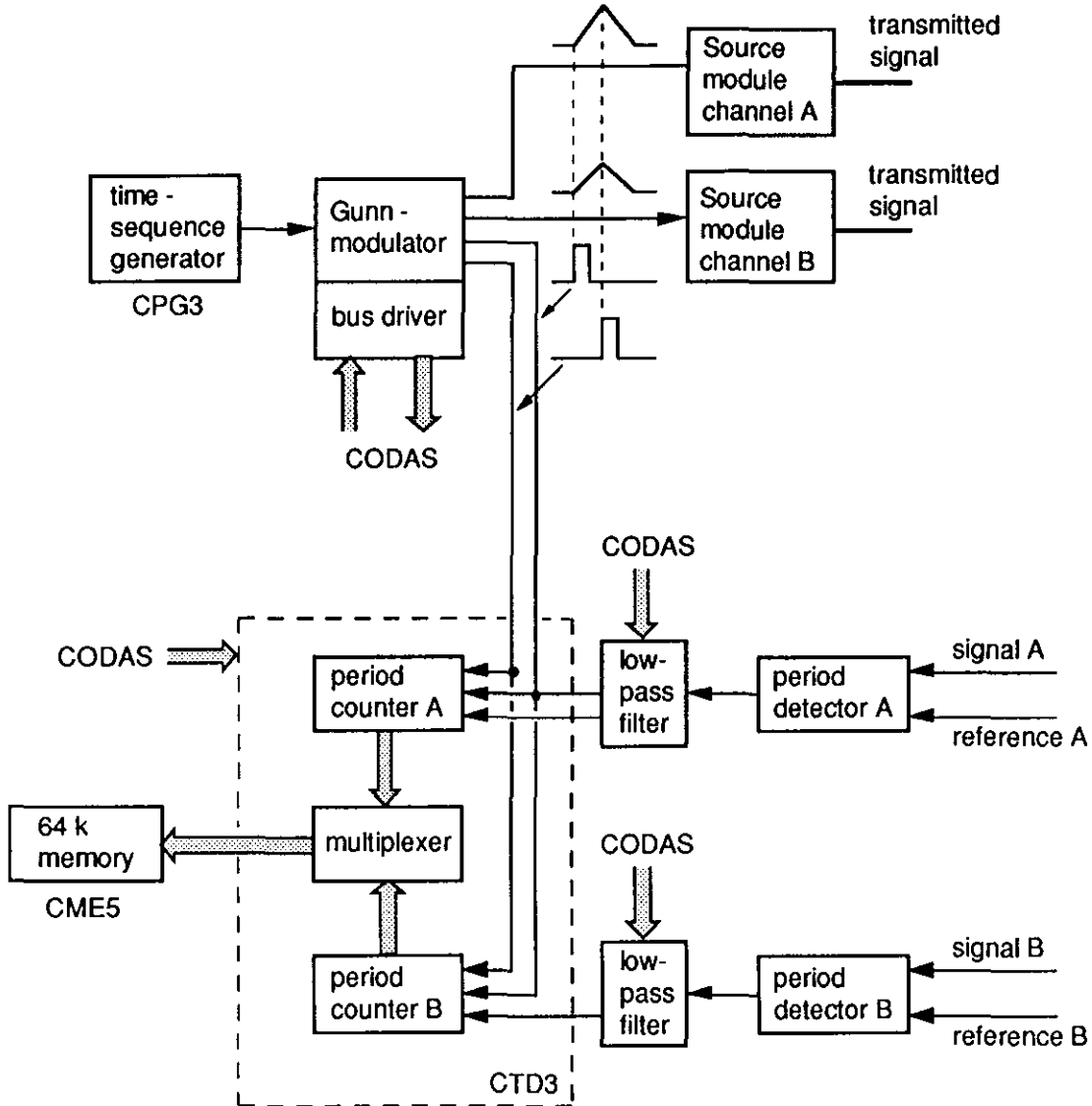


Fig. 5.15. Period counter system.

The CAMAC dual period counters, CTD3, can be pre-conditioned in the following way. The period counters are dual modules (A and B) in which each channel can be switched on or off individually. The dead time can be set from 1 to  $255 \times 20 \mu\text{s}$  with 8 bits to accommodate the filter delay. The clock frequency can be set in steps of octaves from 1.25 MHz to 20 MHz. The maximum accuracy of the period counter can be chosen for a selected sweep time using the different clock frequencies. The counter of the CTD3 starts at the up (c.q. down) of the timing pulse. At the first zero-crossing after the dead time, the number which has been counted is

stored in data word  $t_1$  (c.q.  $t_3$ ); the counting goes on until the end of one period. The second time measured is stored in data word  $t_2$  (c.q.  $t_4$ ). This approach is chosen in order to correct the measurement for the non-linearities in the frequency vs. varactor voltage characteristics of the Gunn-oscillators which are stored in the computer memory. The frequency vs. voltage characteristics can be measured accurately with a spectrum analyser (Hewlett Packard HP-70000) and a 16 bit ADC under computer control.

The times measured when the source is swept up and down in frequency are stored in the memory CME5 in four 16 bit data words. The most significant bit in each word will identify the channel. The frequency modulator for the oscillator, associated with the period counter, is controllable through CODAS; it has the following features:

- the sweep time of the modulator can be set in doubling steps from 200  $\mu$ s to 25.6 ms for a single sweep,
- triggered by the time-sequence generator CPG3, an up and a down ramp are carried out,
- the amplitude of the triangular voltage can be set with 8 bit accuracy to maximum 10 V.

**Coherent detector**

The analogous signal from the coherent detectors (bandwidth 1 MHz), are passed through programmable equal time delay filters and amplifiers, and are recorded by 12 bit analog-to-digital converters CAD4's (LeCroy 8210) and memories CME4's (LeCroy 8800/12) (Fig. 5.16). A time-sequence generator CPG3 controls the sampling rate (up to 1 MHz).

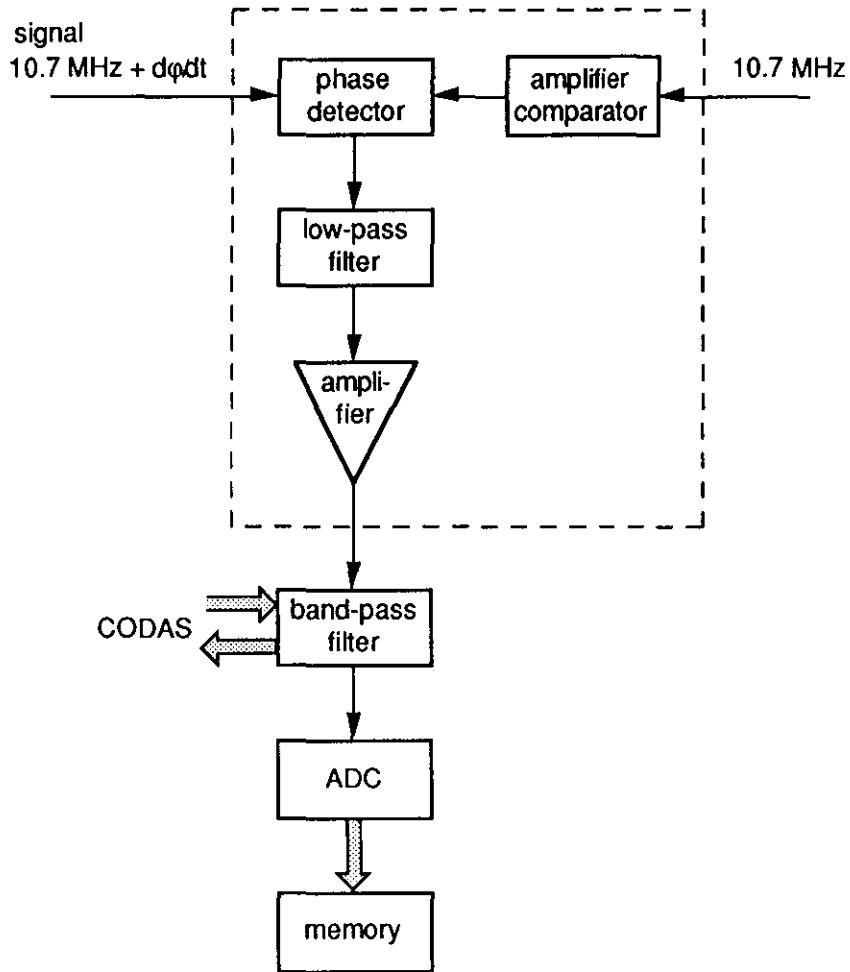


Fig. 5.16. Coherent detector system.

The output of the phase detector [Mini-86] contains phase as well as amplitude changes. This in contrast to the fringe counter and the period counter where only phase changes are measured. Certain frequency bands can be selected with the programmable band-pass filter (cf. Sec. 5.5, p. 118).

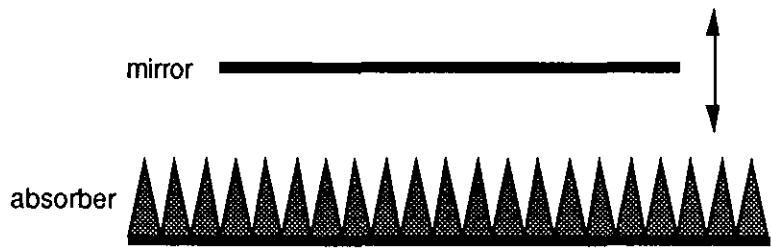
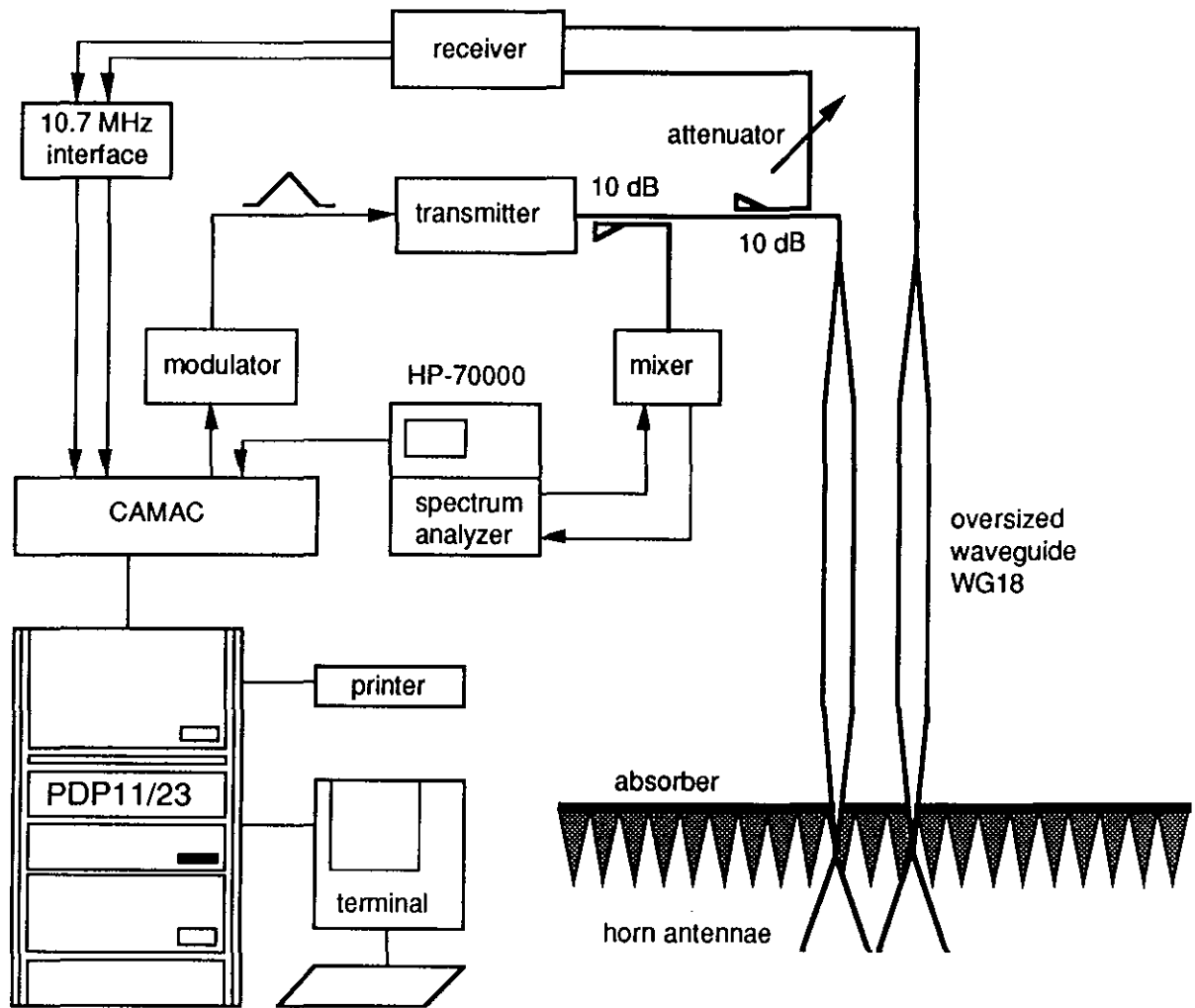


Fig. 5.17. The reflectometer mock-up system.

## **5.4 Performance tests in a mock-up of the JET reflectometer**

### **Introduction**

The individual reflectometer channels of the reflectometer underwent an acceptance test in a reflectometer mock-up at the FOM Instituut voor Plasmafysica Rijnhuizen, before they were installed at the JET experiment. The tests were carried out in the two modes of operation: narrow-band sweep and fixed frequency modes. In the swept frequency mode, intended for radial plasma profile measurements, the distance to a plane mirror is measured. In the fixed frequency mode the magnitude and direction of the movement of the critical density layers can be measured; in the mock-up the change in position of the plane mirror is measured.

### **Description of the test set-up**

A schematic representation of the reflectometer mock-up system is given in Fig. 5.17. The reflectometer consists of a transmitter module, a heterodyne receiver module, interface electronics, and a waveguide system. The transmitter power is guided through a single-mode waveguide and an oversized waveguide WG18 to a horn antenna; in the K and Ka band (frequencies < 40 GHz) only single-mode waveguide is used. Part of the transmitter power is split off, using a 10 dB directional coupler, and is fed to the harmonic mixer of the spectrum analyser for frequency and spectral measurements (this spectrum analyser is only used for verification and for frequency calibration). Another part of the transmitter signal is split off to the reference waveguide. The attenuator sets the reference signal to a value equal to the attenuated value as it will occur in the 50 meter long reference waveguide installed at JET. The transmitted microwave signal is reflected by the movable plane mirror and is received by the heterodyne receiver. Both the reference and the reflected signals are down converted to 10.7 MHz using a local oscillator and two mixers. A phaselock loop maintains the frequency difference of 10.7 MHz between the source and the local oscillator, even when the frequency is swept [Huge-86]. A microwave absorber is used to avoid spurious reflections from pieces of equipment in the room and from the walls. The two 10.7 MHz output signals of the receiver are fed to the phase and coherent detector module, which is connected to a fringe counter, CPD3, and a period counter, CTD3, both CAMAC modules built at the FOM-Instituut voor Plasmafysica Rijnhuizen. The modulator module is only used in the swept frequency mode. All measurements are computer controlled (PDP-11/23).

### Measurement of the distance to the mirror in the swept frequency mode

The swept frequency mode is intended for measurements of radial plasma profiles in JET. A simplified measurement is performed in a mock-up (Fig. 5.17). The mirror can be moved away from or towards the antennae along a test-bench over a range of 1 m to 3 m. The reflectometer measurements made at different positions of the mirror are compared with the position read from the ruler.

As an example, the procedure of a measurement at 18 GHz is given. The single-mode waveguide (WG20) is used in the signal and reference path (the oversized waveguide is only used for higher frequencies). The reference path has a length of 2.602 m, and the signal path is 4.023 m long. The length of the reference path is chosen such that 2 fringes of phase shift occur at the detector when the transmitter is swept over approximately 150 MHz, with the mirror at a distance of 1 m from the antennae.

The time-delay measured at the mixer in the receiver can be expressed as

$$\tau = \frac{1}{2\pi} \times \frac{\Delta\phi}{\Delta f}, \quad (5.1)$$

where  $\tau$  is the difference in delay between the two signals of the two paths. As the period counter measures exactly 1 fringe, i.e.  $\Delta\phi = 2\pi$ , Eq. 5.1 becomes

$$\tau = \frac{1}{\Delta f}. \quad (5.2)$$

The time-delay over a length  $L_g$  of the waveguide is given by

$$\tau_{wg} = \frac{L_g}{c} \frac{\lambda_g}{\lambda} = \frac{L_g}{c} \frac{1}{\sqrt{1 - \frac{f_c^2}{f^2}}}, \quad (5.3)$$

where  $\lambda_g$  is the wavelength in the waveguide,  $\lambda$  the wavelength in free space, and  $f_c$  is the cut-off frequency of the waveguide.

The difference in time-delay between the signal path and reference path in the example becomes

$$\tau = \frac{1}{\Delta f} = \frac{2L}{c} + \frac{4.023}{c} \times \frac{1}{\sqrt{1 - \frac{f_c^2}{f^2}}} - \frac{2.602}{c} \times \frac{1}{\sqrt{1 - \frac{f_c^2}{f^2}}}, \quad (5.4)$$

where  $L$  is the distance from the antennae to the mirror. Equation 5.4 can be written as

$$L = \frac{c}{2\Delta f} - \frac{1.421}{2} \times \frac{1}{\sqrt{1 - \frac{f_c^2}{f^2}}}, \quad (5.5)$$

where  $\Delta f$  and  $f$  are to be measured, as will be explained below.

The frequency of the oscillator in the transmitter module is modulated with a precise triangular voltage pulse. The sweep generator gives also two timing pulses (Fig. 5.15, p. 109) to the period counter at the times of the start of the sweep-up and that of the sweep-down. The triangular voltage applied to the transmitter lags in time by about  $13.8 \mu\text{s}$  as it is fed through an amplifier and a low-pass filter. A correction for this delay has to be made. The amplitude of the triangular voltage can be measured with high precision in the calibration position of the unit \*). The triangular voltage will produce fringes as indicated in Fig. 5.18.

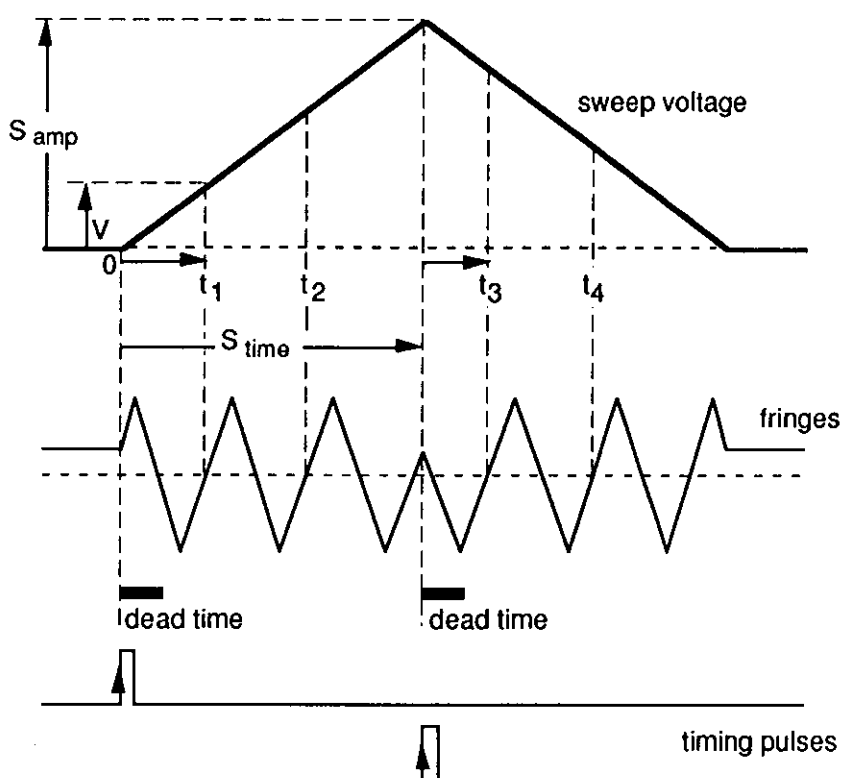


Fig. 5.18. Translation of the zero crossing times into voltages.

The period counter will measure four time intervals: the interval from the start pulse of the sweep-up to the first zero crossing (after the dead time) ( $t_1$ ) and the interval to the moments when the fringe crosses the zero line again from the same direction ( $t_2$ ) (Fig. 5.18).

\*) The modulator can be set in three different positions:

- normal mode, where a single triangular voltage is produced after a trigger pulse,
- repeat mode, where a continuous triangular waveform is produced after a trigger pulse,
- calibration mode, where the output voltage is set to a fixed (DC) voltage corresponding with the top value of the triangular voltage after a trigger pulse.

The other two time intervals are measured from the start pulse of the sweep-down in the same way ( $t_3$  and  $t_4$ ). The measured times can now be converted into four voltages with

$$v_i = t_i \times \frac{\text{amplitude triangular voltage pulse}}{1/2 \text{ sweep time of this pulse}} \quad \text{for } i=1 \text{ to } 4, \text{ (Fig. 5.18).} \quad (5.6)$$

The corresponding four frequencies are then found from a voltage vs. frequency table which is known and characteristic for the Gunn-oscillator used \*). The table contains 100 pairs of numbers. Linear interpolation is carried out between the points. The  $\Delta f$  in the up-sweep is  $f_2 - f_1$  and in the down-sweep  $f_3 - f_4$ . The frequency,  $f$ , in the up-sweep is taken from  $(f_2 - f_1)/2$  and for the down-sweep from  $(f_3 - f_4)/2$ . The cut-off frequency for the given example (WG-20) is 14.051 GHz. With these data Eq. 5.5 yields the distance  $L$ , i.e. the distance from antennae to mirror. Figure 5.19 gives examples of such measurements at 18.6 GHz in the swept frequency mode. The actual position is read from a ruler on the bench along which the mirror is moved.

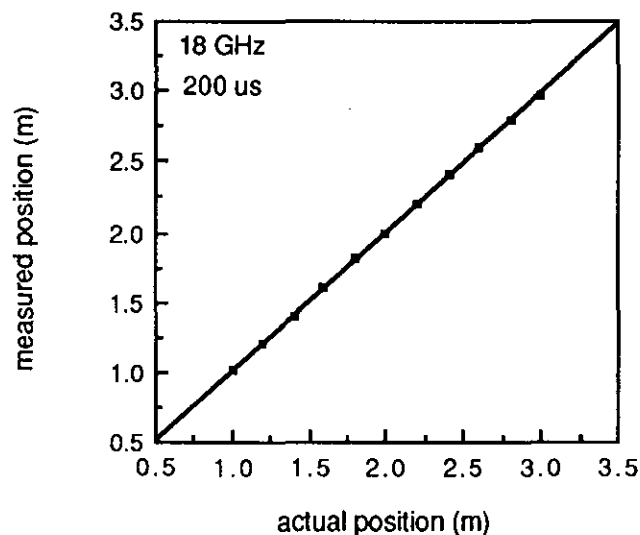


Fig. 5.19. Measurement of the distance of the antennae to a mirror vs. actual position.

Obs. The modulation with a triangular voltage makes it in principle possible to eliminate the phase shift caused by a constant motion of the 'mirror' during the up/down sweep. When the measured phase shifts in the up-sweep and down-sweep are subtracted and divided by 2, the phase shift due to the constant motion is cancelled (cf. Eq. 4.6, p. 84).

\*) The frequency-voltage characteristics of the transmitters are measured with a spectrum analyser (Hewlett Packard HP-70000). The spectrum analyser is set for automatic tracking of the frequency of the transmitter signal. The modulation voltage of the transmitter is set in 100 steps with a 10 bit digital-to-analog convertor, starting at 0 V and up to 10 V. This modulation voltage is measured with an accurate 16 bit analog-to-digital convertor. The spectrum analyser will measure the frequency at each voltage step. The voltages and the corresponding frequencies are stored in a table.

### Measurements of the displacement of the mirror in the fixed frequency mode

In the fixed frequency mode the magnitude and direction of the movement of the critical density layer can be measured. In the mock-up the change in position of the mirror is measured. The phase shift between the reference and reflected signal, both down-converted to 10.7 MHz, are measured during each sample time and written as 16 bit data words into a 64 k memory (LeCroy MM8206/n). The  $1/32$  fraction of a fringe is written in 6 bits and the fringes in 8 bits. The most significant bit contains the channel information. The data words are unfolded with software to phase samples which are then integrated by adding the individual phase steps. The first phase sample is set to zero. The displacement of the mirror, measured with a micrometer, is compared with the reflectometer result. Since the mechanical as well as the frequency stability of the reflectometer is high, the accuracy is only restricted by the fringe counter configuration. The accuracy is 1 bit (the least significant bit: LSB) of the fringe counter sample word or  $1/64$  of the wavelength used. The actual position of the mirror is read from a micrometer with an accuracy of better than 0.01 mm. A typical example is given in Fig. 5.20.

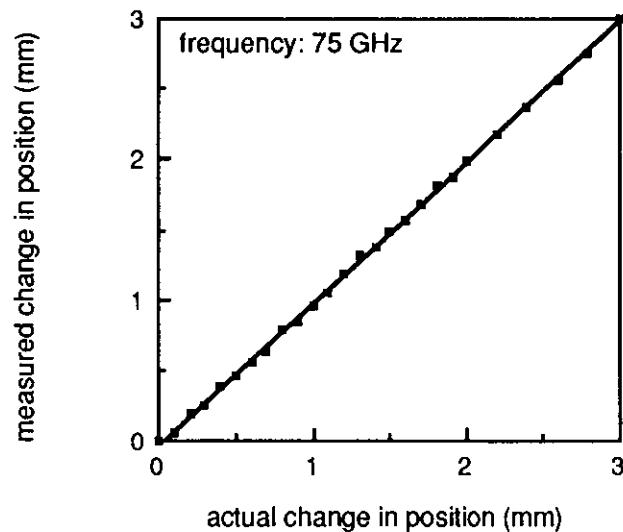


Fig. 5.20. Reflectometer measurement in the fixed frequency mode of the displacement of the mirror vs. actual position.

### 5.5 First results of the multi-channel reflectometer

To ensure proper performance of the reflectometer at JET a number of changes had to be made to the system. The main problems encountered were the following:

- unavoidable high losses in the waveguide system,
- bad location of the antennae,
- strong fluctuations of the density,
- ambitious choice of the bandwidth,
- cross-talk from reference to signal mixer.

The overall losses, from a transmitted signal which is reflected from the far wall of the discharge vessel back to the receiver are, for the nine channels with lower frequencies (18 - 63 GHz), in the order of 60 dB (Fig. 5.2, p. 92). The sensitivity of the reflectometer is high enough (Sec. 5.3, p. 97) to cope with this attenuation. The gain of the signal amplifier (Fig. 5.4, p. 98) had to be raised from 30 dB to ~50 dB, for a number of channels. No good performance is obtained so far from the three channels with higher frequencies (69, 75, and 80 GHz) due to the occurrence of too high attenuation at these frequencies in the combiner and separator system [Mede-87a].

In the first set-up the antennae [Mede-87b] were located in the back of a diagnostic port about 1.2 m away from the plasma edge. This had to be done because of the presence of other equipment in the same port. The antennae were focused in the horizontal plane at the opening of the diagnostic port to avoid reflections from the side walls of the port. Since the antennae are quite far from the plasma surface a small tilt in the reflecting layer will give a strong decrease in signal amplitude. To overcome this difficulty, the antennae are now replaced by two long tapers, at the expense of other equipment, with the front of the antennae about 0.2 m from the plasma edge. This change proved to be a major improvement.

The high fluctuation level of the density makes the reflecting layer far from an ideal microwave reflector. This 'roughness' of the 'mirror' caused frequent sharp decreases in the reflected signal; the result was that the fringe counter often lost many fringes. A reduction of the bandwidth from 2 MHz to a few kHz (crystal filters) made the fringe counter work. The bandwidth of the coherent detector can be chosen over a wide range (Sec. 5.3) using the control program.

It was found that the reference signal at mixer 1 (Fig. 5.4, p. 98) leaked through this mixer (RF to local oscillator isolation: ~ 20 dB), through the isolator (~25 dB isolation), and through the directional coupler to the signal mixer (mixer 2). This caused false interferences when the input signal dropped in amplitude with about 30 dB. This problem is solved with extra attenuators of 30 dB in the four reference waveguides and by raising the gain of the

reference amplifiers by the same amount. The reference signal and the reflected signal are now at the same power level.

An example of the output of the coherent detector compared with the output of the fringe counter is shown below. This is an example of measurements with the coherent detector where the change in the direction of the movement does, fortunately, not fall at or near a top of the fringe signal (Fig. 5.21a); the fringe counter will always give the right direction of the movement (Fig. 5.21b).

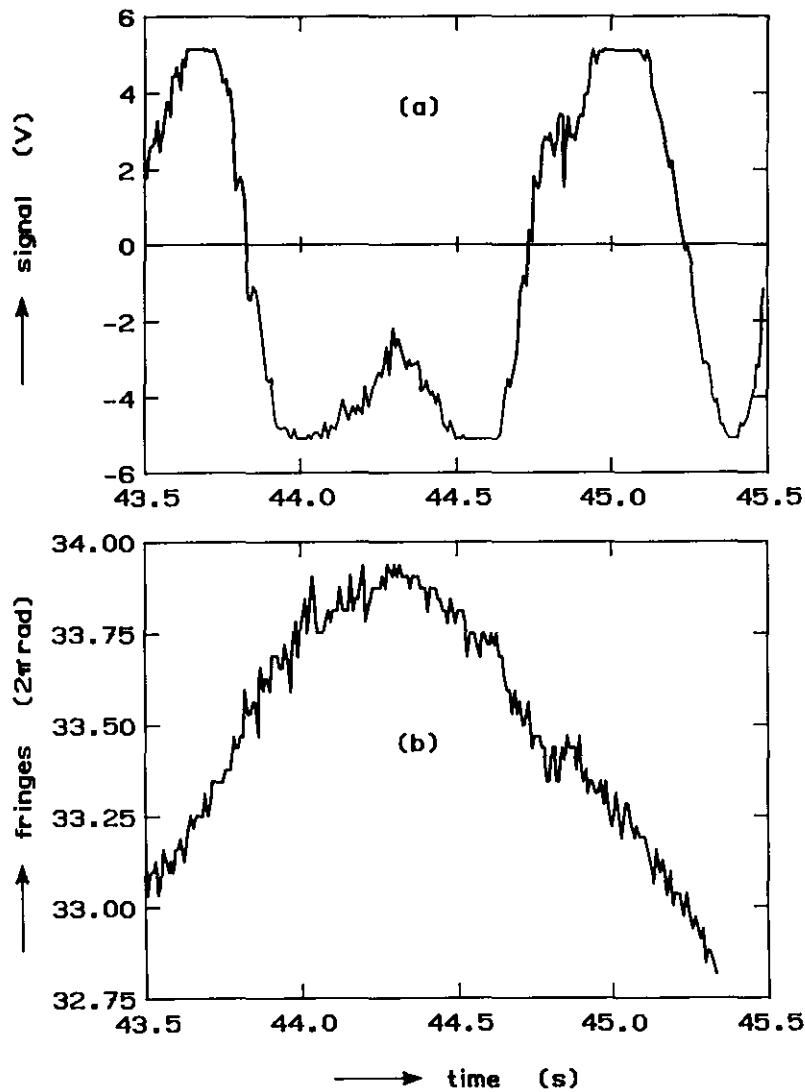


Fig. 5.21. Comparison of the coherent detector (a) and the fringe counter (b) data.

Figure 5.22 and 5.23 show fringe counter signals from a typical JET plasma. More results can be found in the given references [Pren-88a, Pren-88b, Sips-89a, Sips-89b]. The measured number of fringes,  $F$ , can be converted into changes in length,  $\Delta L$ , by using Eq. 4.8 (p. 85)

$$\Delta L \approx \frac{1}{2} \frac{\lambda_0}{0.6} F.$$

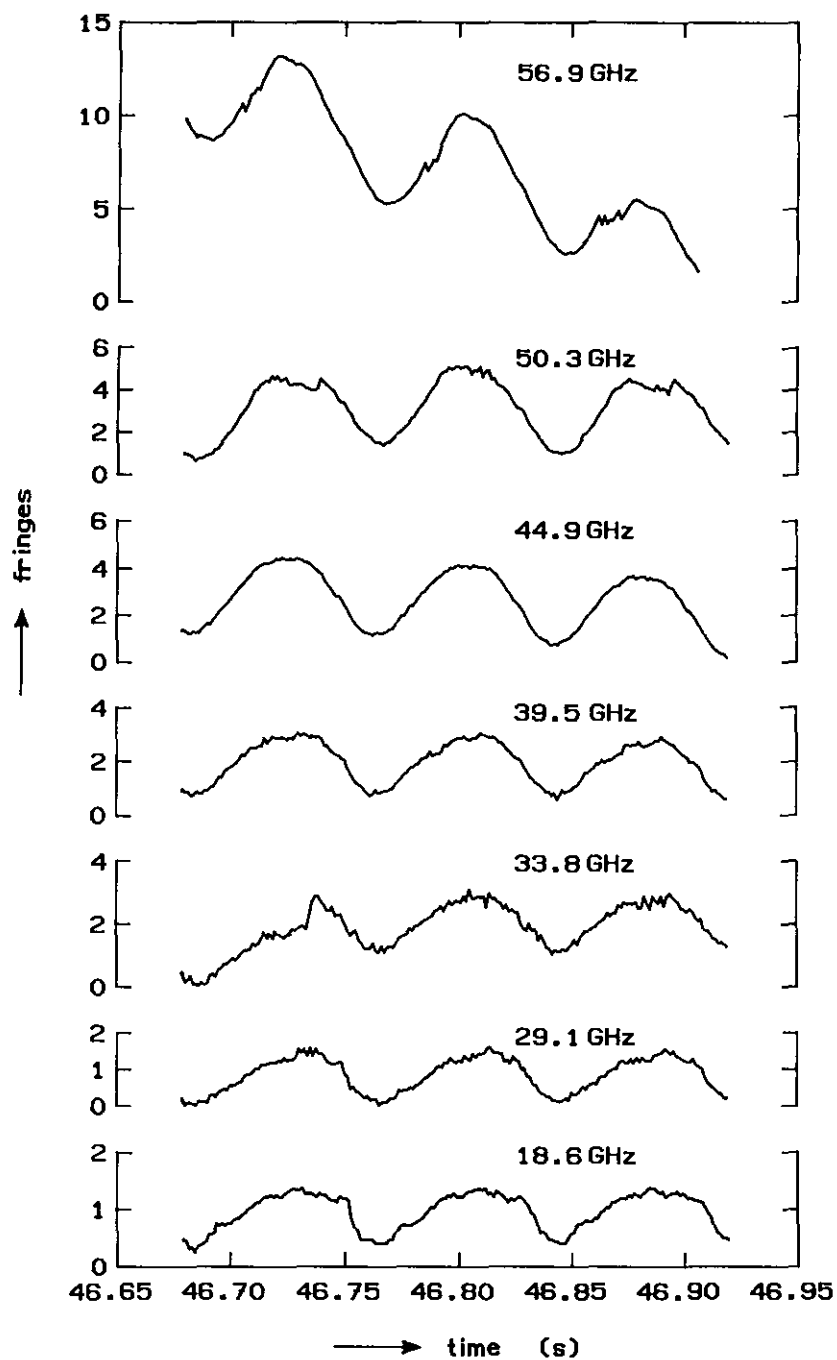


Fig. 5.22. Fringe counter signals showing oscillations of the plasma density.

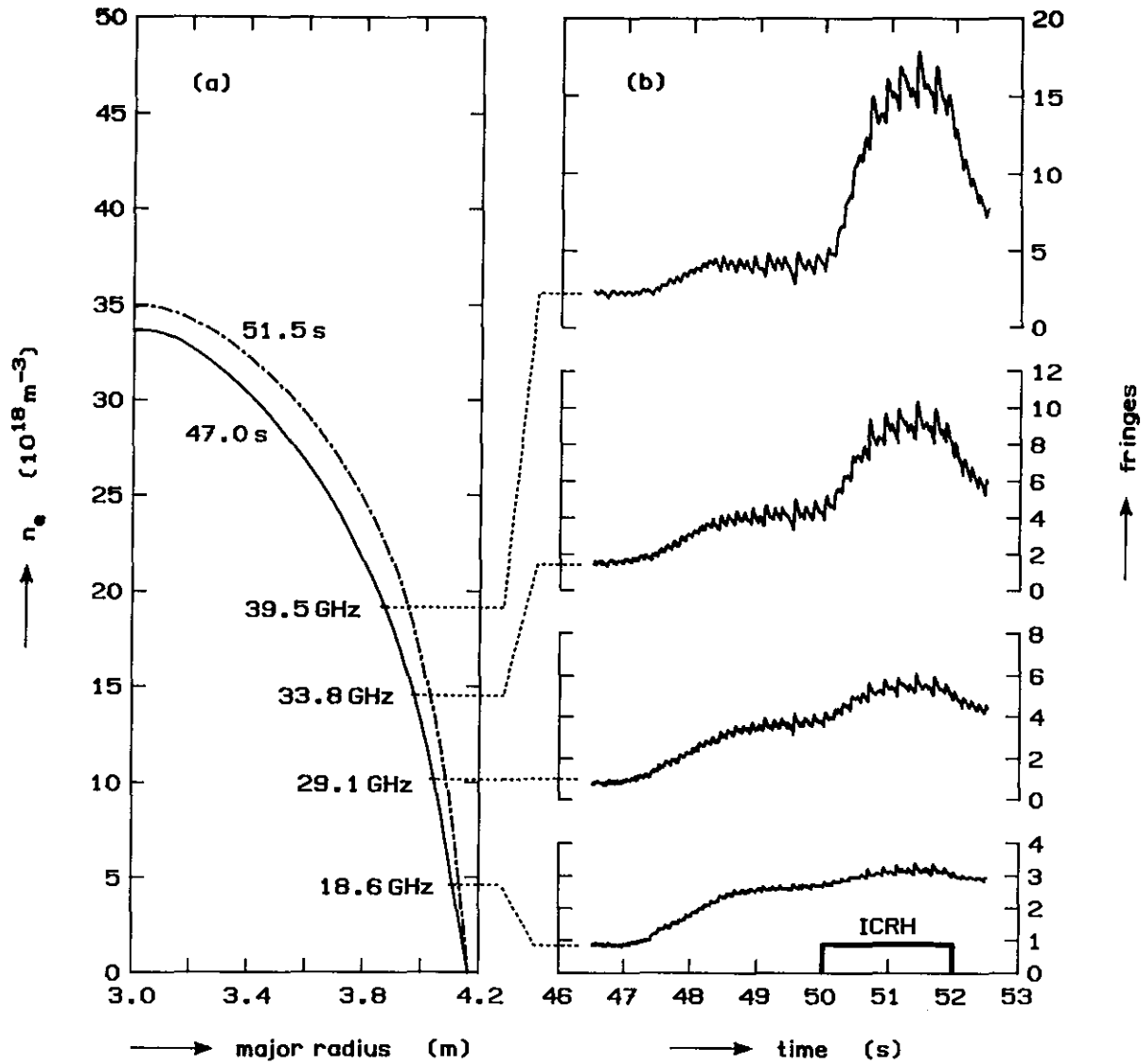


Fig. 5.23. Data of the JET plasma.

a) Density profiles from FIR-laser interferometer at 47.0 s and 51.5 s.

b) Fringe counter signals.

Observe the increase in density and the widening of the profile during the RF heating pulse (Ion Cyclotron Resonance Heating).

Until recently good results could not be obtained from measurements using swept frequencies because the position of the reflecting layer changed too much during the sweep (Eq. 4.6, p. 84). This difficulty could have been overcome by decreasing the sweep time, but that is incompatible with the narrow bandwidth, necessary to filter out fast fluctuations. An other approach (Sips-89c, Pren-90) is to carry out measurements with the fringe counter at a fixed frequency, interrupted by repeated swept frequency operation. The sweep-time is chosen as 6.4 ms, the fixed frequency interval is 27.2 ms (Fig. 5.24). The sweeping of the frequency results in a fringe frequency of about 1 kHz; the detection bandwidth was chosen as 3 kHz.

Good results are obtained when the phase measurements, performed during the intervals when the frequency is swept, are corrected by subtracting the phase changes due to plasma motions. Those are found by extrapolating the phase measurement during the intervals of fixed frequency (baseline correction). In this way the distance to the far wall of the vacuum vessel (2.7 m from the front of the antennae) can be measured with an accuracy of 20 mm, in good agreement with the measurements in the mock-up. The position of the reflecting layer in the plasma can be measured with a somewhat lower accuracy of 50 mm, due to plasma fluctuations.

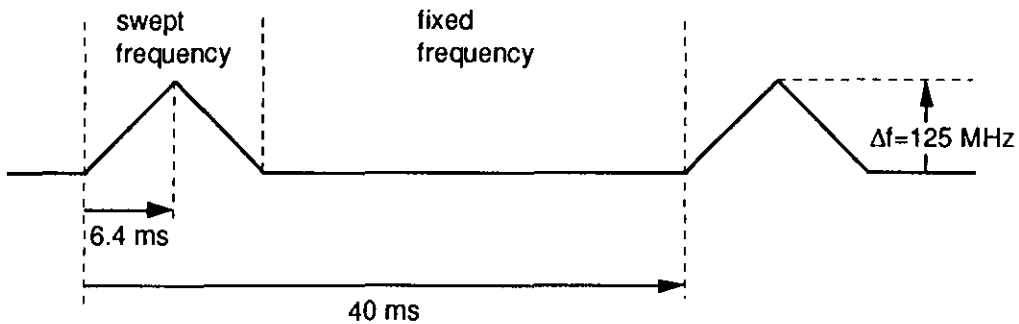


Fig. 5.24. Time sequence of the alternate measurement.

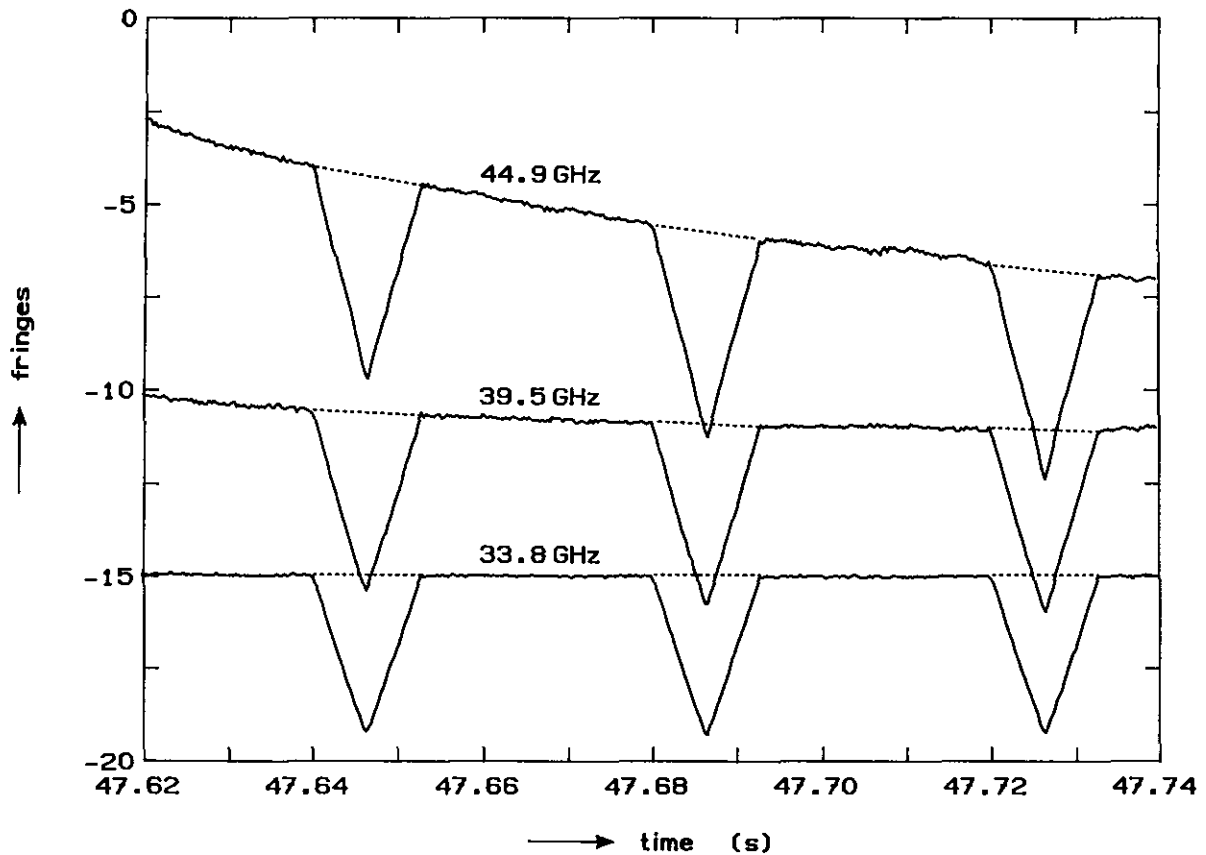


Fig. 5.25. Fringe counter output of three channels in the alternate measurement.

## Appendix C

## PROPOSAL FOR A MULTI-CHANNEL REFLECTOMETER FOR RTP

*Based on the expertise acquired in designing, constructing, and operating the 12-channel microwave reflectometer at JET [Huge-86, Pren-88, Sips-89] a new reflectometer set-up is proposed for the Rijnhuizen Tokamak Project (RTP) at the FOM-Instituut voor Plasmafysica Rijnhuizen.*

A 24-channel reflectometer system is proposed. It should work at frequencies ranging from 27 - 88 GHz and is to be built with the use of single-mode waveguides (Ka-, U-, and E-band). The waves will be launched from both sides of the plasma. The principle of the reflectometer with three channels in the Ka-band (27 - 40 GHz) is shown in Fig. C.1.

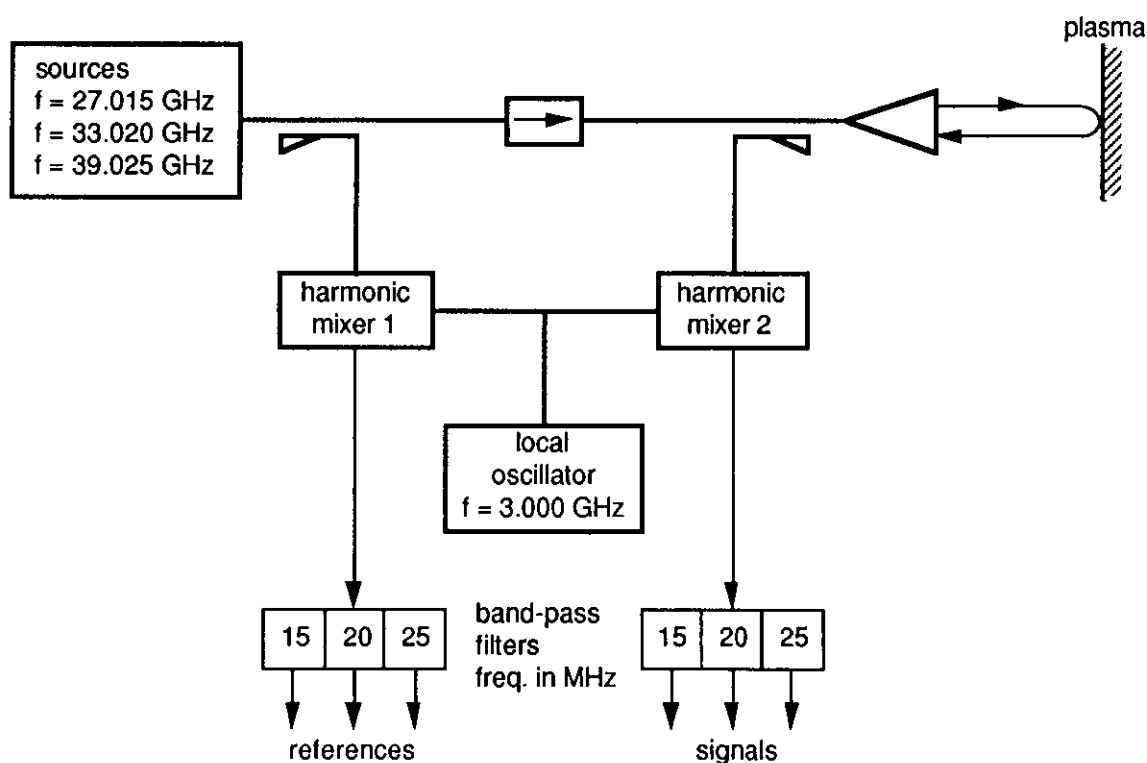


*Fig. C.1. Principle of a three-channel reflectometer in the Ka-band.*

In this system three waves with frequencies of 27.015 GHz, 33.020 GHz and 39.025 GHz, respectively, are launched towards the plasma. One local oscillator at 3 GHz is used for the three channels. The features of the harmonic mixers are such that their output signal contains amongst other combinations also the difference between the  $n$ -th harmonic of the local oscillator (e.g. 27.000 GHz) and the frequency of the incoming signal (e.g. 27.015 GHz).

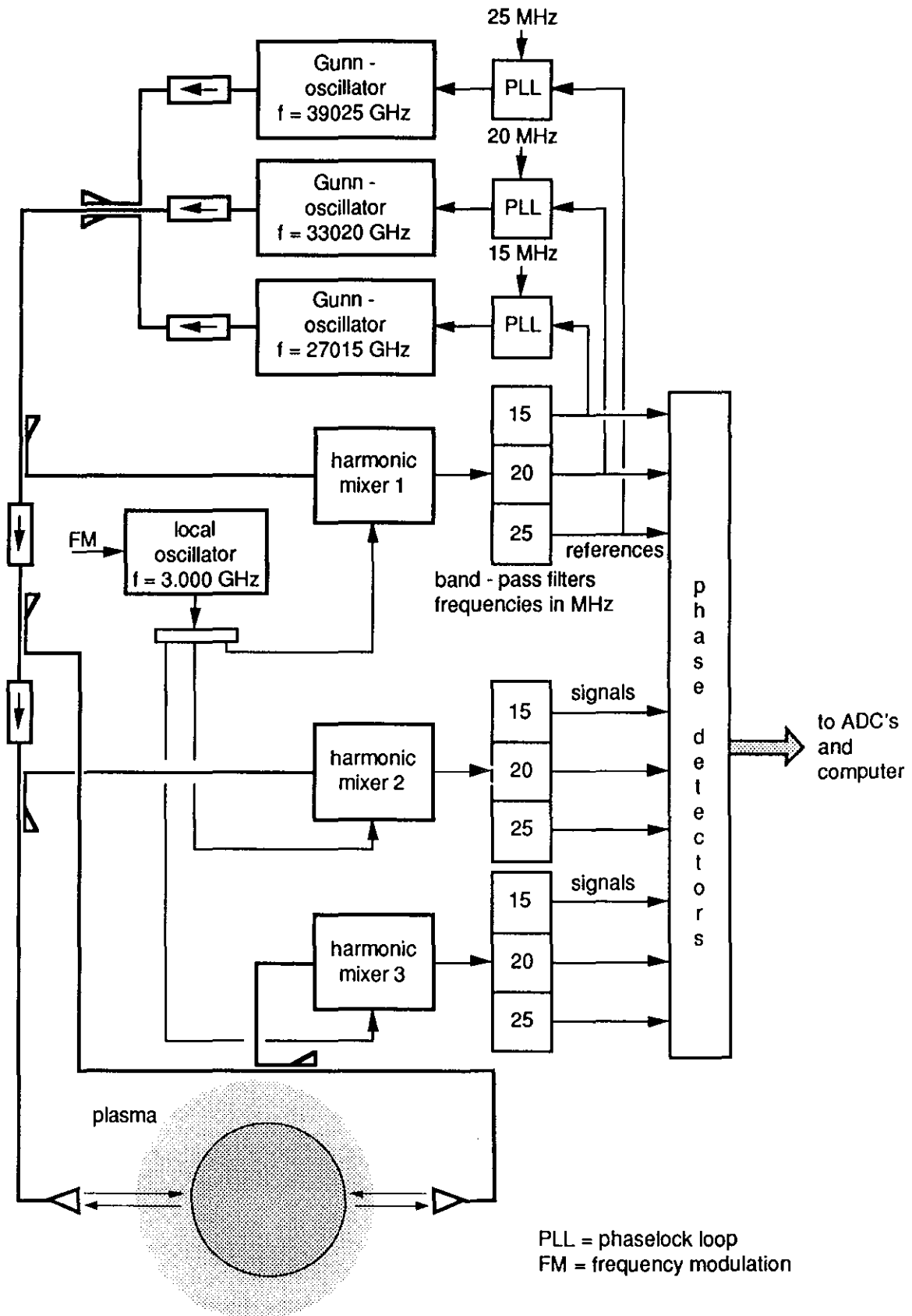


Fig. C.2. Reflectometer set-up in the Ka-band proposed for the RTP-experiment.

The 33 GHz and 39 GHz systems will operate in a similar way. By using different frequency off-sets for the three varactor-tuned Gunn-oscillators the three intermediate frequency signals at 15 MHz, 20 MHz, and 25 MHz, respectively, can be separated with band-pass filters. False mixing products due to intermodulation are rejected by the band-pass filters. The reference signals and the reflected signals are then processed further using phase-detectors and a computer.

A more detailed scheme of the three-channel reflectometer is given in Fig. C.2. The waves will be launched towards the plasma from both sides. A phase detector with high resolution as described in Sec. 1.5 (p. 28) will be used. The output of this phase detector will be recorded using a new data acquisition system with an internal microprocessor. This makes it possible to handle the data with software without being limited by the fixed configuration of a fringe counter. The reflectometer for JET, where each channel consists of two oscillators and two mixers, is about three times more expensive than this new design. This is caused by the fact that the use of harmonic mixers, with ~25 dB conversion loss, was not possible in the JET reflectometer because of the high overall losses in the very extended waveguide system. Two modes of operation will again be possible: a fixed frequency mode for detection of fast movements of the critical density layer and a stepped frequency mode for measuring the distance from the antenna to the critical density layer. A step in frequency (e.g. 100 MHz) will lead to a phase shift which is a direct measure for this distance. This will be done in the following way: the frequency of the local oscillator will be stepped from 3000 MHz to 3010 MHz in e.g. 100  $\mu$ s. The phaselock loops (Fig. C.2) will keep the frequency difference of the local oscillator and the oscillators stable in the stepped frequency mode. This will force the Gunn-oscillators up in frequency to 27.105 GHz, 33.130 GHz, and 39.155 GHz, respectively. The input parameters for the distance measurement (Eq. 5.1, p. 114) are now found in a direct way; the frequency step,  $\Delta f$ , is set and the phase change,  $\Delta\phi$ , is measured. The overall design parameters of the proposed microwave reflectometer are listed in Table. C.1.

*Table. C.1. Design parameters of the RTP reflectometer.*

Number of channels:	24 (12 high and 12 low field side)
Three instruments:	Ka-band 27, 33 and 39 GHz
	U-band 43, 47, 51, 55 and 59 GHz
	E-band 64, 72, 80 and 88 GHz
Resolution in fixed frequency mode	< 1/100 of the relevant wavelength
Sampling frequency in fixed frequency mode	1 MHz
Resolution in stepped frequency mode	< 10 mm
Sampling frequency in stepped frequency mode	10 kHz

The multi-channel reflectometer frequencies with the corresponding critical densities are given in Table 2.

---

*Table 2. Proposed frequencies with corresponding cut-off densities.*

---

Frequency (in GHz)	Critical density (el/m <sup>3</sup> × 10 <sup>19</sup> )
27	0.904
33	1.351
39	1.887
43	2.294
47	2.741
51	3.227
55	3.753
59	4.319
64	5.082
72	6.432
80	7.940
88	9.608

---

## EPILOGUE

*This epilogue could well have been the prologue as the measurement described date from 1963.*

### MEASUREMENTS AT 33 GHZ OF DOPPLER FREQUENCY SHIFT \*)

#### Introduction

Doppler frequency shifts at microwave frequencies have often been used for determining the velocity of moving plasmas [Hey -57, Kolb-59]. In these measurements changes of a standing wave pattern are observed from which the magnitude and not the direction of the plasma velocity can be deduced. Yet, the direction of motion in a reflecting plasma layer is not always obvious in plasma physics experiments. To determine this, the sign of the Doppler frequency shift has to be measured. This can be done using a frequency discriminator in a heterodyne system, yielding sign and magnitude of the frequency variation.

Here the method has been applied to plasmoids, ejected from a hydrogen-loaded titanium gun. The plasmoids are made to move in an evacuated cylindrical waveguide. Both standing wave measurements and frequency shifts measurements are discussed.

#### Plasma gun

The properties of plasmoids ejected from hydrogen-loaded titanium guns were studied as part of the experiments involving the Radial Plasma Gun [Orns-64]. The titanium gun consists of a 10 mm long spiral (10 mm in diameter) wound of 2 mm titanium wire, which is saturated with hydrogen. In the centre of this spiral a trigger pin is mounted, insulated in glass except for a sharp point. Fast rising negative voltage pulses of 20 kV are applied to the trigger pin from a 3000 pF condensator. Field emission initiates a discharge between the pin and the spiral. The discharge current oscillates with a frequency of 2.5 MHz; its maximum amplitude is about 1 kA. The plasma is driven out of the gun by the magnetic pressure connected with the discharge current. Measurements of the density and the velocity of these plasmoids have been carried out.

---

\*) This work was published earlier as Rijnhuizen Report 63-09 (1963).

### Measurements of the cut-off of transmission

In preliminary experiments the plasmoids were shot into an evacuated quartz tube (15 mm in diameter, 0.1 m long). This tube was shielded with foils of microwave absorbing material, with two windows of about 10 mm diameter opposite to each other. A parallel microwave beam (at 120 GHz), focused by means of paraffin lenses, was transmitted through these windows perpendicularly to the quartz tube. Cut-off measurements showed that during about 5  $\mu$ s the density in the plasmoid exceeded  $1.8 \times 10^{20} \text{ m}^{-3}$ , i.e. the cut-off density at 120 GHz [Orns-62]. By observing the arrival of the plasmoid at various distances from the gun through different windows, the velocity could be estimated to be about  $5 \times 10^4 \text{ m s}^{-1}$ . Similar time-of-flight measurements were carried out with microwave beams at 75 GHz and 33 GHz.

### Reflection measurements

The velocity can be determined more accurately from Doppler shift measurements. For these measurements the plasmoids are shot into an evacuated cylindrical waveguide of which the diameter (7.5 mm) was chosen below cut-off at 33 GHz for all possible modes except the  $\text{TE}_{11}$  mode. At 33 GHz the wavelength in vacuum,  $\lambda_v$ , is 9.1 mm and the wavelength in the guide,  $\lambda_g$ , is 14.0 mm. The evacuated waveguide is closed at the far end with a 0.2 mm thick mylar window (voltage standing-wave ratio, VSWR < 1%).

The plasmoid reflects the microwaves and acts as a moving plunger in the waveguide. The phase difference,  $\phi$ , between the incoming wave and the reflected wave is

$$\phi = \frac{2\pi f}{c} L_0 - \frac{\pi}{2} ,$$

where  $f$  = the applied frequency and

$$L_0 = 2 \int_{z=0}^{z=z_1} \mu(z) dz ,$$

is the optical path [Gins-61];

$$\mu(z_0) = 1 \text{ at } z = 0 , \quad \text{i.e. in the vacuum at the front of the plasmoid,}$$

and

$$\mu(z_1) = 0 \text{ at } z = z_1 , \quad \text{i.e. at the layer where the density reaches the cut-off density.}$$

Since the maximum density of the plasmoid far exceeds the critical density ( $1.5 \times 10^{19} \text{ m}^{-3}$  at 33 GHz), the microwave reflection method gives an indication of the motion of the outer layer with the cut-off density which acts as the reflecting 'surface'.

**Changing standing wave patterns**

The velocity of the plasmoid can be deduced from the changes of the standing wave pattern. The pattern results from mixing the reflected signal and the incident signal (Fig. E.1).

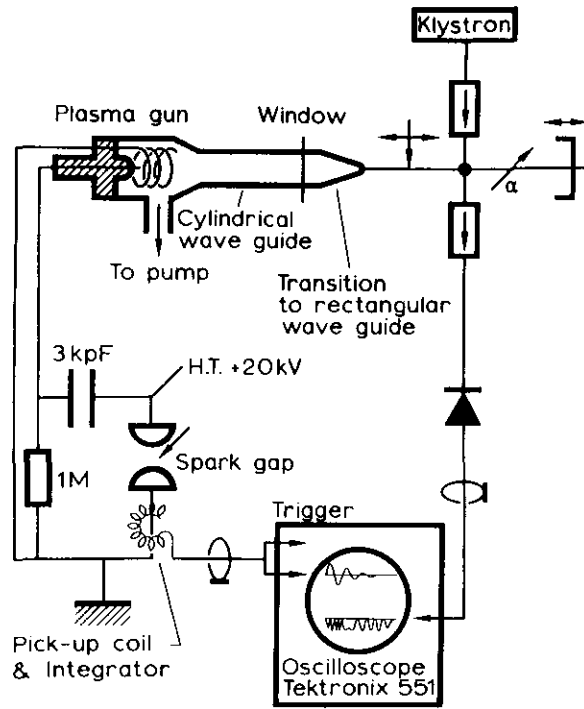


*Fig. E.1. Diagram of the experimental arrangement for measuring changes of the standing wave pattern.*

The pattern of nodes and antinodes passes the quadrantal detector, yielding a beat frequency

$$|\Delta f| = \frac{|v_r|}{\frac{1}{2} \lambda_g},$$

where  $v_r$  is the velocity of the reflector. It can be noted that this description is equivalent with the concept of a Doppler shifted frequency  $f + \Delta f$  interfering with the incident frequency  $f$ . The beat frequency in that case is

$$\Delta f = \frac{2v_r}{v_{ph}} \times f,$$

where  $v_{ph}$  is the phase velocity of the wave in the waveguide:  $v_{ph} = \lambda_g \cdot f$ . From the beat frequency only the velocity can be deduced. The oscillating current in the plasma gun and the beat signal obtained from a crystal detector are shown in Fig. E.2. The fringes can be

distinguished in two different groups: an early group with  $|\Delta f| = 7 \times 10^6$  Hz corresponding to a velocity  $v_r = 5 \times 10^4$  m s<sup>-1</sup> and a later group with  $|\Delta f| = 2 \times 10^6$  Hz corresponding to  $v_r = 1.5 \times 10^4$  m s<sup>-1</sup>.

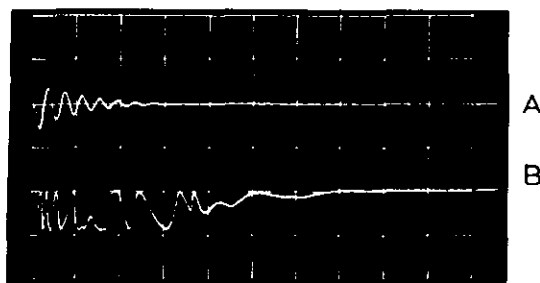


*Fig. E.2. a) Current in the plasma gun 2 kA/div.  
b) Changing standing wave pattern 10 mV/div.  
Sweep 1  $\mu$ s/div.*

If the reflected signal is not coupled out at the far end but through a hole in the cylindrical wall of the waveguide at only 20 mm distance from the plasma gun, two groups of three fringes (i.e.  $3 \times \frac{1}{2} \lambda_g$ ) are separated by an interval during which the signal is cut off. Apparently, the reflecting layer of the plasmoid proceeds in the waveguide during the first microsecond. When the oscillating current in the gun decreases, the plasma production and acceleration stops. Axial and radial diffusion of charged particles reduce the density and possibly change the shape of the axial density distribution. As a result, the reflecting 'surface' moves backward. The diffusion process was not analysed in more detail because the behaviour of the plasma, mixed with the accelerating magnetic field inside the narrow metal tube, was not of particular interest.

### Frequency shift measurements

In order to distinguish between backward and forward motions of the reflecting plasma, a method to measure the actual frequency shift was developed (Fig. E.3).

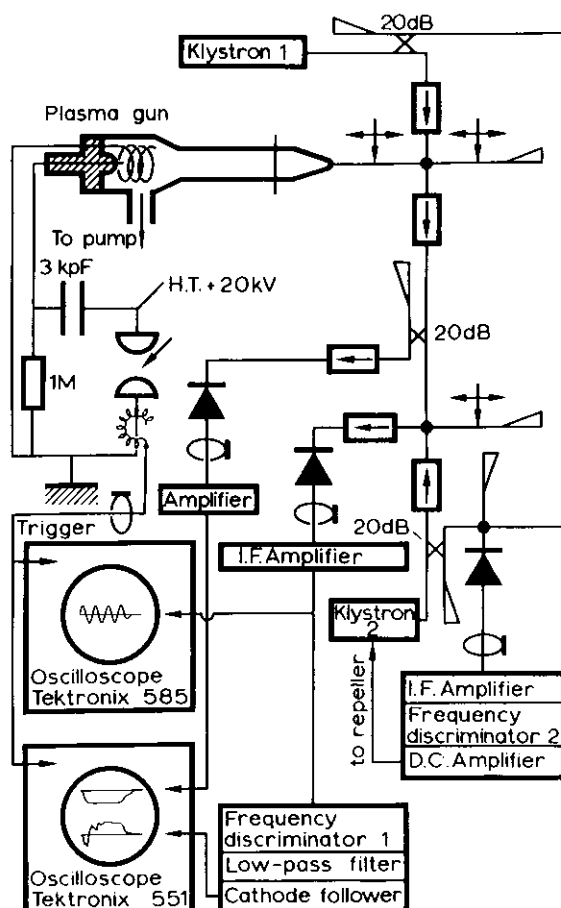
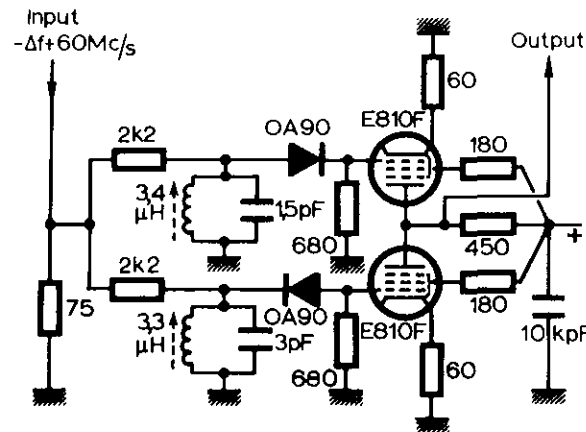


Fig. E.3. Diagram of the experimental arrangement for measuring Doppler frequency shift.

In this case the reflected signal of frequency  $f \pm \Delta f$  is not mixed with the original signal of frequency  $f$  from klystron 1. All spurious reflections from stationary obstacles in the waveguide assembly are carefully tuned away by sliding screws. The signal reflected by the plasma is mixed with the signal from a local oscillator (klystron 2) of which the frequency is automatically controlled in such a way that it oscillates at a frequency which differs by 60 MHz from klystron 1 \*).

\*) The automatic control (Fig. E.3) [Rein-53] is achieved by passing the interference signal from the two klystrons, detected by a crystal rectifier, through a 4 MHz wide frequency discriminator 2 with its centre frequency at 60 MHz (Fig. E.6). A deviation  $\Delta f$ , in the oscillation frequency of one of the klystrons causes an output from the discriminator circuit. The output is amplified and is subsequently fed to the repeller of the local oscillator, which is thus tuned to make the frequency difference again 60 MHz.

The mixed signal is rectified at the crystal detector (1N26) which is terminated by a  $75\ \Omega$  resistance in order to obtain a fast response of about 2 ns. As the output of the crystal is quadratical, the beat frequency is  $\Delta f + 60\ \text{MHz}$ . This intermediate frequency signal is amplified and fed into the fast responding ( $\sim 10\ \text{ns}$ ), 20 MHz wide, frequency discriminator 1 which has its centre frequency at 60 MHz (Fig. E.4).



*Fig. E.4. Circuit diagram of frequency discriminator 1.*

Essentially, the discriminator consists of two LC resonance circuits, with resonant frequencies of 48 MHz and 72 MHz. The outputs of these circuits are subtracted (Fig. E.5).

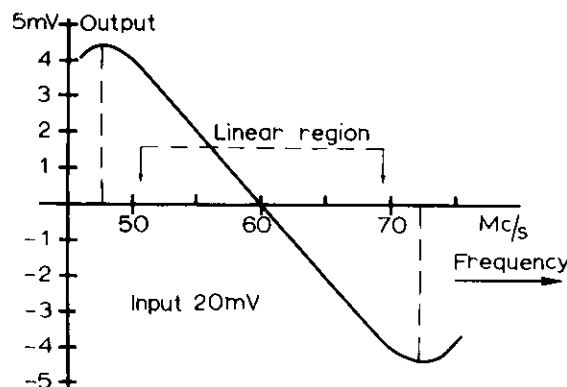


*Fig. E.5. Performance of frequency discriminator 1.*

The resulting output is linearly proportional to the frequency over a 20 MHz wide range when a constant-amplitude input signal is applied to the circuit. The output voltage is passed through a low-pass filter (15 MHz) in order to suppress spurious signals and is subsequently measured with an oscilloscope. The measured signal is linearly proportional to  $\Delta f$ . The output has been calibrated by measuring the amplitude of the intermediate frequency pulse with an oscilloscope

(Tektronix 585) and comparing it to the output of the discriminator when a pulse of known amplitude is applied from a tuneable oscillator (45 MHz to 75 MHz).

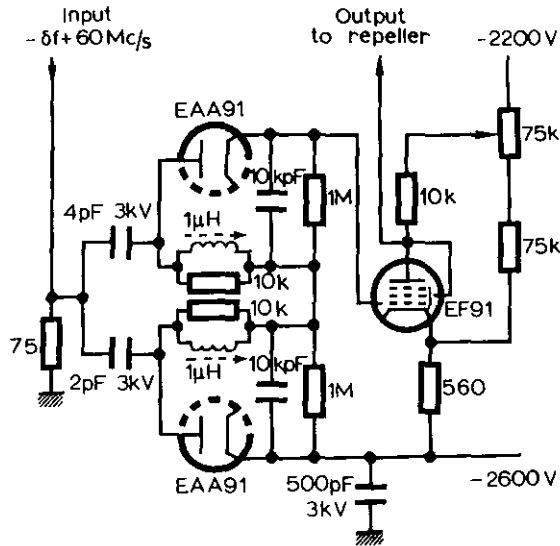


Fig. E.6. Circuit diagram of frequency discriminator 2.

As the Doppler frequency shift is

$$\Delta f = \frac{2v_r}{v_{ph}} \cdot f = \frac{v_r}{\frac{1}{2}\lambda_g},$$

the velocity of the plasmoid can be calculated from the measured frequency shift. Moreover, the sign of the output voltage yields the direction of the motion. Simultaneously with this measurement part of the pure reflected signal is detected, passed through an amplifier and fed to the oscilloscope in order to measure the duration of the phenomenon. The flatness of this signal shows how well the original frequency is tuned out since no fringes occur. Therefore, the frequency measurement is not disturbed by amplitude modulation effects.

Figure E.7 shows a typical example of the measurement.

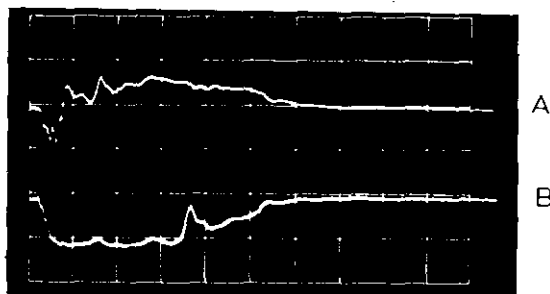


*Fig. E.7. a) Output of the frequency discriminator 5 mV/div (corresponding to a frequency shift of 13 MHz/div, i.e. a velocity of  $9 \times 10^4 \text{ m s}^{-1}$ ).  
b) Reflected microwave signal 10 mV/div.  
Sweep  $1 \mu\text{s/div}$ .*

It can be observed that during the first microsecond the negative frequency shift is high. For a short while it even exceeds 12 MHz corresponding to a forward velocity of  $8 \times 10^4 \text{ m s}^{-1}$ . During the 2nd to 5th microsecond the backward velocity of the reflecting 'surface' is about  $2 \times 10^4 \text{ m s}^{-1}$ . Many details can be distinguished: the motion appears to be rather irregular.

## REFERENCES

- [Anab-87] E. Anabitarte, E.G. Bustamente, M.A.G. Calderón, and J.M. Senties, *Int. J. of Infrared & Millim. Waves*, **8** (1987) 733
- [Anab-88] E. Anabitarte, E.G. Bustamente, M.A.G. Calderón, J.M. Senties, A.P. Navarro, and J. Sánchez, *J. Phys. D: Phys.* **21** (1988) 1384
- [Bick-87] R.J. Bickerton, *JET and the prospect for nuclear fusion*, JET-P(87)59, JET Joint Undertaking, Abingdon
- [Bobe-68] C. Bobeldijk et al., *Proc. 3rd Int. Conf. on Plasma Phys. and Contr. Nucl. Fusion Res., Novosibirsk (1968) Vol. 1*, p. 287
- [Bobe-73] C. Bobeldijk, R.J.J. van Heijningen, and P.C.T. van der Laan, *Third Int. Symp. on Toroidal Plasma Confinement, Garching (1973) paper G5*
- [Born-83] M. Bornatici, R. Cano, O. De Barbieri, and F. Engelmann, *Nuclear Fusion* **23** (1983) 1153
- [Boro-86] A.M. Borozenets, A.I. Skibenko, K.N. Stepanov, and I.P. Fomin, *High Temp. (USA)* **24** (1986) 440. Translation from *Teplofizika Vysokikh Temperatur*, **24** (1986) 570
- [Bott-87] H. Bottollier-Curtet and G. Ichtchenko, *Rev. Sci. Instrum.* **58** (1987) 539
- [Budd-61] K.G. Budden, *Radio waves in the ionosphere*, University Press, Cambridge (1961)
- [Cald-85] M.A.G. Calderon and F. Simonet, *Int. J. of Infrared & Millim. Waves*, **7** (1985) 605
- [Chen-77] F.F. Chen, *Introduction to plasma physics*, Plenum Press, New York (1977)
- [Cost-86] A.E. Costley, *Course and Workshop on Basic and Advanced Diagnostic Techniques for Fusion Plasmas, Varenna (1986) Vol. II*, p. 379 (Invited lecture)
- [Doan-81] J.L. Doane, E. Mazzucato, and G.L. Schmidt, *Rev. Sci. Instrum.* **52** (1981) 12
- [Doyl-89] E.J. Doyle, T. Lehecka, S. Burns, E. Olson, N.C. Luhmann, Jr. and W.A. Peebles, *Bull. Am. Phys. Soc.* **34** (1989) 2116
- [Efth-85] P.C. Efthimion et al., *Rev. Sci. Instrum.* **56** (1985) 908
- [Fess-83] J.A. Fessey, C.W. Gowers, and C.A.J. Hugenholtz, *8th Int. Conf. on Infrared and Millimeter Waves, Miami (1983)*, (Post deadline paper)
- [Fess-85] J.A. Fessey, C.W. Gowers, C.A.J. Hugenholtz, and K. Slavin, *JET plasma electron density measurements from 2-mm wave interferometer*, JET-P(85)04, JET Joint Undertaking, Abingdon
- [Fess-87] J.A. Fessey, C.W. Gowers, C.A.J. Hugenholtz, and K. Slavin, *J. Phys. E* **20** (1987) 169
- [Gard-79] F.M. Gardner, *Phase-lock techniques*, (Second edition) John Wiley & Sons, New York (1979)
- [Ginz-61] V.L. Ginzburg, *The propagation of electromagnetic waves in plasma*, Pergamon Press, Oxford (1970)
- [Gott-77] N. Gottardi, *Iterative method of evaluating local electron density in asymmetrical plasma distributions*, IPP III/39, Max-Planck-Institut für Plasmaphysik, Garching (1977)
- [Gowe-82] C.W. Gowers and C. Lamb, *J. Phys. E* **15** (1983) 343
- [Heal-65] M.A. Heald and C.B. Wharton, *Plasma diagnostics with microwaves*, John Wiley, New York (1965)
- [Hey -57] J.S. Hey, J.T. Pinson, and P.G. Smith, *Nature* **179** (1957) 1184
- [Herm-66] H. Hermansdorfer, *Z. Naturforsch.* **21a** (1966) 1471
- [Horo-83] P. Horowitz and W. Hill, *The art of electronics*, University Press, Cambridge (1983)
- [Hubb-87] A.E. Hubbard, *Measurement of electron density on JET by microwave reflectometry*, Thesis Imperial College of Science and Technology, London, May 1987
- [Hubb-87a] A.E. Hubbard, A.E. Costley and C.W. Gowers, *J. Phys. E: Sci. Instrum.* **20** (1987) 423
- [Huge-70] C.A.J. Hugenholtz, *J. Phys. E* **3** (1970) 318
- [Huge-70a] C.A.J. Hugenholtz, *J. Phys. E* **3** (1970) 750

136 *References*

- [Huge-73] C.A.J. Hugenholtz and A.J. Putter, *Microwave interferometer with digital read-out for large numbers of fringes*, RR 73-81, FOM-Instituut voor Plasmafysica Rijnhuizen, Nieuwegein (1973)
- [Huge-74] C.A.J. Hugenholtz, *Rev. Sci. Instrum.* **45** (1974) 1474
- [Huge-76] C.A.J. Hugenholtz and B.J.H. Meddens, *A CO<sub>2</sub>-laser interferometer with direct read-out of phase-shift*, RR 76-100, FOM-Instituut voor Plasmafysica Rijnhuizen, Nieuwegein (1976)
- [Huge-79] C.A.J. Hugenholtz and B.J.H. Meddens, *Rev. Sci. Instrum.* **50** (1979) 1123
- [Huge-81] C.A.J. Hugenholtz, *Proposed 2-mm interferometer for JET*, Internal Report 81/064, FOM-Instituut voor Plasmafysica Rijnhuizen, Nieuwegein
- [Huge-82] C.A.J. Hugenholtz and B.J.H. Meddens, *Rev. Sci. Instrum.* **53** (1982) 174
- [Huge-82a] C.A.J. Hugenholtz, *Horn antenna matched to oversized waveguide and vacuum window for the JET 2-mm microwave interferometer*, Internal Report 82/001, FOM-Instituut voor Plasmafysica Rijnhuizen, Nieuwegein
- [Huge-86] C.A.J. Hugenholtz and A.J. Putter, *Technical description of the sources, detection systems and data acquisitions for the JET multichannel reflectometer*, RR 86-170, FOM-Instituut voor Plasmafysica Rijnhuizen, Nieuwegein (1986)
- [Huge-86a] C.A.J. Hugenholtz and A.J. Putter, *Course on Basic and Advanced Diagnostic Techniques for Fusion Plasmas*, Varenna (1986) Vol. II, p. 469
- [Huge-88] C.A.J. Hugenholtz and A.J. Putter, *Bull. Am. Phys. Soc.* **33** (1988) 1967
- [Hutc-87] I.H. Hutchinson, *Principles of plasma diagnostics*, University Press, Cambridge (1987).
- [Koecc-80] F. Koechlin, private communication
- [Kolb-59] A.C. Kolb, *Proc. IVth Int. Conf. on Ion. Phenomena in Gases*, Uppsala (1959) Vol. IV, p. 1021
- [Lehe-88] T. Lehecka, W.A. Peebles, N.C. Luhmann, Jr., S.R. Burns, and E. Olson, *Rev. Sci. Instrum.* **59** (1988) 1620
- [Lisi-61] G. Lisitano and M. Tutter, *Z. Naturforsch.* **16a** (1961) 692
- [Luhm-84] N.C. Luhmann and A.A. Peebles, *Rev. Sci. Instrum.* **55** (1984) 279
- [Mans-88] M. Manso et al., *Proc. 15th Eur. Conf. on Contr. Fusion and Plasma Heating*, Dubrovnik (1988) Vol. 12B, Part III, p. 1127
- [Medd-74] B.J.H. Meddens and R.J. Taylor, *A multiradian mm-interferometer using a digital phase comparator*, RR 74-85, FOM-Instituut voor Plasmafysica Rijnhuizen, Nieuwegein (1974)
- [Mede-87a] F. Medeiros and N. Williams, *A multi-octave millimeter wave combiner and separator network*, Radio Frequency Technology Division, ERA Technology Ltd., Leatherhead, UK (1987)
- [Mede-87b] F. Medeiros and N. Williams, *A multi-octave millimeter wave focusing antenna*, 17th European Microwave Conf., Rome (1987) p. 201
- [Mini-86] *Mini-Circuits, 29 Most frequently asked questions about phase detectors*, Mini-Circuits, Brooklyn, NY (1986)
- [More-48] T. Moreno, *Microwave transmission design data*, Dover Publications Inc., New York, (1948)
- [Okre-68] E.C. Okress, *Microwave Power Engineering*, Academic Press, New York (1968)
- [Omar-75] M.A. Omar, *Elementary solid state physics*, Addison-Wesley, Reading, MA (1975)
- [Orli-88] D.V. Orlinskij and G. Magyar, *Nuclear Fusion* **28** (1988) 611
- [Orms-62] L.Th.M. Ornstein and C.A.J. Hugenholtz, *A rapidly responding 2.5 mm microwave set-up*, RR 62-06, FOM-Instituut voor Plasmafysica Rijnhuizen, Jutphaas (1962)
- [Orms-63] L.Th.M. Ornstein, C.A.J. Hugenholtz, and H.A. van der Laan, *Proc. VIth Int. Conf. on Ionization in Gases*, Paris (1963) Vol. IV, p. 161
- [Orms-64] L.Th.M. Ornstein, *A radial plasma gun*, Thesis University of Utrecht, September 1964

- [Orns-70] L.Th.M. Ornstein and C.A.J. Hugenholtz, *A miniaturized microwave probe to measure local plasma densities*, Conference on Diagnosis of High-Temperature Plasma, Sukhumi, USSR (1970)
- [Orns-79] L.Th.M. Ornstein et al., Proc. 9th Eur. Conf. on Contr. Fusion and Plasma Phys., Oxford (1979) Paper D2.6, p. 92
- [Pren-88a] R. Prentice, P. Cripwell, A.E. Costley, J.A. Fessey, J.C.M. de Haas, A.E. Hubbard, C.A.J. Hugenholtz, T. Oyevaar, M. Paume, A.J. Putter, A.C.C. Sips, and K. Slavin, Proc. 15th Eur. Conf. on Contr. Fusion and Plasma Heating, Dubrovnik (1988) Vol. III, p. 1115
- [Pren-88b] R. Prentice, H.E. Clarke, P. Cripwell, A.E. Costley, J.A. Fessey, J.C.M. de Haas, A.E. Hubbard, C.A.J. Hugenholtz, T. Oyevaar, M. Paume, A.J. Putter, A.C.C. Sips, and K. Slavin, Bull. Am. Phys. Soc. **33** (1988) 2029
- [Pren-90] R. Prentice, A.C.C. Sips, J.A. Fessey, and A.E. Costley, Proc. 17th Eur. Conf. on Contr. Fusion and Plasma Heating, Amsterdam (1990)
- [Putt-84] A.J. Putter and C.A.J. Hugenholtz, Proc. 13th Symp. on Fusion Technology, Varese (1984) Vol. 2, p. 42
- [Putt-85] A.J. Putter and C.A.J. Hugenholtz, *Technical information manual for the 2-mm microwave interferometer electronics*, Internal Report 85/001, FOM-Instituut voor Plasmafysica Rijnhuizen, Nieuwegein
- [Rebu-84] P.H. Rebut et al., Proc. 10th Int. Conf. on Plasma Phys. and Contr. Nucl. Fusion Res., London (1984) Vol. 1, p. 167
- [Rein-53] F.J. Reintjes and G.T. Coate, *Principles of Radar*, McGraw-Hill, New York (1953)
- [Shmo-61] J. Shmoys, J. Appl. Phys. **32** (1961) 689
- [Simo-84] F. Simonet, *Measurement of electron density profile by microwave reflectometry on tokamaks*, EUR-CEA-FC-1225, Fontenay-aux-Roses, France (1984)
- [Simo-85] F. Simonet, Rev. Sci. Instrum. **56** (1985) 664
- [Sips-89a] A.C.C. Sips, A.E. Costley, J.C.M. de Haas, and R. Prentice, Proc. 16th Eur. Conf. on Contr. Fusion and Plasma Phys., Venice (1989) Part I, p. 99
- [Sips-89b] A.C.C. Sips, J.C.M. de Haas, G.M.D. Hogewei, R. Prentice, and A.E. Costley, Bull. Am. Phys. Soc. **34** (1989) 2055
- [Sips-89c] A.C.C. Sips, private communication
- [Slui-70] F.W. Sluijter, J. Opt. Soc. Am. **60** (1970) 8
- [Sout-61] G.C. Southworth, *Principles and applications of waveguide transmission*, Van Nostrand, Princeton, NJ (1961)
- [Stix-62] T.H. Stix, *The theory of plasma waves*, McGraw-Hill, New York (1962)
- [Tang-84] A. Tanga, C.W. Gowers, C.A. Hugenholtz, P. Morgan, and F.C. Schüller, *Global particle balance and recycling in first JET discharges*, JET-P(84)09, JET Joint Undertaking, Abingdon
- [Vero-82] D. Veron, Workshop on Diagnostics for Fusion Reactor Conditions, Brussels, CEC, EUR 8351-I EN (1982) p. 199
- [Vero-83] D. Veron, Workshop on Diagnostics for Fusion Reactor Conditions, Brussels, CEC, EUR 8351-II EN (1983) p. 283



## INHOUD

De tokamak is de belangrijkste experimentele opstelling ter wereld geworden in het onderzoek naar de mogelijkheid om elektrisch vermogen op te wekken door beheerste thermonucleaire versmelting. Om thermonucleaire condities te bereiken is het noodzakelijk het plasma, in het bijzonder de energie-inhoud daarvan, voldoende lang op te sluiten. De opsluiting wordt beperkt door warmtegeleiding, convectieve processen en straling. Gedetailleerde analyse van experimenten laat zien dat warmteverliezen door elektronen de klassieke voorspellingen met twee orden van grootte te boven gaan, terwijl de warmteverliezen door ionen dicht bij de theoretische voorspellingen liggen.

Om de levensvatbaarheid van de tokamak naar waarde te kunnen schatten is het noodzakelijk plasmaparameters te meten. Een groot aantal meetmethoden zijn gebaseerd op de analyse van straling die van het plasma komt. Dit kan straling zijn die geëmitteerd wordt door het plasma of straling uitgezonden door een externe bron die door het plasma heen gaat en er door wordt beïnvloed. Microgolfmethoden spelen daarbij een belangrijke rol.

Meettechnieken met behulp van microgolven hebben reeds vele jaren een belangrijke rol gespeeld bij thermonucleaire experimenten. De meest gebruikte technieken kunnen worden onderverdeeld in een aantal categorieën:

- detectie van de elektronencyclotron- of synchrotron straling; dit geeft informatie over de temperatuur van de elektronen in het plasma,
- studie van collectieve verstrooiing van invallende golven waarmee dichtheidsfluctuaties in plasma kunnen worden gevolgd,
- interferometrie om de elektronendichtheid van het plasma te meten,
- reflectometrie om de lokatie van specifieke dichtheidslagen in het plasma te bepalen, vaak in combinatie met metingen van de fluctuaties van die lagen,
- polarimetrie om de lokale verdeling van de magnetische veldsterkte in het plasma te meten.

Dit is een grote verscheidenheid aan meetmethoden, elk gebaseerd op de wisselwerking van elektromagnetische golven en plasma. De voortplanting van elektromagnetische golven in plasma's is uitvoerig behandeld door verschillende schrijvers [Chen-77, Ginz-61, Heal-65, Stix-62]. Hoewel de wisselwerking van elektromagnetische golven met plasma's nogal ingewikkeld is, kan de beschrijving toch zeer vereenvoudigd worden voor tokamak plasma's aangezien in het hier gebruikte frequentie gebied de ionen oneindig zwaar mogen worden beschouwd. In tokamak plasma's is de elektronentemperatuur in het algemeen  $\leq 10$  keV zodat de gemiddelde thermische snelheid van de elektronen veel kleiner is dan de snelheid van de elektromagnetische golven die dicht bij de lichtsnelheid is; dit heeft tot gevolg dat de

relativistische effecten in het algemeen te verwaarlozen zijn. De elektronen-ionen botsingsfrequentie is veel lager dan de frequentie van de golven waardoor ook de botsingsdemping te verwaarlozen is.

In dit proefschrift worden twee diagnostieken beschreven: Interferometrie en Reflectometrie. De principes van deze technieken kunnen als volgt worden aangegeven. De fasesnelheid van een elektromagnetische golf die zich door een plasma voortplant is afhankelijk van de dichtheid: de brekingsindex is  $\mu(n_e) = c/v$ , waar  $c$  de lichtsnelheid is en  $v$  de fasesnelheid van de elektromagnetische golf in het plasma met een elektronendichtheid  $n_e$ . Bij een zekere –kritische– dichtheid,  $n_c$ , wordt de fasesnelheid oneindig, met andere woorden de elektromagnetische golf van een zekere frequentie kan zich niet verder voortplanten door het plasma maar wordt gereflecteerd \*).

Elektromagnetische golven die door het plasma worden gezonden kunnen worden gebruikt om de elektronen dichtheid te meten met een interferometer, mits de juiste frequency is gekozen, d.w.z. voor zover  $n_e$  kleiner dan  $n_c$  blijft. Interferometrie is in feite de meting van de faseverandering t.g.v. de aanwezigheid van het plasma. Microgolfinterferometrie is een basistechniek om de plasmadichtheid in thermonucleaire experimenten te meten als functie van tijd. Wanneer de plasmadichtheid niet homogeen is, maar een zekere ruimtelijke verdeling heeft (b.v. een parabolische), zal de golf langs het pad door het plasma variërende afbuigingseffecten ondergaan en dus geen rechte lijn volgen. De resulterende afbuigingshoek hangt af van de gekozen golflengte, van de waarde van  $n_e/n_c$  en van de ruimtelijke gradiënt van  $n_e$ . Om de afbuiging zo klein mogelijk te houden moet de golflengte ver van de z.g. „cut-off” gekozen worden, dit is zo kort mogelijk, maar wel zo lang dat de variatie van de faseverschuiving tengevolge van de aanwezigheid van plasma nog goed te detecteren is. Kortere golflengtes vereisen echter een hogere mechanische stabiliteit van het instrument om effecten van valse faseveranderingen tengevolge van trillingen te vermijden. De keuze van de werk-frequentie houdt dus altijd een compromis in en is tevens afhankelijk van de beschikbaarheid van de microgolfoscillatoren. In het algemeen worden interferometers met één meetbundel gebruikt. De microgolfbundel met een kleine divergentie wordt in het algemeen parallel aan de dichtheidsgradiënt door het centrum van het plasma gezonden, dus de verstoring van de meting door afbuigingseffecten is relatief klein. Interferometrie kan dichtheidsprofielen opleveren wanneer een aantal (parallele) bundels worden gebruikt. Aangezien geïntegreerde lijndichtheden

---

\*) Dit is natuurlijk maar bij benadering waar. Reflectie is in feite een continu effect in een inhomogeen medium. Echter binnen de toepassingsgrenzen van de z.g. WKB (Wenzel-Kramers-Brillouin) benadering (dit is in feite zo lang de beschouwde golflengte zeer kort is t.o.v. de schaallengte van de inhomogeniteit) komt het effect van deze inhomogeniteit voornamelijk tot uiting in de fase van de golf en reflectie treedt niet op of is totaal.

worden gemeten moet de informatie worden omgezet, b.v. door Abel-inversie, om een dichtheidsprofiel te vinden. Veel-kanaalsinterferometers voor grote thermonucleaire plasma-experimenten worden kolossale obstakels in de volle ruimte rond zulke experimenten en bezetten tevens vele observatievensters. Het is niet te verwachten dat dit soort instrumenten in de volgende generatie van thermonucleaire proefopstellingen nog zullen worden toegepast.

Bij reflectometrie wordt een golf met een bepaalde frequentie naar het plasma gezonden en vrijwel geheel gereflecteerd door de laag in de nabije omgeving van de kritische dichtheid. Het faseverschil van de uitgezonden en de gereflecteerde golven bevat informatie over de positie van de reflecterende laag. Reflectometers kunnen op twee manieren worden bedreven: met vaste frequentie zijn bewegingen van een reflecterende laag te volgen, terwijl met een frequentiezwaai de absolute positie is te bepalen. Aangezien de golf zich door plasma voortplant alvorens de golf reflecteert bij de „cut-off” laag, moet ook de faseverandering in deze transparante laag in beschouwing worden genomen. Daar de kritische dichtheid afhankelijk is van de frequentie, is de toepassing van golven met een aantal verschillende frequenties noodzakelijk om een dichtheidsprofiel te bepalen, aan de kant waar de reflectometer geplaatst is. Reflectometermetingen van beide kanten zijn nodig om een compleet dichtheidsprofiel van een plasma te bepalen. Reflectometrie is in ontwikkeling in verscheidene laboratoria, want één van de aantrekkelijke kanten van reflectometrie vergeleken met meer-kanaalsinterferometrie is het feit dat de opstelling weinig ruimte vergt. Een ander voordeel van reflectometrie t.o.v. meer-kanaalsinterferometrie is dat lagere frequenties gebruikt kunnen worden; er kan dan gekozen worden uit een groter aantal typen oscillatoren.

## SAMENVATTING

### Deel 1. Interferometrie

Hoofdstuk 1 geeft een inleiding over interferometrie waarin ook enige de theoretische achtergrond wordt gegeven. Verschillende microgolffonderdelen worden beknopt besproken. Uitvoerig wordt ingegaan op fase-modulatietechnieken, waarmee het mogelijk is om faseverschuiving ondubbelzinnig te meten. Een aantal digitale fasedetectoren, waarmee een grote nauwkeurigheid is te bereiken, worden besproken.

Hoofdstuk 2 geeft een beschrijving van de 2-mm microgolffinterferometer, ontworpen en gebouwd voor de JET-tokamak, het gezamenlijk Europese thermonucleaire experiment in Culham, Engeland. Berekeningen van de golfpijpv verliezen, verliezen van de microgolfbundel door het plasma en de te verwachten signaal-ruisverhouding worden gegeven. Resultaten van plasmadichtheidsmetingen laten een zeer goede fase-oplossing zien (1 op 5000).

Hoofdstuk 3 beschrijft CO<sub>2</sub>-laser interferometers, gebouwd voor het RINGBOOG-experiment, een gasdekentokamak in het FOM-Instituut voor Plasmafysica Rijnhuizen. Het eerste instrument is een één-kanaalsinterferometer, die om eenduidige fase-informatie te verkrijgen, gebruik maakt van een bewegende spiegel. In een tweede instrument wordt gebruik gemaakt van twee „Bragg-cell” modulatoren. Een derde instrument heeft 15 kanalen en maakt gebruik van een lintvormige bundel waarmee een compleet „fase-beeld” van het plasma op een detector-rij wordt verkregen.

### Deel 2. Reflectometrie

Hoofdstuk 4 is een inleiding over reflectometrie, waarin de verschillende mogelijkheden en beperkingen van de methode worden besproken. Een afleiding is gegeven van de relatie tussen de fasemetingen en de daarbij behorende dichtheidsprofielen.

Hoofdstuk 5 geeft een uitvoerige beschrijving van de 12-kanaals heterodyne reflectometer ontworpen en gebouwd voor JET. De reflectometer kan op de eerder genoemde twee manieren functioneren. Metingen aan een model, gebruik makend van een metalen spiegel, laten zien dat de gestelde nauwkeurigheidseisen kunnen worden bereikt. Tenslotte worden de eerste metingen met de reflectometer aan het JET-plasma getoond.

In een appendix wordt een voorstel beschreven voor een 24-kanaals reflectometer voor de RTP-tokamak in Nieuwegein.

De epiloog geeft een terugblik naar de jaren 60 met de beschrijving van een heterodyne reflectometer, waarmee snelheden van snel bewegende plasmoiden werden gemeten.

## DANKWOORD

De vrijheid en plezierige werksfeer waarin ik mij heb kunnen ontwikkelen op het FOM-Instituut voor Plasmafysica Rijnhuizen, Nieuwegein heb ik altijd zeer gewaardeerd.

De jarenlange samenwerking met Luuk Ornstein, nu mijn promotor, die mij vaak heeft geïnspireerd tot het bedenken van nieuwe meetsystemen, wil ik graag memoreren.

Veel dank ben ik verschuldigd aan Antoon Putter zonder wie de twee meetsystemen voor JET, beschreven in dit proefschrift, niet mogelijk waren geweest. De plezierige medewerking van o.a. Theo Oyevaar, Henny van Ramele, George Sips en mijn Engelse collega's John Fessey, Chris Gowers, Robin Prentice en Karin Slavin bij de bouw en het inbedrijfstellen van de twee diagnostieksystemen voor JET wil ik graag noemen.

De vele collega's bij het FOM-Instituut voor Plasmafysica, in het bijzonder Bert van der Laan en Ben Meddens, die mij in het verleden hebben geholpen wil ik graag bedanken.

## CURRICULUM VITAE

Ik ben geboren op 3 juni 1937 te Klaaswaal. Mijn technische opleiding heb ik genoten aan de HTS voor Elektronica in Hilversum. De opleiding werd met goed gevolg in 1958 afgesloten met het behalen van het diploma „Hogere Elektronicus”. Gedurende mijn militaire dienst (1959-1960) kreeg ik een radaropleiding en werd daarna leraar aan de radarschool. Vanaf September 1960 was ik, in dienst bij de Stichting voor Fundamenteel Onderzoek der Materie, werkzaam op het FOM-Instituut voor Plasmafysica Rijnhuizen in het toenmalige Jutphaas. Ik specialiseerde mij al snel, in samenwerking met L.Th.M. Ornstein, op microgolf-diagnostieken. Van juni 1972 tot juli 1973 werd ik gedetacheerd bij het Alcator-project aan het Massachusetts Institute of Technology (MIT) in Cambridge, USA. Ik ontwierp en bouwde er o.a. een microgolfinterferometer. In 1973 en 1974 ben ik gedurende enige tijd bij de Associatie Euratom-CNEN Laboratorium Gaz Ionizzati in Frascati, Italië, adviseur geweest voor het ontwerpen van millimeter diagnostiek voor het grote FT-tokamak experiment. In 1981 verwierf ik een contract bij de Joint European Torus (JET) te Culham, Engeland, voor het ontwerp van een éénkanaals-microgolfinterferometer. Daarop volgde (1982-1984) een detachering bij JET in Engeland. In deze periode werd de 2-mm microgolfinterferometer gebouwd. In 1985 maakte ik voorstudies voor een heterodyne reflectometersysteem, hetgeen resulteerde in een nieuw JET studiecontract. In 1986 volgde een omvangrijk contract voor een 12-kanaals heterodyne microgolfreflectometer, die werd gebouwd in samenwerking met A.J. Putter c.s. Het installeren van de reflectometer werd in 1988 voltooid. In 1988 ben ik als adviseur opgetreden voor het Centro de Electrodinâmica da Universidade Técnica de Lisboa, Lissabon, Portugal, voor de reflectometer, die door de groep wordt gebouwd voor de ASDEX-tokamak te Garching, Duitsland. Per 1 januari 1987 werd ik bevorderd tot wetenschappelijk medewerker bij de stichting FOM.

**ADDENDUM TO**  
**MICROWAVE INTERFEROMETER AND REFLECTOMETER TECHNIQUES FOR**  
**THERMONUCLEAR PLASMAS**

by  
C.A.J. Hugenholtz

*RIJNHUIZEN REPORT 90-192 (1990)*

The above report was distributed, for reasons of convenience, in the form of a doctoral thesis, which allowed only limited possibility for acknowledgement (in Dutch). The author wishes to distribute this addendum, in order to acknowledge in more detail the role of others in the work described. The addendum is to be considered an integral part of the Rijnhuizen report 90-192.

**Part 1, Interferometry**

Well-known interferometer techniques and specific experience in this field were used to build the 2-mm wave interferometer for JET under a development contract between the Association Euratom-FOM and the JET-project. The responsibility for the design, construction, and operation in the early phase, was undertaken by the author who worked under attachment to JET under the supervision of Dr. L.C.J.M. de Kock. In a later phase this responsibility was transferred by JET to Mr. C.W. Gowers. The good cooperation with Mr. J.A. Fessey, Mr. C.W. Gowers, Dr. L.C.J.M. de Kock, and Miss K. Slavin is gratefully acknowledged.

**Part 2, Reflectometry**

The concept of the multi-channel reflectometer for JET was proposed by Dr. A.E. Costley [Cost-86], who also supervised the work of Dr. A.E. Hubbard on the design and construction of the first single-channel homodyne reflectometers for JET [Hubb-87 and Hubb-87a]. The initial feasibility work for the multichannel reflectometer consisting of computer simulations and proof of principle experiments was carried out on JET by Dr. A.E. Hubbard and published by Prentice et al [Pren-86].

The multi-channel reflectometer for JET was designed and built with Mr. R. Prentice as JET responsible officer. The FOM-Instituut voor Plasmafysica undertook –under contract with JET– the design, construction, and installation of the sources, heterodyne detection systems, data-acquisition systems, and the reference waveguides. The FOM effort was coordinated by the author in close cooperation with Mr. A.J. Putter and his group.



The commissioning of the reflectometer was performed jointly by the FOM Task Agreement Team, i.e. Mr. J.W.. Oosterbeek, Mr. T. Oyevaar, and Ir. A.C.C. Sips, and Mr. J.A. Fessey, Mr. H. Clarke, and Miss. K. Slavin of the JET Team. The work was supervised by Mr. R. Prentice in collaboration with the author. The good cooperation with all those mentioned is gratefully acknowledged

The Rijnhuizen report basically describes the technical solutions chosen for the reflectometer systems. The results at the end of chapter 5 were included in order to demonstrate the performance of the reflectometer and the author is grateful to Mr. R. Prentice for his permission to include unpublished data.

[Pren-86] R. Prentice, A.E. Costley, J.A. Fessey, and A.E. Hubbard, Course and Workshop on Basic and Advanced Diagnostic Techniques for Fusion Plasmas, Varenna (1986), EUR 10797 EN, Vol II, p. 451